UNLIMITED
UNCLASSIFIED

Canada

# A SUMMARY OF TRANSONIC NATURAL LAMINAR FLOW AIRFOIL DEVELOPMENT AT NAE

by

M. Khalid and D.J. Jones

National Aeronautical Establishment

OTTAWA
MAY 1990

AERONAUTICAL NOTE
NAE-AN-65
NRC NO. 31608

National Research Council Canada
Conseil national de recherches Canada

## NATIONAL AERONAUTICAL ESTABLISHMENT

## SCIENTIFIC AND TECHNICAL PUBLICATIONS

### AERONAUTICAL REPORTS

**Aeronautical Reports (LR):** Scientific and technical information pertaining to aeronautics considered important, complete, and a lasting contribution to existing knowledge.

**Mechanical Engineering Reports (MS):** Scientific and technical information pertaining to investigations outside aeronautics considered important, complete, and a lasting contribution to existing knowledge.

**AERONAUTICAL NOTES (AN):** Information less broad in scope but nevertheless of importance as a contribution to existing knowledge.

**LABORATORY TECHNICAL REPORTS (LTR):** Information receiving limited distribution because of preliminary data, security classification, proprietary, or other reasons.

Details on the availability of these publications may be obtained from:

Graphics Section,
National Research Council Canada,
National Aeronautical Establishment,
Bldg. M-16, Room 204,
Montreal Road,
Ottawa, Ontario
K1A 0R6

## ÉTABLISSEMENT NATIONAL D'AÉRONAUTIQUE

## PUBLICATIONS SCIENTIFIQUES ET TECHNIQUES

### RAPPORTS D'AÉRONAUTIQUE

**Rapports d'aéronautique (LR):** Informations scientifiques et techniques touchant l'aéronautique jugées importantes, complètes et durables en termes de contribution aux connaissances actuelles.

**Rapports de génie mécanique (MS):** Informations scientifiques et techniques sur la recherche externe à l'aéronautique jugées importantes, complètes et durables en termes de contribution aux connaissances actuelles.

**CAHIERS D'AÉRONAUTIQUE (AN):** Informations de moindre portée mais importantes en termes d'accroissement des connaissances.

**RAPPORTS TECHNIQUES DE LABORATOIRE (LTR):** Informations peu disséminées pour des raisons d'usage secret, de droit de propriété ou autres ou parce qu'elles constituent des données préliminaires.

Les publications ci-dessus peuvent être obtenues à l'adresse suivante:

Section des graphiques,
Conseil national de recherches Canada,
Établissement national d'aéronautique,
Im. M-16, pièce 204,
Chemin de Montréal,
Ottawa (Ontario)
K1A 0R6

UNLIMITED
UNCLASSIFIED

# A SUMMARY OF TRANSONIC NATURAL LAMINAR FLOW AIRFOIL DEVELOPMENT AT NAE

# RÉSUMÉ DES RECHERCHES DE L'ÉNA SUR DES PROFILS AÉRODYNAMIQUES À ÉCOULEMENTS LAMINAIRES NATURELS TRANSSONIQUES

by/par

M. Khalid and D.J. Jones

National Aeronautical Establishment/
Établissement national d'aéronautique

AERONAUTICAL NOTE
NAE-AN-65
NRC NO. 31608

OTTAWA
MAY 1990

Y.Y. Chan, Head/Chef
High Speed Aerodynamics Laboratory/
Laboratoire d'aérodynamique à hautes vitesses

G.F. Marsters
Director/directeur

90-05826/


## SUMMARY

This report contains an analysis of the experimental results obtained from four supercritical natural laminar flow (NLF) airfoils investigated in the NAE High Reynolds Number Test Facility. The airfoils have maximum thickness to chord ratios of 0.10, 0.13, 0.16 and 0.21 and were designed for a lift coefficient of $C_L$ = 0.6. Their design Mach numbers were 0.8, 0.76, 0.72 and 0.68 respectively and the design chord Reynolds number was 12.5 million. It was found that all the airfoils showed the presence of a drag bucket close to design conditions and long lengths (in some cases about 70%) of natural laminar flow at Reynolds number 6.7 million. The minimum drag for the airfoils was found to range from 0.0045 to 0.0051, representing far lower levels than any airfoil dominated by turbulent boundary layer. It is also indicated that with transition fixed at about 10% chord the drag levels were similar to other airfoils with turbulent boundary layers.

## RÉSUMÉ

Le présent rapport contient une analyse des résultats expérimentaux obtenus pour quatre profils aérodynamiques à écoulements laminaires naturels surcritiques qui ont fait l'objet de recherches à l'installation d'essai pour les nombres de Reynolds élevés. Les profils ont des rapports épaisseur/corde maximaux de 0,10, 0,13, 0,16 et 0,21, et sont conçus pour un coefficient de portance de $C_L$ = 0,6. Leurs nombres de Mach théoriques sont de 0,8, 0,76, 0,72 et 0,68 respectivement, et le nombre de Reynolds théorique des cordes est de 12,5 millions. Les résultats révèlent que tous les profils présentent un godet de traînée au voisinage des conditions théoriques et des longueurs importantes (parfois d'environ 70 %) d'écoulement laminaire naturel au nombre de Reynolds de 6,7 millions. La traînée minimale pour les profils varie entre 0,0045 et 0,0051, ce qui est de beaucoup inférieur à celle de tout profil dominé par une couche limite turbulente. À noter aussi que, pour une transition fixée à environ 10 % de la corde, la traînée est voisine de celle d'autres profils avec couches limites turbulentes.

CONTENTS


| | Page |
|---|---|
| Summary | (iii) |
| List of Tables | (vi) |
| List of Figures | (vii) |
| Symbols | (xiii) |
| 1.0 INTRODUCTION | 1 |
| 2.0 DISCUSSION OF EXPERIMENTAL RESULTS | 4 |
| 2.1 LIFT PERFORMANCE | 4 |
| 2.1.1 Lift versus angle of attack | 4 |
| 2.1.2 Lift curve slope versus Mach number | 5 |
| 2.1.3 Maximum lift and lift at separation onset versus Mach number | 7 |
| 2.2 PITCHING MOMENT RESPONSE | 9 |
| 2.2.1 Pitching moment versus Mach number | 9 |
| 2.3 AIRFOIL DRAG | 11 |
| 2.3.1 Drag Polars | 11 |
| 2.3.1.1 Transition Free Drag Polars at $Re/c=6.7 \times 10^6$ | 11 |
| 2.3.1.2 Transition Fixed Drag Polars at $Re/c= 6.7 \times 10^6$ | 13 |
| 2.3.1.3 Transition Free Drag Polars at $Re/c=12.5 \times 10^6$ | 14 |
| 2.3.1.4 Transition Fixed Drag Polars at $Re/c=12.5 \times 10^6$ | 14 |
| 2.3.2 Drag versus Mach number | 15 |
| 2.4 DRAG COMPARISON AGAINST OTHER AIRFOILS | 16 |
| 2.5 FLOW VISUALIZATION | 17 |
| 2.6 PRESSURE DISTRIBUTIONS | 19 |
| 3.0 COMPARISONS OF GRUMFOIL WITH THE EXPERIMENTAL DATA | 21 |
| 4.0 CONCLUSION | 25 |

5.0 ACKNOWLEDGMENTS 26

6.0 REFERENCES 26

## List of Tables


| | | Page |
|---|---|---|
| Table 1. | Some interesting Drag Features of the four NLF airfoils | 31 |
| Table 2. | Comparison with the NACA 66 Series | 32 |
| Table 3. | GRUMFOIL and Experimental Results for 10% Airfoil: Transition points and Drag Values. R/c = 6.7 million, $C_L$ = 0.6. | 33 |

## List of Figures


| | | Page |
|---|---|---|
| 1. | The Four Airfoils tested in the NAE Facility | 35 |
| 2. | Features of Design Velocities | 36 |
| 3. | NAE 2- Dimensional Test Section | 37 |
| 4. | Coefficient of lift versus angle of attack $C_{LB}$ versus $\alpha$ | 38 |
| 5. | Lift curve slope versus Mach Number $\partial C_L/\partial\alpha$ versus M, Re= 6.7 X $10^6$ (Free Transition). | 39 |
| 6. | Lift curve slope versus Mach Number $\partial C_L/\partial\alpha$ versus M, Re=12.5 X $10^6$ (Free Transition). | 40 |
| 7. | Linear Compressibility $\partial C_L/\partial\alpha$ v $1/\sqrt{(1-M^2)}$ ( Free Transition) | 41 |
| 8. | Lift curve slope versus Mach Number $\partial C_L/\partial\alpha$ versus M, Re= 6.7 X $10^6$ (Transition Fixed). | 42 |
| 9. | Lift curve slope versus Mach Number $\partial C_L/\partial\alpha$ versus M, Re=12.5 X $10^6$ (Transition Fixed). | 43 |
| 10. | Linear Compressibility $\partial C_L/\partial\alpha$ v $1/\sqrt{(1-M^2)}$ (Fixed Transition) | 44 |
| 11. | Maximum lift and lift at separation versus Mach number $CL_{MAX}$, $CL_{SEP}$ versus M, Re/c=6.7 X $10^6$ (Free Transition) | 45 |
| 12. | Maximum lift and lift at separation versus Mach number $CL_{MAX}$, $CL_{SEP}$ versus M, Re/c=12.5 X $10^6$ (Free Transition) | 46 |
| 13. | Maximum lift and lift at separation versus Mach number $CL_{MAX}$, $CL_{SEP}$ versus M, Re/c=6.7 X $10^6$ (Transition Fixed) | 47 |
| 14. | Maximum lift and lift at separation versus Mach number $CL_{MAX}$, $CL_{SEP}$ versus M, Re/c=12.5X $10^6$ (Transition Fixed) | 48 |
| 15. | Pitching moment coefficient $C_M$ versus Mach number M, Re/c= | |

Page

6.7 X $10^6$ , $C_{LB}$ =0.6 (Free Transition) 49

16. Pitching moment coefficient $C_M$ versus Mach number M, Re/c= 6.7 X $10^6$ , $C_{LB}$ =0.6 (Transition Fixed) 50

17. Pitching moment coefficient $C_M$ versus Mach number M, Re =12.5 X $10^6$ , $C_{LB}$ =0.6 (Free Transition) 51

18. Pitching moment coefficient $C_M$ versus Mach number M, Re =12.5 X $10^6$ , $C_{LB}$ =0.6 (Transition Fixed) 52

19. The wake rake location relative to the airfoil. 53

20. Wake drag coefficient versus lift coefficient, $C_{DW}$ versus $C_{LB}$ , (Free Transition), Re/c=6.7 X $10^6$ , M = 0.2 & 0.3. 54

21. Wake drag coefficient versus lift coefficient, $C_{DW}$ versus $C_{LB}$ , (Free Transition), Re/c=6.7 X $10^6$ , M = 0.5. 55

22. Wake drag coefficient versus lift coefficient, $C_{DW}$ versus $C_{LB}$ , (Free Transition), Re/c=6.7 X $10^6$ , M = 0.6. 56

23. Wake drag coefficient versus lift coefficient, $C_{DW}$ versus $C_{LB}$ , (Free Transition), Re/c=6.7 X $10^6$ , M = 0.7. 57

24. Wake drag coefficient versus lift coefficient, $C_{DW}$ versus $C_{LB}$ , (Free Transition), Re/c=6.7 X $10^6$ , M = 0.76, 0.74. 58

25. Wake drag coefficient versus lift coefficient, $C_{DW}$ versus $C_{LB}$ , (Free Transition), Re/c=6.7 X $10^6$ , M = 0.80 & 0.81 59

26. Wake drag coefficient versus lift coefficient, $C_{DW}$ versus $C_{LB}$ , (Transition Fixed), Re/c=6.7 X $10^6$ , M = 0.2 60

27. Wake drag coefficient versus lift coefficient, $C_{DW}$ versus $C_{LB}$ , (Transition Fixed), Re/c=6.7 X $10^6$ , M = 0.6 61

28. Wake drag coefficient versus lift coefficient, $C_{DW}$ versus $C_{LB}$ , (Transition Fixed), Re/c=6.7 X $10^6$ , M = 0.68-0.72 62

Page

29. Wake drag coefficient versus lift coefficient, $C_{DW}$ versus $C_{LB}$ , (Transition Fixed), Re/c=6.7 X $10^6$ , M = 0.74-0.80 63

30. Wake drag coefficient versus lift coefficient, $C_{DW}$ versus $C_{LB}$ , (Free Transition ), Re/c=12.5 X $10^6$ , M = 0.5 64

31. Wake drag coefficient versus lift coefficient, $C_{DW}$ versus $C_{LB}$ , (Free Transition ), Re/c=12.5 X $10^6$ , M = 0.6 65

32. Wake drag coefficient versus lift coefficient, $C_{DW}$ versus $C_{LB}$ , (Free Transition ), Re/c=12.5 X $10^6$ , M = 0.7 66

33. Wake drag coefficient versus lift coefficient, $C_{DW}$ versus $C_{LB}$ , (Free Transition ), Re/c=12.5 X $10^6$ , M = 0.74 - 0.76 67

34. Wake drag coefficient versus lift coefficient, $C_{DW}$ versus $C_{LB}$ , (Free Transition ), Re/c=12.5 X $10^6$ , M = 0.78,0.80 68

35. Wake drag coefficient versus lift coefficient, $C_{DW}$ versus $C_{LB}$ , (Transition Fixed ), Re/c=12.5 X $10^6$ , M = 0.6 69

36. Wake drag coefficient versus lift coefficient, $C_{DW}$ versus $C_{LB}$ , (Transition Fixed ), Re/c=12.5 X $10^6$ , M = 0.7-0.72 70

37. Wake drag coefficient versus lift coefficient, $C_{DW}$ versus $C_{LB}$ , (Transition Fixed ), Re/c=12.5 X $10^6$ , M = 0.76 71

38. Wake drag coefficient versus lift coefficient, $C_{DW}$ versus $C_{LB}$ , (Transition Fixed ), Re/c=12.5 X $10^6$ , M = 0.80 72

39. Wake drag coefficient versus Mach number $C_{DW}$ versus M, (Free Transition) $C_{LB}$ = 0.3, Re/c=6.7 X $10^6$ . 73

40. Wake drag coefficient versus Mach number $C_{DW}$ versus M, (Free Transition) $C_{LB}$ = 0.5, Re/c=6.7 X $10^6$ . 74

41. Wake drag coefficient versus Mach number $C_{DW}$ versus M, (Free Transition) $C_{LB}$ = 0.6, Re/c=6.7 X $10^6$ . 75

42. Wake drag coefficient versus Mach number $C_{DW}$ versus M, (Free Transition) $C_{LB}$ = 0.7, Re/c=6.7 X $10^6$ . 76

Page

43. Wake drag coefficient versus Mach number $C_{DW}$ versus M, (Transition Fixed) $C_{LB}$ = 0.3, Re/c=6.7 X $10^6$ . 77

44. Wake drag coefficient versus Mach number $C_{DW}$ versus M, (Transition Fixed) $C_{LB}$ = 0.5, Re/c=6.7 X $10^6$ . 78

45. Wake drag coefficient versus Mach number $C_{DW}$ versus M, (Transition Fixed) $C_{LB}$ = 0.6, Re/c=6.7 X $10^6$ . 79

46. Wake drag coefficient versus Mach number $C_{DW}$ versus M, (Transition Fixed) $C_{LB}$ = 0.7, Re/c=6.7 X $10^6$ . 80

47. Wake drag coefficient versus Mach number $C_{DW}$ versus M, (Free Transition ) $C_{LB}$ = 0.3, Re/c=12.5 X $10^6$ . 81

48. Wake drag coefficient versus Mach number $C_{DW}$ versus M, (Free Transition ) $C_{LB}$ = 0.5, Re/c=12.5 X $10^6$ . 82

49. Wake drag coefficient versus Mach number $C_{DW}$ versus M, (Free Transition ) $C_{LB}$ = 0.6, Re/c=12.5 X $10^6$ . 83

50. Wake drag coefficient versus Mach number $C_{DW}$ versus M, (Free Transition ) $C_{LB}$ = 0.7, Re/c=12.5 X $10^6$ . 84

51. Wake drag coefficient versus Mach number $C_{DW}$ versus M, (Transition Fixed ) $C_{LB}$ = 0.3, Re/c=12.5 X $10^6$ . 85

52. Wake drag coefficient versus Mach number $C_{DW}$ versus M, (Transition Fixed ) $C_{LB}$ = 0.5, Re/c=12.5 X $10^6$ . 86

53. Wake drag coefficient versus Mach number $C_{DW}$ versus M, (Transition Fixed ) $C_{LB}$ = 0.6, Re/c=12.5 X $10^6$ . 87

54. Wake drag coefficient versus Mach number $C_{DW}$ versus M, (Transition Fixed ) $C_{LB}$ = 0.7, Re/c=12.5 X $10^6$ . 88

55. Drag comparison with other airfoils using $C_{DW}$. 89

56. Flow Visualization, NAE 72-060-16:1, M = 0.8, Re/c=6.7 X $10^6$ $C_L$ = 0.6 90

57. Flow Visualization, NAE 76-060-13:1, M = 0.8, Re/c=6.7 X $10^6$ 91

Page

$\alpha$ = 0.33

58. Flow Visualization, NAE 80-060-10:1, M = 0.8, Re/c=6.7 X $10^6$
$\alpha$ = 1.39 92

59a. Pressure Distribution At The Design Conditions, Re/c=12.5X$10^6$ 93

59b. Pressure Distribution Under Free Transition Conditions
Re/c =12.5 X $10^6$ 94

60. Pressure Distribution Under Free Transition Conditions
Re/c=6.7 X $10^6$ 95

61a. GRUMFOIL versus Experiment. 'Sidewall' Correction of -0.15
Applied. Transition Fixed 10% Airfoil. 96

61b. GRUMFOIL versus Experiment. 'Sidewall' Correction of
-0.008 Applied. Transition Fixed 10% Airfoil. 97

62. Sidewall Correction Computed According to Murthy using
Tunnel measured values of $\delta^*$. 98

63a. Comparison of GRUMFOIL and Experiment, Transition Fixed.
10% airfoil $C_L$ = 0.298 99

63b. Comparison of GRUMFOIL and Experiment, Transition Fixed.
10% airfoil $C_L$ = 0.471 100

63c. Comparison of GRUMFOIL and Experiment, Transition Fixed.
10% airfoil $C_L$ = 0.663 101

63d. Comparison of GRUMFOIL and Experiment, Transition Fixed.
10% airfoil $C_L$ = 0.796 102

64a. Comparison of GRUMFOIL and Experiment, Free Transition
10% airfoil $C_L$ = 0.333 103

64b. Comparison of GRUMFOIL and Experiment, Free Transition
10% airfoil $C_L$ = 0.486 104

64c. Comparison of GRUMFOIL and Experiment, Free Transition
10% airfoil $C_L$ = 0.601 105

Page

64d. Comparison of GRUMFOIL and Experiment, Free Transition 10% airfoil $C_L$ = 0.697 106

64e. Comparison of GRUMFOIL and Experiment, Free Transition 10% airfoil $C_L$ = 0.767 107

64f. Comparison of GRUMFOIL and Experiment, Free Transition 10% airfoil $C_L$ = 0.810 108

65a. Comparison of GRUMFOIL and Experiment, Transition Fixed 10% airfoil $C_L$ = 0.376 109

65b. Comparison of GRUMFOIL and Experiment, Transition Fixed 10% airfoil $C_L$ = 0.522 110

65c. Comparison of GRUMFOIL and Experiment, Transition Fixed 10% airfoil $C_L$ = 0.618 111

65d. Comparison of GRUMFOIL and Experiment, Transition Fixed 10% airfoil $C_L$ = 0.717 112

65e. Comparison of GRUMFOIL and Experiment, Transition Fixed 10% airfoil $C_L$ = 0.798 113

66a. Convergence of GRUMFOIL for case in Fig 64c. 114

66b. $\delta^*$ computed by GRUMFOIL Code for case in Fig. 64c. 115

66c. Shape factor predicted by GRUMFOIL for case in Fig. 64d. 116

66d. Momentum Thickness predicted by GRUMFOIL for case in Fig. 64d. 117

66e. Skin friction as predicted by GRUMFOIL for case in Fig. 64d. 118

66f. Entrainment coefficient predicted by GRUMFOIL for case in Fig. 64d 119

67. A comparison of experimental and GRUMFOIL drag values $C_L$ = 0.6. 10% Airfoil. 120

## Symbols

| Symbol | Definition |
|---|---|
| b | model span |
| c | chord length |
| $C_{DW}$ | wake drag coefficient $D_W/(q_\infty S)$ |
| $C_L$ | lift coefficient, $L/(q_\infty S)$ |
| $C_M$ | pitching moment coefficient about 1/4 chord negative nose down |
| $C_p$ | pressure coefficient, $(p-p_\infty)/q_\infty$ |
| $D_W$ | wake drag |
| L | model lift force |
| M | Mach number |
| q | dynamic pressure, $(1/2\rho_\infty U_\infty^2)$ |
| Re | Reynolds number per unit length |
| $R_c$, Re/c | Reynolds number based on model chord length |
| p | local static pressure |
| $p_\infty$ | free stream static pressure |
| S | model reference area (c.b) |
| t/c | maximum thickness to chord length of the model |
| x/c | relative distance along airfoil chord |
| U | flow velocity |
| $\alpha$ | angle of attack |
| $\rho$ | density |
| $\delta$ | airfoil maximum thickness to chord ratio |
| $\delta^*$ | boundary layer displacement thickness |
| $\partial C_L/\partial\alpha$ | lift curve slope at $C_L = 0.0$ |

Subscripts

| | |
|---|---|
| B | balance measurement |
| c | refers to Mach numbers. This is the tunnel value corrected for upper and lower walls. |
| $\infty$ | free stream conditions |
| SEP | flow separation conditions |

# 1. INTRODUCTION

Future transport aircraft will benefit from improved airfoil designs that reduce wing section drag. Toward that objective, the National Aeronautical Establishment and Boeing Canada de Havilland Division have had an ongoing program of research and development aimed at developing improved supercritical airfoils suitable for future regional transport aircraft. The purpose of this report is to provide a compendium of the results obtained over several years of designing and testing four supercritical airfoils that are capable of supporting extensive regions of natural laminar flow (NLF) in suitably favorable conditions. This technology will provide substantial reduction in drag or alternatively allow substantial increases in wing thickness for a given Mach number and lift coefficient.

When designing these airfoils, one of the foremost objectives was to ensure that good aerodynamic characteristics were retained when the boundary layers were made turbulent from near the noses of the airfoils. This situation can be expected to prevail occasionally, for premature transition can be caused by some type of surface contamination or free stream turbulence. However, for circumstances where conditions are sufficiently "clean" the natural laminar flow (NLF) airfoils are designed to support laminar flow back to 45 to 70% chord on their upper surfaces and up to 40 to 50% chord on their lower surfaces. This extent of laminar flow will lead to drag

reduction of at least 50% relative to the same airfoils with turbulent boundary layers.

Validating the performance of NLF-capable airfoils at high Reynolds number becomes difficult in wind tunnels due to the need for very low turbulence levels and for extremely fine tolerances on small models. Measurements made in 1978 by Elfstrom in the NAE Two Dimensional Test Facility [1] showed turbulence levels were about 0.30% at Reynolds numbers of 14-20 million . Calculations made using this level of turbulence with the method of Van Driest and Blumer [2] suggested there was little prospect for extensive NLF under these conditions. However, subsequent tests at NAE showed lower turbulence levels of about 0.16% as a result of new screens being installed [3] and edgetone noise effects from the porous walls being reduced.

Four airfoils were designed and tested. They ranged from 10% to 21% in maximum thickness to chord. Their geometries are shown in Fig.1. The airfoil designations shown in Fig.1 e.g., NAE 76-060-13(1) indicate the design Mach number, design lift, maximum thickness to chord and, in brackets the version of the airfoil. The design lift coefficient selected for the airfoils was 0.6 to suit aircraft operating over long ranges and at high altitudes. The airfoils were designed using BGK computer code at Re/c =12.5 $x10^6$ with turbulent boundary layer and accelerated flow up to the shock wave, in anticipation that accelerated flow would lead to delayed transition and extended runs of laminar flow. Note that the trailing edge thickness

(~0.5%) of the 16 and 21% airfoils is larger than that of the thinner airfoils(~0.1%). The thinner trailing edge for later designs was believed to be more advantageous for NLF design as observed in Reference 4.

Some features of the design velocity distribution for the airfoils are summarized in Fig. 2. At the design condition the peak Mach numbers on the upper surface were kept to 1.10-1.12 to give low wave drag, and the velocity gradients were made slightly favorable to encourage NLF. A moderate amount of aft loading was used to enhance performance, subject to the constraints that pitching moment coefficients should not be less than -0.14 at the design conditions. Boundary-layer calculations were made with almost fully turbulent conditions which showed good margins from flow separation on the upper and lower surfaces of the airfoils at their respective design conditions.

The airfoils were tested in the NAE 0.38m X 1.5m two-dimensional wind tunnel over a range of chord Reynolds numbers from 6.7 to 16.7 million . The tunnel is a blowdown type with the top and bottom walls having normal holes giving a porosity of 20.5%, and the sidewalls having controlled suction in the region of the model. The model of the 16% t/c (thickness to chord) airfoil was made of 12 inches chord and the models of the other airfoils were 10 inches chord. Fig. 3 shows the schematics of the 2 D test section (0.38 m X 1.5 m) which is mounted in the 1.5 m X 1.5 m test section of the NAE trisonic

wind tunnel for these tests. See Reference 5 for more detailed description of this facility.

It should be noted that all airfoils were tested at the same unit Reynolds number. Thus the chord Reynolds number for the 16% thick airfoil is 1.2 times larger than that of the other three airfoils. In the following text, the Reynolds numbers quoted are referred to the 10 inch chord airfoils, except otherwise indicated, the Reynolds number for the 16% thick airfoil is 1.2 times the cited value.

This report will first review the experimentally determined characteristics of all the airfoils under both fixed transition (usually 7% and 15% on the upper and lower surfaces respectively) and free transition conditions. A later section will compare computed results from a recent code GRUMFOIL with the experimental data for the 10 and 13% airfoils. Unfortunately, transition free computed results on the 13% airfoil are not available as convergence problems were encountered with the GRUMFOIL computer code. Other comparisons of theory with experiment for all the airfoils under transition fixed conditions can be found in Ref. 6 while Ref. 7 gives more information on the two thicker airfoils.

## 2. DISCUSSION OF EXPERIMENTAL RESULTS

### 2.1 LIFT PERFORMANCE

#### 2.1.1 Lift versus angle of attack

Figure 4 shows the transition free $C_{LB}$ versus $\alpha$ performances for all the four airfoils at Mach number of M= 0.3 and Reynolds number of 6.7 X $10^6$ ( 16% thick airfoil at M= 0.2 and Re/c =5.9 X $10^6$ $ft^{-1}$ ). $C_{L\ MAX}$ appears to increase with the thickness of the airfoil starting from a low of about 1.19 at $\alpha$= 9.18 deg for the 10 % thick (t/c) airfoil, to the highest $C_{L\ MAX}$ value of 1.68 at $\alpha$ = 13.67 deg for the 21 % thickness airfoil. The $C_{L\ MAX}$ value for the 10% airfoil is well below the other thicker airfoils. The leading edge of the 10% airfoil has a nose radius much smaller than the other thicker airfoils, and as explained in Ref. [8], a decrease in the nose radius can be responsible for a substantial drop in the $C_{L\ MAX}$ value for the same airfoil.

In Fig. 4 the $C_{L\ MAX}$ values in most cases are well defined and the $C_{LB}$ versus $\alpha$ are fairly linear. At $\alpha$ = 0.0 the $C_{LB}$ values range from 0.275 for 10% thick airfoil to 0.445 for 21% thick airfoil. The increase must result from increasing camber for thicker airfoils, see Fig 1. At other Reynolds numbers, the angle of attack was not traversed up to sufficiently high $\alpha$'s to provide a complete $C_{LB}$ v $\alpha$ picture.

### 2.1.2 Lift curve slope versus Mach number

Figures 5 and 6 show the transition free cases of $\partial C_L/\partial\alpha$ (at $C_L$ = 0.0) against Mach number for the four airfoils at Reynolds numbers of 6.7 X$10^6$ and 12.5 X $10^6$ respectively. From Figure 5 it appears that $\partial C_L/\partial\alpha$ values remain

somewhat steady up to M = 0.5 after which point they show an increasing trend, reaching a maximum at or close to the individual design Mach number of the airfoil. This increasing trend with Mach number is consistent with Prandtl-Glauert theory (compressibility effect) which predicts a linear increase with respect to the parameter $\simeq 1/\sqrt{(1-M^2)}$ when close to transonic Mach Numbers. Similar trends have been observed for a NACA 230 series airfoil tested in DVL (Deutsche Versuchsanstalt fur Luftfahrt) 2.7m wind tunnel Ref [8]. The $\partial C_L/\partial\alpha$ data for the higher Reynolds number case $12.5 \times 10^6$ are somewhat lower than those at the lower Reynolds number $6.7 \times 10^6$ . The thicker turbulent boundary layer effectively decambers the airfoil leading to lower $\partial C_L/\partial\alpha$.

To investigate linear compressibility similitude amongst the four airfoils, $\partial C_L/\partial\alpha$ data at Re = 6.7 and 12.5 million under free transition conditions were also plotted against $1/\sqrt{(1-M^2)}$.The data shown in Fig 7 seem to collapse well for $M \leq 0.64$ suggesting similarity in performance at subsonic Mach numbers. Note also that $\partial C_L/\partial\alpha$ is fairly linear with the parameter $1/\sqrt{(1-M^2)}$ up to an abscissa value of about 1.25.

Figures 8 and 9 are the plots for the transition fixed values of $\partial C_L/\partial\alpha$ against Mach number at Reynolds numbers of $6.7 \times 10^6$ and $12.5 \times 10^6$ respectively. There is no data available for $M \leq 0.6$. For the Mach number range covered in these plots $0.6 \leq M \leq 0.8$ , in general there is an increase in $\partial C_L/\partial\alpha$ values with Mach number, with some airfoils showing a

distinct maximum towards the upper end of the range. Under transition fixed conditions it is noted that for a given Mach number the thinner boundary layer at $Re/c = 12.5 \times 10^6$ gives rise to higher $\partial C_L/\partial\alpha$ values than their counterparts at $6.7 \times 10^6$. Linear compressibility was again studied by plotting $\partial C_L/\partial\alpha$ against $1/\sqrt{(1-M^2)}$ for the transition fixed data in Fig 10. Again, the data seem to collapse only for the subsonic Mach numbers $M \leq 0.67$.

It should be mentioned that von-Karman [9] transonic similitude was also investigated for the above data under transition fixed and free conditions. This exercise was carried out by plotting $\partial C_L/\partial\alpha((\gamma+1)M^2/\delta^2)^{0.333}$ against $(1-M^2)/(\delta(\gamma+1)M^2)^{0.666}$ ( For the sake of brevity this plot is not shown). No satisfactory collapse of data for the four airfoils was noted.

Comparison of transition free data at $Re/c = 6.7 \times 10^6$ (Figure 5) against the corresponding turbulent airfoil data (Figure 8) shows that there is a decrease in $\partial C_L/\partial\alpha$ values once the laminar flow is lost. However, at the higher Reynolds number of $12.5 \times 10^6$, the difference in (compare Figures 6 and 9) $\partial C_L/\partial\alpha$ values for the transition free and transition fixed runs is not as noticeable.

### 2.1.3 Maximum lift and lift at separation onset versus Mach number

Figures 11 and 12 show the free transition lift performance of the four airfoils against Mach number at chord Reynolds numbers of $6.7 \times 10^6$ and $12.5 \times 10^6$ respectively. For each airfoil the $C_{L\ sep}$ performance is also shown along with the $C_{L\ max}$. $C_{L\ sep}$ in each case is obtained by plotting $C_p$ at or close to a chord station $x/c = 0.96$ versus $C_{LB}$, and then determining the point on the curve where $\partial C_p/\partial C_L = -0.4$, Ref.10. Lift corresponding to the drag rise Mach numbers was also evaluated ( based on a $\partial C_D/\partial M = 0.1$ method) from appropriate drag polars and is also shown in Figures 11 and 12.

When discussing the performance of these airfoils as a group it must be understood that each one of them has been designed to perform best at its own design conditions. For example at M =0.7 the 21% airfoil is at or close to its design lift condition whereas the 10 % airfoil is far from its design Mach number value. Equally the 10% is designed for M=0.8, where its lift performance is, and expected to be better than the other three. In general a glance at Figure 11 indicates that for all the airfoils both $C_{L\ max}$ and $C_{L\ sep}$ decrease with increasing Mach number. Another interesting point to note is that at higher Mach numbers $M \geq 0.7$ , there is a tendency for thinner airfoils to show higher $C_{L\ max}$ values and vice versa for $M \leq 0.7$ which is indicative of different lift developing mechanism in different Mach number regimes.

The drag rise Mach number data in both Reynolds number cases (Figures 11 and 12) also conforms to the design

constraints of each airfoil and cannot be discussed in a comparative sense.

Figures 13 and 14 show the corresponding transition fixed data for the four airfoils at chord Reynolds numbers of $6.7 \times 10^6$ and $12.5 \times 10^6$ respectively. The general behavior of $C_{L\ max}$ and $C_{L\ sep}$ again shows a decreasing trend with the increase of Mach number with the overall levels of lift (in most cases) being a little bit below the transition free counterparts. There is no radical shift in drag rise Mach number in going from transition free to turbulent conditions for the two thicker airfoils, however, the thinner 13 % and 10 % airfoils do appear to show a drop in drag rise Mach number when the turbulent flow conditions are forced.

As expected in almost all of the above lift versus Mach number plots $C_{L\ sep}$ values always trail the corresponding $C_{L\ max}$ data.

## 2.2 PITCHING MOMENT RESPONSE

### 2.2.1 Pitching Moment versus Mach Number

Figures 15 and 16, respectively show the transition free and transition fixed pitching moment versus Mach number of the four airfoils at $C_{LB} = 0.6$ and chord Reynolds Number of $6.7 \times 10^6$. For the transition free results in Figure 15 , it is clear that both the thickness (t/c) and the Mach

number have the effect of increasing the magnitude of the pitching moment. As mentioned earlier, at the design Mach number these airfoils were supposed to have a pitching moment greater than -0.14. With the exception of the 10% airfoil which appears to have a pitching moment value of about -0.14 at M=0.8, all others fall well below this constraint at their respective design Mach numbers. The 16 % airfoil (NAE 72-060-16:1) perhaps displays the largest pitching moment magnitude $|C_M|$ in almost the entire Mach number range ( with the exception of a small interval $0.68 \leq M \leq 0.72$ in which the 21% airfoil takes over).

The transition moves forward with the increase of the Reynolds number and a thicker boundary layer with a comparatively smaller loading at the aft portion causes a reduction in the pitching moment magnitude as shown by the comparison of the turbulent airfoil data in Figure 16 to the free transition data in Figure 15. The pitching moment magnitude still shows a similar trend with thickness and Mach number as was observed for the transition free case in Figure 15.

Figure 17 and 18 respectively show a similar transition free and transition fixed comparison at $C_{LB} = 0.6$ and a still higher chord Reynolds number of $12.5 \times 10^6$. The transition free data in Figure 17 once again show that the airfoils thickness and increase of Mach number have the effect of increasing the magnitude of the pitching moment. Note that the 16 % airfoil even at this higher Reynolds number of $12.5 \times 10^6$ seems to provide the largest pitching moment at almost all Mach number

conditions. It is also interesting to note that for the transition free data in Figure 17, the thicker airfoils 21 and 16 % appear to show a bottoming out of the pitching moment response followed by (in case of 21% airfoil) a short reversal caused by a trailing edge separation. Under transition fixed conditions in Figure 18 the overall trends remain generally similar to their transition free counterparts.

## 2.3 AIRFOIL DRAG

The wake drag was measured by the standard sidewall-mounted traversing rake supporting four pitot probes, The method is based on measuring the momentum deficit in the wake. Reference 11 gives details of the instrumentation. The signal from probe 4 is ignored as it is sometimes affected by the disturbed sidewall boundary layer. The total effective drag $C_{DW}$ is usually computed from an average of the remaining three probes, see Figure (19).

### 2.3.1 Drag Polars

#### 2.3.1.1 Transition Free Drag Polars at Re = 6.7 x $10^6$

Figures 20 to 25 present transition free drag polars for the four airfoils at Re = 6.7 X $10^6$ for the Mach number range from 0.3 to 0.7. For the 16 % airfoil , the low Mach number ( M = 0.2 ) measurements were made at Re = 6 X$10^6$ and are thus duly presented for comparison.

At M = 0.3 in Figure 20 , in the lower drag region of the polars with $0.0 \leq C_{LB} \leq 0.75$ , the drag increases with the thickness of the airfoil, with the thinnest 10 % airfoil, occupying the lowest drag level of about 0.0046 which increases to a value of about 0.0080 for the 21 % airfoil. At M =0.5 in Figure 21, a similar trend is repeated except in the region $0.5 \leq C_{LB} \leq 0.75$, where the 10 % airfoil has very similar drag characteristics as the 13% airfoil.

The drag polar for the 16% airfoil was not available at M = 0.6 in Figure 22. Drag polars for the remaining airfoils are shown. Except for one point at $C_{LB} = 0.198$, the drag polar for the 21% airfoil is notably higher than the polars for the other two airfoils which at least in the range $0.3 \leq C_{LB} \leq 0.7$ show very similar drag levels. Figure 23 shows the drag polars for the four airfoils at M = 0.7. This Mach number is very close to the design Mach number value of the 21 % airfoil and , near the design lift condition in the range $0.3 \leq C_{LB} \leq 0.6$, this airfoil displays the lowest drag. This, as will be addressed later, is due to extensive NLF at this condition.

At Mach number M=0.76 , the drag polar for the thickest 21 % airfoil was not measured as the conditions here, are well past the drag rise Mach number for this airfoil. The polars for the remaining three airfoils, shown in Figure 24, are fairly similar and crisscross each other in the range $0.3 \leq C_{LB} \leq 0.7$. For the thinnest airfoil (to show the Mach number effect), the drag polar at M = 0.74 is also included (plotted using symbol

+). Only the thinnest two airfoils were tested at high Mach numbers of 0.8 and 0.81. The 10 % airfoil which at these Mach numbers is performing at or close to its design conditions gives significantly less drag than the 13 %, see Figure 25. The 13 % airfoil is almost into drag rise but still displays good drag features for $C_L$ between 0.2 and 0.5.

### 2.3.1.2 Transition Fixed Drag Polars at Re = $6.7 \times 10^6$

Transition fixed drag polars are given in Figures 26 to 29. In comparison, the data collected for the transition fixed cases is less detailed . The low Mach number and Reynolds number case shown in Figure 26 suggests that from the drag viewpoint there is very little to choose between the two airfoils. At these flow conditions the boundary layer displays similar characteristics irrespective of the thickness of the airfoil. At a higher Mach number of M = 0.6 in Figure 27 on the other hand, an increase in drag is noted with the thicker airfoils.

Figures 28 and 29 show the transition fixed drag polars at Mach numbers $0.68 \leq M \leq 0.8$. Since this Mach number range includes the design Mach number of all the airfoils , the minimum drag levels here are considerably higher than their counterparts in transition free polars. In other words, the generous extent of natural laminar flow available is lost once the transition is fixed giving rise to the resulting wake drag levels. For example the 13 % airfoil here in Figure 29 at M = 0.76 gives a minimum drag level of 0.0102 compared to a minimum

drag level of only about 0.0045 under natural laminar flow conditions in Figure 24. It should be stressed however that the 'turbulent flow' drag levels are still competitive with airfoils specifically designed for early transition.

### 2.3.1.3 Transition Free Drag Polars at Re = 12.5 X $10^6$

Figures 30 to 34 show transition free polars at a higher Reynolds number of Re = 12.5 X $10^6$ in the Mach number range 0.5 to 0.8. Since at this high Reynolds number the airfoils do not support as much laminar flow as they did at the lower chord Reynolds number case of 6.7 X $10^6$ , the airfoils have comparatively higher drag particularly in cases close to their design Mach numbers. Consider for example the 10 % airfoil in Figure 34, which shows drag values of about 0.0064 to 0.0080 for $C_{LB} \leq 0.6$. This drag level was as low as 0.0048 - 0.0060 for the same $C_{LB}$ limits at a lower chord Reynolds number of 6.7 X $10^6$ in Figure 25.

### 2.3.1.4 Transition Fixed Drag Polars at Re = 12.5 X $10^6$

Transition fixed studies were also done at chord Reynolds number of Re = 12.5 X $10^6$. The drag trends as observed in the drag polars for the Mach numbers M = 0.6 to 0.8, shown in Figures 35 to 38, in general remain the same as under transition free high Reynolds number polars in Figure 30 to 34. Only the actual drag levels are somewhat higher. Compare for instance the transition fixed results for the three thicker airfoils at M =

0.6 in Figure 35 to their transition free counterparts in Figure 31. It appears that even at Re/c = 12.5 X $10^6$ the airfoils carry some laminar flow which is lost when the transition is fixed giving the increment in drag as depicted by the preceding comparison. Compare also the drag polar for the 13 % airfoil under transition fixed conditions at M = 0.76 to its transition free counterpart in Figure 33. Some contribution to the increased drag under transition fixed conditions must come from the trip drag of the transition strip.

To show the Reynolds number effect on drag one may compare the transition fixed data at Reynolds number of Re/c = 12.5 X $10^6$ to its transition fixed counterpart at Re = 6.7 X $10^6$ . Drag polars for the 13 % and 21 % thick airfoils in Figures 27 and 35 can be used this comparison. Based on the fact that for similar boundary layers the local skin friction $C_f \propto 1/R_e(x)^{1/5}$ , one would expect lower drag values for the high Reynolds number case. This is certainly borne out by the comparison of the transition fixed data in Figures 27 and 35.

### 2.3.2 Drag versus Mach number

The drag polars of the four airfoils are also cross plotted in the form of wake drag $C_{DW}$ as a function of the Mach number M for a number of selected $C_{LB}$ cases. Both the transition free and transition fixed data at Reynolds numbers of 6.7 X $10^6$ and 12.5 X $10^6$ are plotted at $C_{LB}$ = 0.3, 0.5,0.6 and 0.7. The plots are presented in Figures 39 to 54.

Since airfoil drag has already been discussed at length in the previous section , only some interesting features of drag at Re/c = 6.7 X $10^6$ ( where a long extent of laminar flow was observed) will be highlighted here. Very often in the $C_{LB}$ v M type of plots for NLF supercritical airfoils we witness the drag 'bucket phenomenon', which as the name suggests represents a noticeable depression in the drag levels close to the design Mach numbers. Indeed it is at or close to these flow conditions where as much as 65 to 70% laminar flow (10% airfoil) has been observed Ref.7. Also see section 2.5.

For comparison of drag performances between airfoils and the extent of the bucket region for the case Re/c = 6.7 X $10^6$, consult table 1 and Figures 39 to 42.

## 2.4 Drag Comparison Against Other Airfoils

Drag, at design conditions at the lower Reynolds numbers, obtained from the current set of NLF airfoils as seen in Figure 55 is considerably less than all the 2 D airfoils tested in this facility to date. Hoerner's turbulent shock free drag curve also provided in Figure 55 represents a minimum envelope for all of the other airfoils shown. It must be realized that some of the airfoils included in this comparison used fixed transition strips and thus lost the benefit of NLF, whereas others did make use of NLF and still produced drag levels comparable with those of fixed transition. This could

have been due to unfavorable pressure gradients ( as in the 'peaky' type airfoils ) or tunnel turbulence levels at the time of testing. Recent improvements Ref. 11 to the NAE 5 ft X 5 ft wind tunnel might have cleaned up some of this turbulence. The turbulence levels averaged to about 0.16% at the conditions where the current airfoil tests were conducted.

Inspection of Figure 55 shows that minimum drag levels given by our four airfoils are indeed well below Hoerner's curve, especially at $Re/c = 6.7 \times 10^6$ where the drag levels for the four airfoils range between 0.0057 and 0.0064.

To compare with still other data we consider the NACA 66 series, which is a family of low drag airfoils. It must however be noted that the NACA 66 series airfoils are earlier designs and are most suited for low speed and low lift applications. A comparison between the aerodynamic performance of the present NAE airfoils and NACA 66 series airfoils is shown in table 2. Instead of further cluttering up Figure 55, a minimum drag $C_{DW\ (min)}$ comparison along with other important aerodynamic parameters such as $C_{L\ (max)}$ and $\partial C_L/\partial\alpha$ (at design M ), between NAE airfoils and the airfoils selected from NACA 66 series is carried out in table 2.

## 2.5 FLOW VISUALIZATION

Some flow visualization data were also recorded to

substantiate the extent of the natural laminar flow. The flow visualization was obtained by spraying the airfoils with a thin film of oil containing a dye which fluoresced in ultraviolet light. The application required some care as a film that was too thick could cause premature transition which would alter the airfoil characteristics markedly at low Reynolds numbers.

Figure 56 shows the flow visualization record of the 16% thick airfoil at Re/c = 6.7 X$10^6$, M = 0.75 and $C_L$ = 0.6 which correspond to the conditions where drag bucket was experienced from the wake drag data (see Fig 41) . Various regions of the flow are described on the figure. It appears that at Re/c = 6.7 X$10^6$ laminar flow extends up to 70 % chord which coincides with the shock location. The disturbances due to the pressure taps caused a transition wedge of sufficient spanwise extent to influence the centerline probe of the wake traverse apparatus. Although the models were cleaned very thoroughly between runs, the flow visualization record showed a few isolated transition wedges due to minute particles from tunnel contamination during the run.

Figure 57 shows a flow visualization record for the 13% thick airfoil close to the conditions where minimum bucket drag was measured for this airfoil , see Fig 41. The test conditions corresponded to M = 0.78, Re/c = 6.7 X $10^6$ and $\alpha$ = 0.33. The two black strips on the airfoil were the tapes used to cover the pressure taps on the airfoil. The laminar flow in the wider clean spanwise portion of the airfoil runs well up to ≈65% of

the chord length. The transition wedge emanating from the corner of the tape is fairly noticeable up to this station ($x/c \approx 0.65$) where it gets muddled into the overall turbulent flow. Note the presence of two distinct specks of dirt in the segment between the two strips giving rise to earlier transition wedges.

For the 10% thick airfoil, the flow visualization record is shown in Fig 58, at conditions $M = 0.8$, $Re/c = 6.7 \times 10^6$ and $\alpha = 1.39$, which again correspond to the bucket conditions in Fig 41. A laminar flow length of well up to 60% is measured in this case. Note the presence of the transition wedge on the right hand side caused by a dirt particle.

## 2.6 PRESSURE DISTRIBUTIONS

Figures 59a and 59b respectively compare the transition fixed and free pressure distributions on the four airfoils at design conditions, i.e. $C_L \approx 0.6$, the Reynolds number of $Re/c = 12.5 \times 10^6$ and their respective design Mach numbers. To obtain long lengths of laminar flow one would expect the favorable or flat roof top pressures to drive the shock as far downstream as possible. This is best represented by the pressure distributions on the upper surface of the 10 and 13 % airfoils. The 10 % airfoil was able to delay shock until 66% of the chord under both free and fixed transition conditions. For the 13 % airfoil the shock location was about 50 % under the design transition fixed conditions and about 45 % under off design transition free conditions. The 21 and the 16 % produced favorable pressure

distributions only up to about 20 % of the chord followed by a gentle adverse pressure gradient (the gradient is more noticeable for the 16 % airfoil) under transition fixed conditions. Under transition free conditions the 21 % airfoil seems to show a flatter and longer roof top pressure distribution when compared to its transition fixed counterpart. Note also a more pronounced pressure recovery after shock for the 21% airfoil under transition free conditions.

The pressure levels also tend to be a little higher under fixed transition conditions giving rise to a stronger shock than the smearing of the pressure levels for the free transition case producing weaker shock.

The bottom surface shows favorable pressure gradient for all airfoils up to a distance of about 45 to 50 % of the chord for both cases considered above.

To provide another comparison, Figure 60 shows the free transition data at Re/c = 6.7 X $10^6$, with the $C_L$ and Mach number again corresponding to the design conditions of the airfoils. The 10 % airfoil still continues to show a remarkably flat roof top pressure distribution on the top surface, stretching up to about 65 % of the chord length even at this off design transition free condition. The 13 % and 21% airfoils too maintain a steady flat pressure distribution up to about 45 % of the chord length indicating the presence of substantial lengths of laminar flow. The 16 % airfoil, however shows a noticeable

adverse pressure gradient past the 20% chord length signaling the onset of relatively earlier transition. The bottom surfaces have once again maintained favorable pressure gradients up to 45 to 50 % of the chord lengths.

Notice the presence of a small 'kink' in the 16 % pressure data at about 3 % of the chord length on all three figures which was very likely caused by the presence of a leaky pressure port.

## 3. COMPARISONS OF GRUMFOIL WITH THE EXPERIMENTAL DATA

In reference 6 some comparisons were made between our experimental data on the present airfoils and the computer codes BGK [12], GRUMFOIL [13-14] and DRELA [15]. The comparisons indicated that GRUMFOIL and DRELA were quite close to good agreement with GRUMFOIL being marginally better. Thus in the paper we will consider only this code and concentrate our attention on the 10% and 13% airfoils. We will also include studies on the free transition cases as well as the fixed transition cases given in Reference 6. It was found that in the free transition cases it was more difficult to obtain a solution - the code is more robust if transition is fixed and even here a good initial guess for the solution is usually needed. To this end NAE altered the GRUMFOIL input logic to accept successive inputs of M, $C_L$, Re, XTU and XTL. A solution procedure then starts with the previous final solution. For the first input line it is best to start with a low Mach number and lift, and transition far forward.

The GRUMFOIL code has 3 options for determining transition. These are based on Crabtree's correlation [16], Michel's [17] and that of Stevens, Gordia and Braden [18]. The latter two, for our test data, did not give convergent solutions so we were limited to using Crabtree's correlation. Using experimental data at Reynolds numbers up to 7 million based on 3 different airfoils and a flat plate, Crabtree was able to show that a reasonable curve through the mean data could be obtained by plotting, at transition, the boundary layer Reynolds number $U\theta/\nu$ against a pressure gradient parameter $U'\theta^2/\nu$. The GRUMFOIL code uses a similar curve to predict transition.

The comparison of theory with experiment must be done carefully as the wind tunnel Mach number cannot be defined with 100% accuracy. The top and bottom wall correction due to Mokry and Ohman [19] has been used at NAE for several years and is similar to corrections applied in other porous wall tunnels. At NAE we have always assumed that sidewall interference is negligible since sidewall suction is applied in the vicinity of the airfoil. However recent work by Lynch [20-21] indicates that there may be a correction due to sidewall boundary layer as applying the suction does not result in a perfectly parallel flow at the walls. Murthy has computed a correction due to sidewall boundary layer variation $\partial\delta^*/\partial x$ for the NAE facility. His work [22] is based on an assumption of 2-D growth of the boundary layer with no lateral variation. This assumption is questionable but it does lead to a correction of a right order of magnitude when applied to test data by Lynch [20-21] and

Jones et al [6]. However even these comparisons are questionable since a $C_p$ comparison cannot be made as the scaling used for $C_p$ is in error (see [6]). In the comparisons in the present report we will always use the ratio $p/p_o$ since these are wind tunnel measured quantities which are invariant with free stream conditions $M_\infty$ and $p_\infty$.

The difficulties in getting a good match are shown in Figure. 61. Here, transition is fixed at 7% and 15% on the upper and lower surfaces respectively. It can be seen that applying the full correction indicated by Murthy ($\Delta M \simeq -0.015$), in Fig. 61a, the upper surface distribution is well predicted but the lower surface pressures are too low. By increasing the computational Mach number such that $\Delta M = -0.008$ we see, from Fig. 61b, that the lower surface matches well but the upper surface is not well predicted.

An interesting feature shown in Fig. 61 are the 'ripples' in the upper surface pressure distribution. These are thought to be due to oblique waves emanating from the interference of the sidewall with the airfoil leading edge. These have been noticed by Boeing [23] who also have flow viz pictures showing this effect. To verify that it was not a 'poor model' effect in our case we ran a computation using design coordinates and measured coordinates. The results were almost identical indicating that the model was accurately made.

Until the sidewall effect is understood more clearly

(NAE may use a full 5' span model to minimize sidewall effects) we will use in this report the correction as evaluated according to formulae by Murthy [22] and shown in Fig. 62. Some typical surface pressure comparisons are shown in Fig. 63-65. The first set, Fig. 63, is for the 10% foil with transition fixed at 7% and 15% while the remaining set are for the 10% (free transition) and 13% (fixed). For one of the cases, Fig 64c, the convergence and boundary layer parameters are shown in Fig 66.

Note that for the free transition case on the 13% airfoil solutions are not available. Several attempts were made to run GRUMFOIL in a mode where transition was either determined using Crabtree's criterion or fixed at the specified input value- whichever came first (KT =1, XTANU > 0, XTRANL >0). Since convergence is difficult when transition is far back, the code was operated by moving the transition back in successive solutions. While this approach worked in some cases for the 10% airfoil, it failed in our attempts for the 13%. It seems that during the iterations the transition point moved backwards and forwards without stabilizing. It may be that a more gradual change from laminar to turbulent flow would help rather than having a sudden change.

Generally the trends shown by the predictions are quite good especially in the fixed transition cases. The free transition results are more difficult to obtain and the code will often not converge to a steady state. Thus it is not possible to do all the comparisons one would like in this case.

Even so in the cases that did converge most of the trends seem reasonable (e.g. transition moving downstream as the pressure gradient becomes more favorable) and the code shows a prediction of the 'drag bucket' even though the drag level is too high (Fig. 67). This drag data from GRUMFOIL was obtained using $R_c$ = 6.7 million with $C_L$ about 0.6 and increasing the Mach number in steps from 0.489 to 0.802 ($M_c$ from 0.5 to 0.82). The computed transition points and other data are given in Table 3. Also shown in Fig. 67 are the data for $R_c$ =11 million and 16.7 million. It can be seen here that the drag trend with Reynolds number is not correct since the lower Reynolds number data, with transition further aft, should be predicting lower drag. Note that the data is not complete for the higher Reynolds numbers as convergence problems are encountered at these conditions.

## 4.0 CONCLUSIONS

Four NLF airfoils having thicknesses of 0.1, 0.13, 0.16 and 0.21 have been investigated both theoretically and experimentally in the High Speed Aerodynamics Laboratory of NAE.

At or close to the design flow conditions as much as 70% natural laminar flow has been observed on some airfoils.

The minimum drag levels ($C_{DW}$) for the four airfoils range from a low of about 0.0045 to a high of about 0.0051.

A complete comparison of experimental results with GRUMFOIL

calculations was not possible due to non convergence of the code in a large number of transition free cases. The cases with fixed transition were less likely to fail. The available results for the 10% airfoil in free transition indicate a correct prediction of the drag bucket at a Mach number of about 0.8.

Having investigated the NLF concept in 2 D, there is a need to verify some of these results in 3 D by similarly investigating a generic reflection plane (preferably) or complete model in NAE's 5 ft High Reynolds number Trisonic Facility. Ultimately, we hope to apply this NLF concept to a real flight experiment which may involve gloving a portion of the wing of a Flight Research T33 trainer aircraft.

## 5. ACKNOWLEDGMENTS

The work reported in this paper was carried out under a collaborative program between DeHavilland Aircraft of Canada (presently, Boeing of Canada DeHavilland Division) and the National Aeronautical Establishment. The authors are grateful to B. Eggleston and and R.J.D. Poole for their cooperation.

## 6. REFERENCES

1. Elfstrom, G. M., 'Skin Friction Measurements on two Relatively Thick Airfoils at High Reynolds Numbers', NRC/NAE Aero Note NAE AN 23, Nov. 1984.

2. Van Driest, E.R. and Blumer, C.B., 'Boundary Layer Transition: Free stream Turbulence and Pressure Gradient Effects,' AIAA Journal, Vol. 1, June 1963, pp. 1303-1306.

3. Ohman, L.H., et al., Recent Improvements to the NAE 5 ft X 5 ft Blowdown Wind Tunnel NRC Report AN-31, 1985.

4. Sommers, D. M. 'Design and Experimental Results of a Natural Laminar Flow Airfoil for General Aviation Applications, 'NASA TP 1861, June 1985.

5. Ohman, L. H., 'The NAE High Reynolds Number 15 in X 15 in, Two-Dimensional Test Facility', NAE LTR-HA-4, April 1970.

6. Jones, D. J., Khalid, M. and Eggleston, B., 'Comparison of Theory and Experiment for four Supercritical, Low Drag Airfoils,' AGARD CP-437, Paper P8-1, May 1988.

7. Eggleston, B., Jones, D. J.,Poole, R.J.D. and Khalid, M., 'Thick Supercritical Airfoils with Low Drag and Natural Laminar Flow', Journal of Aircraft, Vol 24 , N0 6, June 1987.

8. Riegels, F. W,' Airfoil Sections', Results From Wind Tunnel Investigations, Theoretical Foundations, translated from the German by D.G. Randall. London, Butterworths 1961.

9. Liepmann, H. W. and Roshko, A., ' Elements of Gasdynamics', John Wiley and Sons, Inc. 1956.

10. Eggleston, B; Jones, D.J. and Elfstrom, G. M. ' Development of Modern Airfoil Sections for High Subsonic Cruise Speeds', Atlantic Aeronautical Conference , March 1979.

11. Ohman, L. H., 'The NAE 15" X 60" Two- Dimensional Test Facility; New Features and Some Related Observations, Results of New Centre Line Calibration at 20.5% Porosity'. NRC Report LTR-HA-15, 1973.

12. Bauer, F.,Garbedian, P. R. and Korn D.,'Supercritical Wing Sections III', Lecture Notes in Economics and Mathematical Systems. No. 150, 1977.

13. Melnik,R.E,., Chow,R.R., Mead, H.R. and Jameson,A.,'An improved Viscid/Inviscid Interaction Procedure for Transonic Flow over Airfoils', NASA CR-3805, October 1985.

14. Mead, H. R. and Melnick, R. E. GRUMFOIL: 'A Computer Code for the Viscous Transonic Flow over Airfoils', NASA CR-3806, October 1985.

15. Drela, M., 'Two-Dimensional Transonic Aerodynamic design and Analysis Using the Euler Equations', Ph. D Thesis, MIT, 1985.

16. Crabtree, L. F. 'Prediction of Transition in the Boundary Layer on an Airfoil', J. Royal ,Aeron. Soc.,vol. 62, July 1958.

17. Michel, R., 'Determination of Transition Point and

Calculation of Drag of Wing Sections in Incompressible Flow' Publication No. 58, ONERA, 1952.

18. Stevens, W., Gordia, S., and Braden, J., 'Mathematical Model for Two-Dimensional Multi-Component Airfoils in Viscous Flow', NASA CR 1843, 1971.

19. Mokry, M. and Ohman, L. H., 'Application of the Fast Fourier Transform to Two-Dimensional Wind Tunnel Wall Interference', Journal of Aircraft, vol,17. june 1980.

20. Lynch, F. T., Bui, M. H. and Patel, D. R., 'Some Fundamental Concepts in the Design, Analysis and Testing of Transonic Airfoils', Douglas Co. Paper 7579, October 1985.

21. Lynch, F. T. and Johnson, C., B., 'Wind tunnel Sidewall Boundary Layer Effects in Transonic Airfoil testing- Some Correctable but Some Not', Paper No. 18, AGARD Symposium on Aerodynamic Data Accuracy and Quality. September 1987.

22. Murthy, M., 'Corrections for Attached Sidewall Boundary Layer Effects in Two-Dimensional Airfoil Testing', NASA CR 3873, 1985.

23. Private Communication from Mark Anderson, Boeing Commercial Airplane Co., Feb. 1989 .

## TABLE 1: SOME INTERESTING DRAG FEATURES OF THE FOUR NLF AIRFOILS AT Re = 6.7 x $10^6$ $ft^{-1}$ (TRANSITION FREE)

| AIRFOILS | | | | |
|---|---|---|---|---|
| CONDITIONS | $C_{LB}$ = 0.3 | $C_{LB}$ = 0.5 | $C_{LB}$ = 0.6 | $C_{LB}$ = 0.7 |
| **NAE 68-060-21:1** | | | | |
| Bucket region | 0.66 ≤ M ≤ 0.712 | 0.66 ≤ M ≤ 0.712 | 0.66 ≤ M ≤ 0.71 | 0.64 ≤ M ≤ 0.71 |
| $C_{DW\ (min)}$ = 0.0051 | $C_L$ = 0.497 at M = 0.68 and Re = 6.7 X $10^6$ $ft^{-1}$ | | | |
| $M_{DR}$ based $\partial C_D/\partial M$=0.1 | 0.703 | 0.700 | 0.712 | 0.689 |
| $C_{DW}$ (bucket min) | 0.0057 | 0.0058 | 0.0064 | 0.0072 |
| **NAE 72-060-16:1** | | | | |
| Bucket region | 0.7 ≤ M ≤ 0.77 | 0.70 ≤ M ≤ 0.76 | 0.70 ≤ M ≤ 0.76 | 0.72 ≤ M ≤ 0.76 |
| $C_{DW\ (min)}$ = 0.0051 | $C_L$ = 0.464 at M = 0.75 and Re = 6.7 X $10^6$ $ft^{-1}$ | | | |
| $M_{DR}$ based $\partial C_D/\partial M$=0.1 | 0.764 | 0.752 | 0.748 | 0.758 |
| $C_{DW}$ (bucket min) | 0.0057 | 0.0051 | 0.0056 | 0.0070 |
| **NAE 76-060-13:1** | | | | |
| Bucket region | 0.72 ≤ M ≤ 0.80 | 0.74 ≤ M ≤ 0.80 | 0.72 ≤ M ≤ 0.79 | 0.72 ≤ M ≤ 0.80 |
| $C_{DW\ (min)}$ = 0.0045 | $C_L$ = 0.300 at M = 0.76 and Re = 6.7 X $10^6$ $ft^{-1}$ | | | |
| $M_{DR}$ based $\partial C_D/\partial M$=0.1 | 0.772 | 0.779 | 0.78 | 0.783 |
| $C_{DW}$ (bucket min) | 0.0045 | 0.0051 | 0.0056 | 0.0078 |
| **NAE 80-060-10:1** | | | | |
| Bucket region | 0.74 ≤ M ≤ 0.82 | 0.74 ≤ M ≤ 0.82 | 0.74 ≤ M ≤ 0.82 | 0.74 ≤ M ≤ 0.81 |
| $C_{DW\ (min)}$ = 0.0045 | $C_L$ = 0.540 at M = 0.81 and Re = 6.7 X $10^6$ $ft^{-1}$ | | | |
| $M_{DR}$ based $\partial C_D/\partial M$=0.1 | 0.812 | 0.811 | 0.819 | 0.800 |
| $C_{DW}$ (bucket min) | 0.0052 | 0.0048 | 0.0058 | 0.0080 |

Individual drag rise Mach number $M_{DR}$ for each case is appropriately identified on the $C_{DW}$ V M plots.

## TABLE 2: COMPARISON WITH THE NACA 66 SERIES

| AIRFOILS | t/c | $C_L$(des) | $C_L$ (max) | $\partial C_L/\partial\alpha$ at M (des) | $C_D$ (min) |
|---|---|---|---|---|---|
| NAE 68-060-21:1 | 0.21 | 0.60 | 1.6800 | 0.176 | 0.0051 |
| NACA $66_4$ -221 | 0.21 | --- | 1.4900 | 0.111 | 0.0042 |
| NAE 72-060-16:1 | 0.16 | 0.60 | 1.6400 | 0.198 | 0.0051 |
| NACA $66_2$ -215 | 0.15 | 0.25 | 1.4500 | 0.106 | 0.0035 |
| NAE 76-060-13:1 | 0.13 | 0.60 | 1.6200 | 0.196 | 0.0045 |
| NACA $66_1$ -212 | 0.12 | 0.15 | 1.4500 | 0.106 | 0.0035 |
| NAE 80-060-10:1 | 0.10 | 0.60 | 1.1900 | 0.240 | 0.0045 |
| NACA 66 -210 | 0.10 | 0.15 | 1.2800 | 0.110 | 0.0033 |

**TABLE 3: GRUMFOIL AND EXPERIMENTAL RESULTS FOR THE 10% AIRFOIL: TRANSITION POINTS AND DRAG VALUES.**

**$R_c = 6.7 \times 10^6$, $C_L \approx 0.6$**

| $M_c$ | $C_{D_W}$ | $C_{D_B}$ | $C_{DF}$ | $C_{D_\infty}$ | $C_{D_{wave}}$ | $X_{T_u}$ | $X_{T_L}$ (%) |
|---|---|---|---|---|---|---|---|
| 0.5 | 0.0075 | 0.0076 | 0.0051 | 0.0071 | 0.0005 | 11 | 55 |
| 0.7 | 0.0074 | 0.0087 | 0.0055 | 0.0081 | 0.0006 | 6 | 54 |
| 0.74 | 0.0077 | 0.0084 | 0.0051 | 0.0078 | 0.0006 | 12 | 54 |
| 0.76 | 0.0067 | 0.0081 | 0.0049 | 0.0072 | 0.0009 | 21 | 54 |
| 0.78 | 0.0070 | 0.0078 | 0.0046 | 0.0066 | 0.0012 | 36 | 54 |
| 0.79 | 0.0060 | 0.0078 | 0.0044 | 0.0064 | 0.0014 | 42 | 54 |
| 0.8 | 0.0060 | 0.0077 | 0.0042 | 0.0061 | 0.0016 | 48 | 52 |
| 0.81 | 0.0057 | 0.0067 | 0.0034 | 0.0058 | 0.0009 | 70 | 52 |
| 0.82 | 0.0100 | 0.0114 | 0.0036 | 0.0055 | 0.0059 | 70 | 50 |

NOTATION

$C_{D_W}$ EXPERIMENTAL WAKE DRAG

GRUMFOIL:

$C_{D_B}$ TOTAL DRAG INCLUDING BASE DRAG

$C_{DF}$ SKIN FRICTION

$C_{D_\alpha}$ BASED ON MOMENTUM THICKNESS FOR DOWNSTREAM

$C_{D_{wave}}$ DRAG DUE TO THE SHOCK WAVE

$X_T$ TRANSITION POINTS ON THE UPPER AND LOWER SURFACES

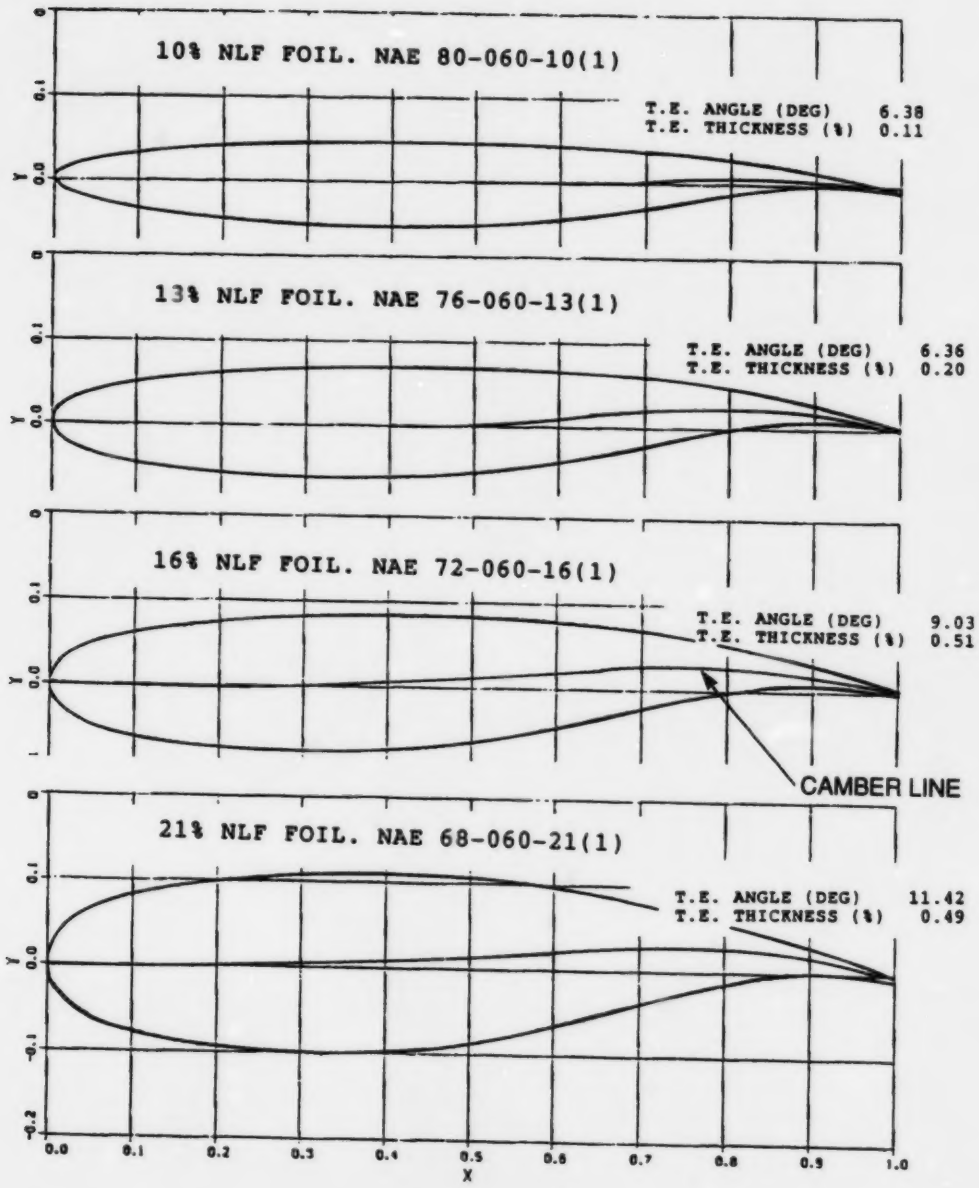


**FIG. 1: THE FOUR AIRFOILS TESTED IN THE NAE FACILITY**

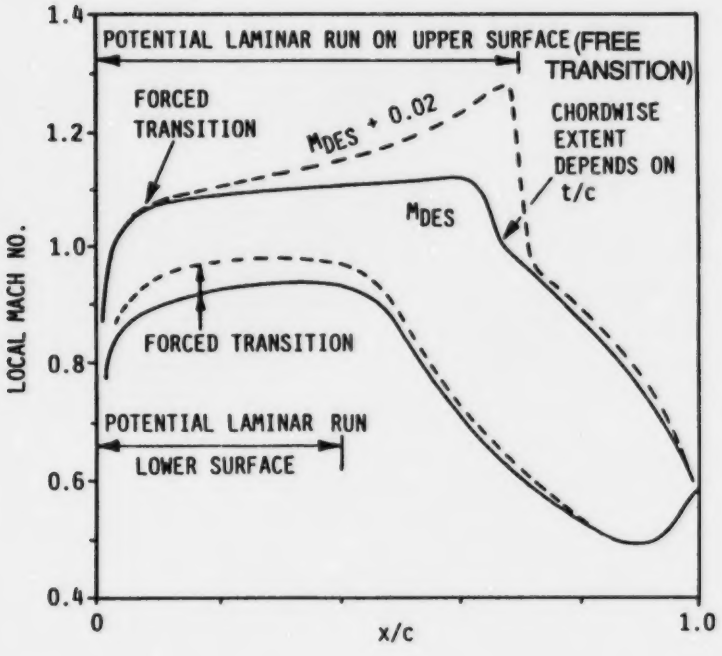


**FIG. 2: FEATURES OF DESIGN VELOCITIES**

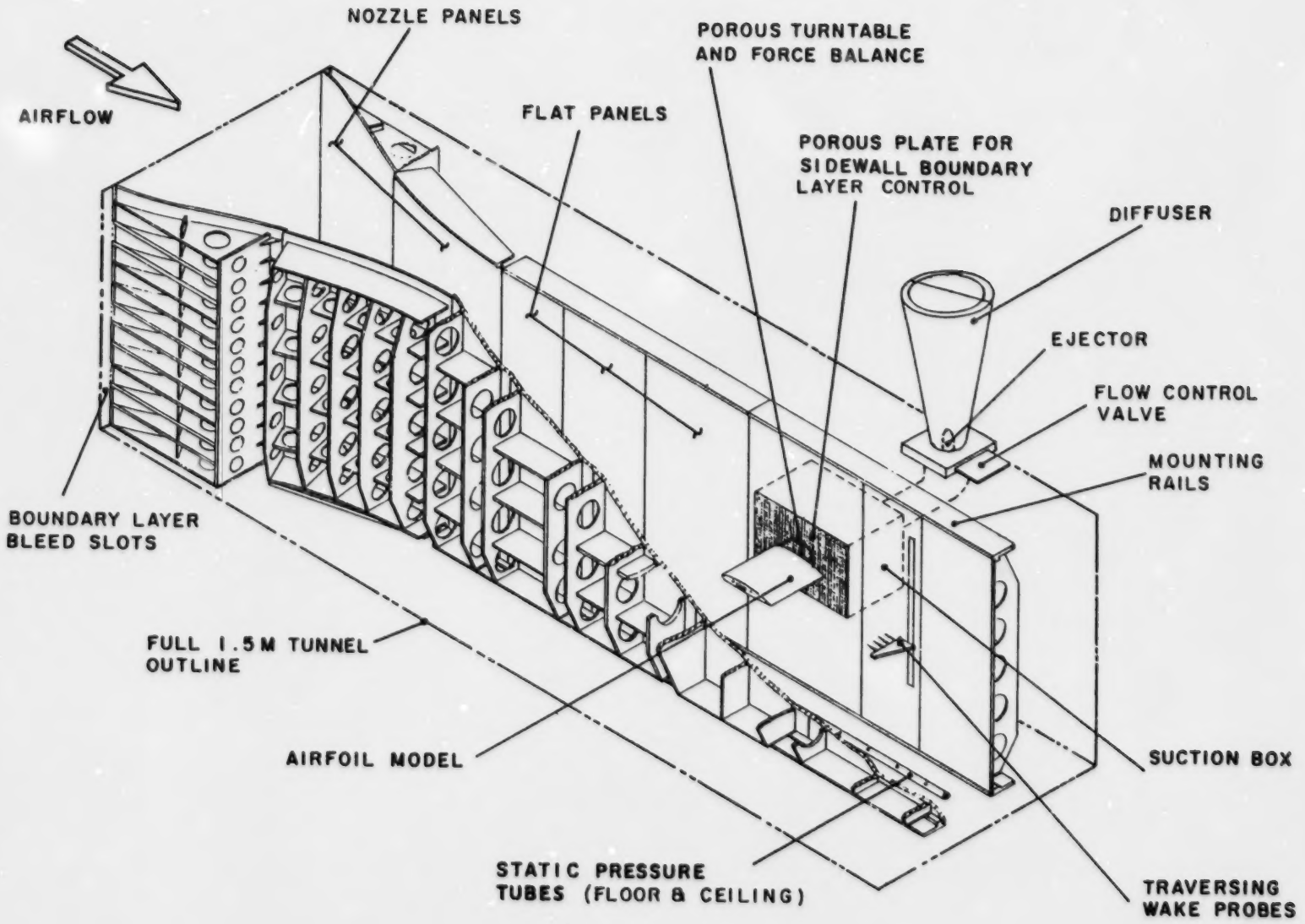


**FIG. 3: NAE 2-DIMENSIONAL TEST SECTION**

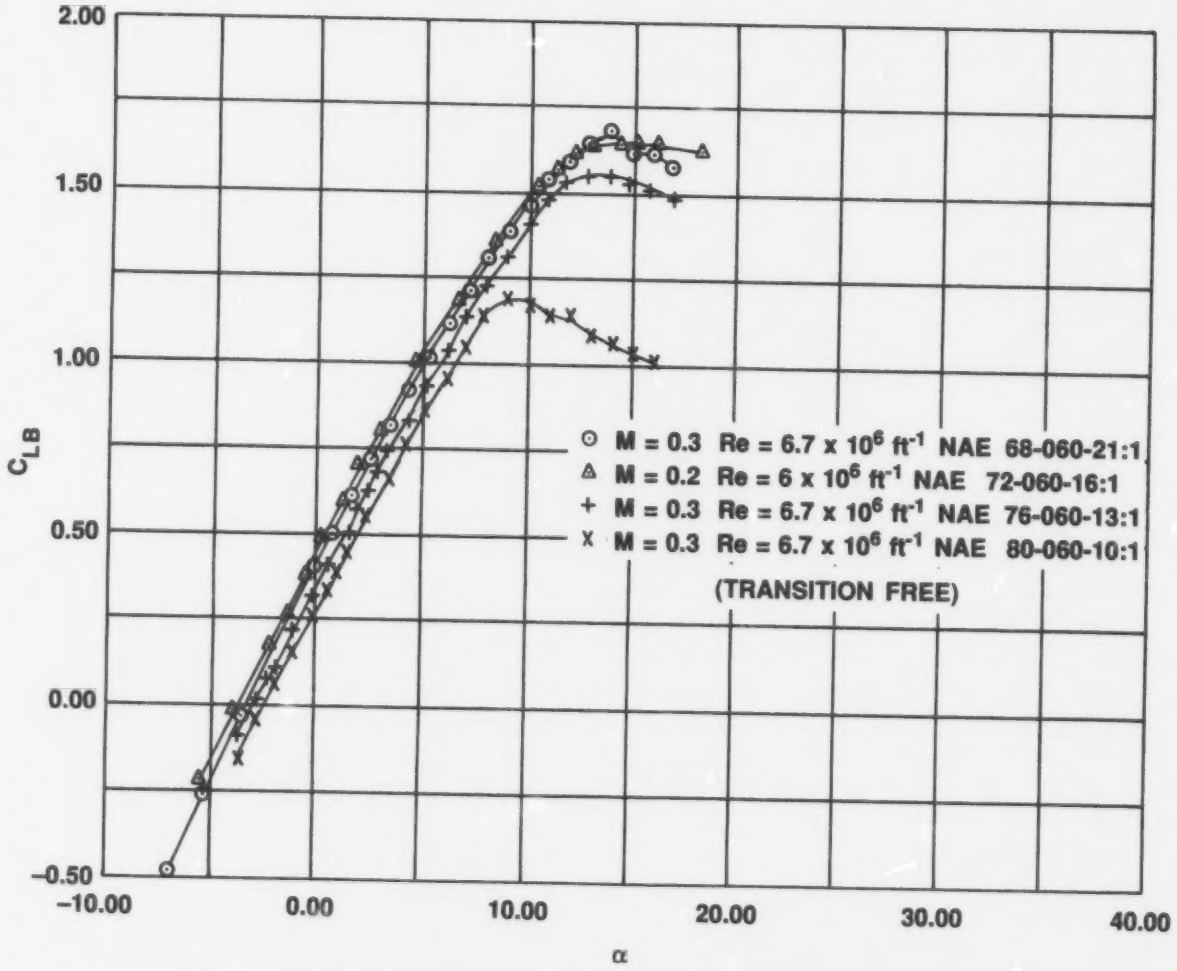


**FIG. 4: COEFFICIENT OF LIFT VERSUS ANGLE OF ATTACK**
**$C_{LB}$ VERSUS α**

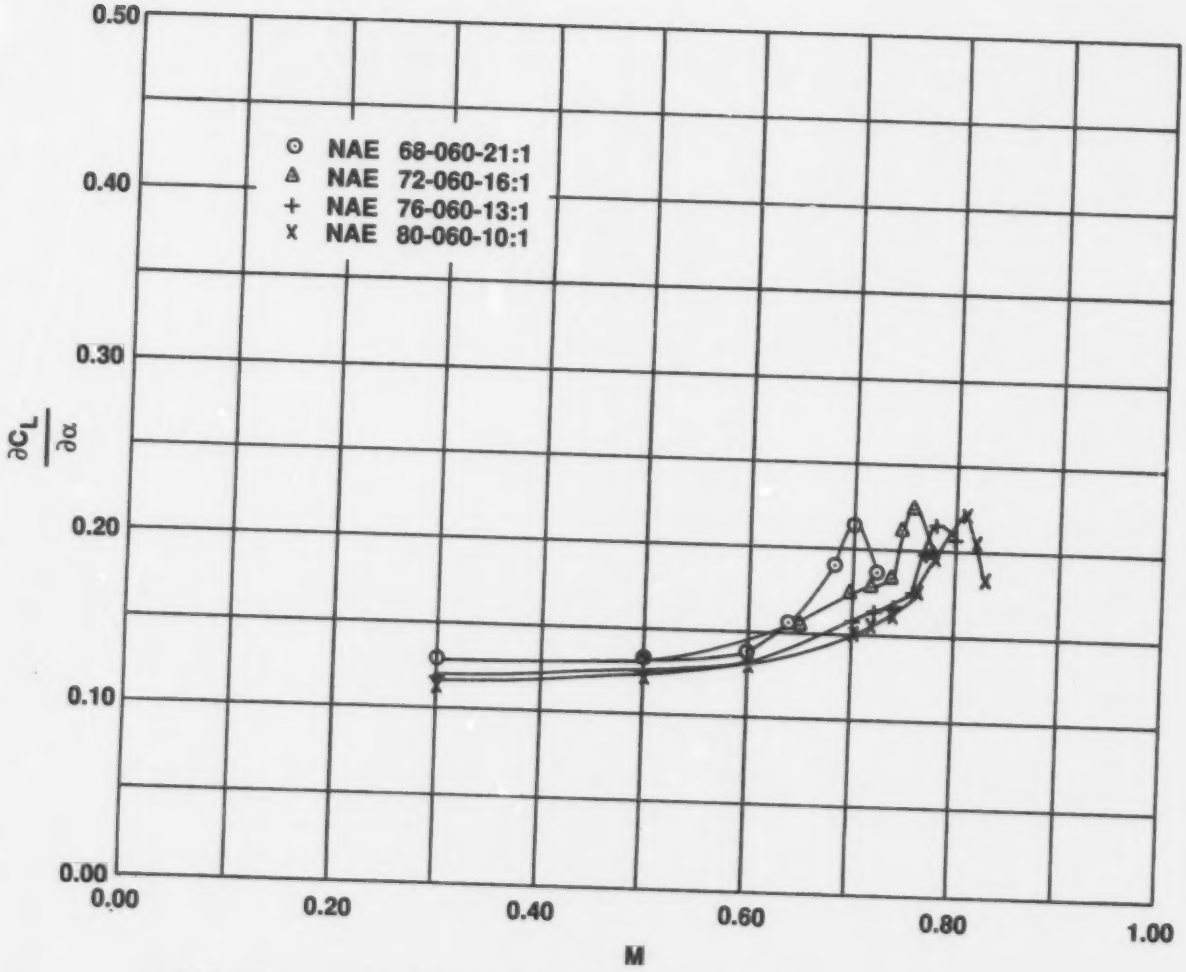


FIG. 5: LIFT CURVE SLOPE VERSUS MACH NUMBER $\frac{\partial C_L}{\partial \alpha}$ VERSUS M, Re = 6.7 x $10^6$ (FREE TRANSITION)

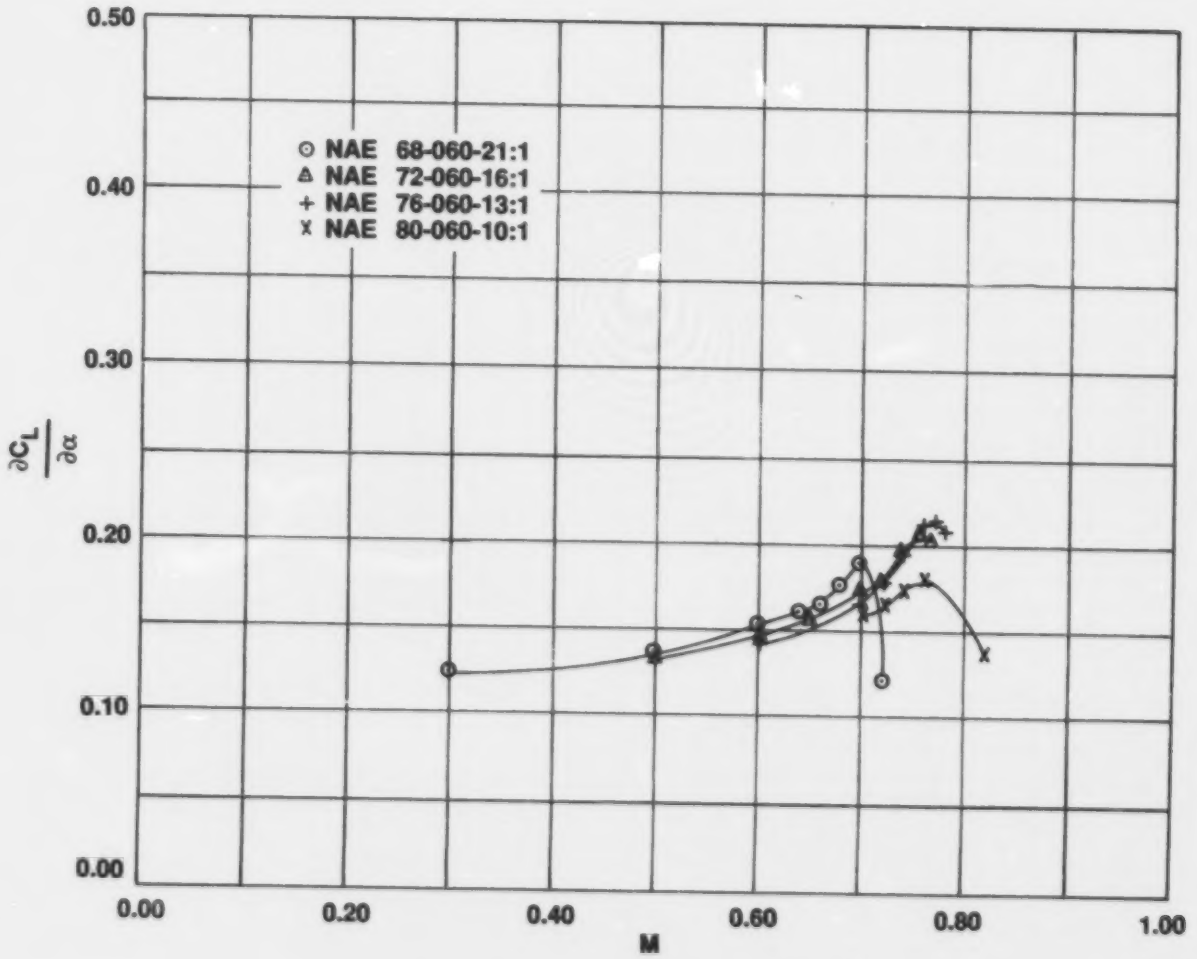


FIG. 6: LIFT CURVE SLOPE VERSUS MACH NUMBER $\frac{\partial C_L}{\partial \alpha}$ VERSUS M, Re = 12.5 x $10^6$ (FREE TRANSITION)

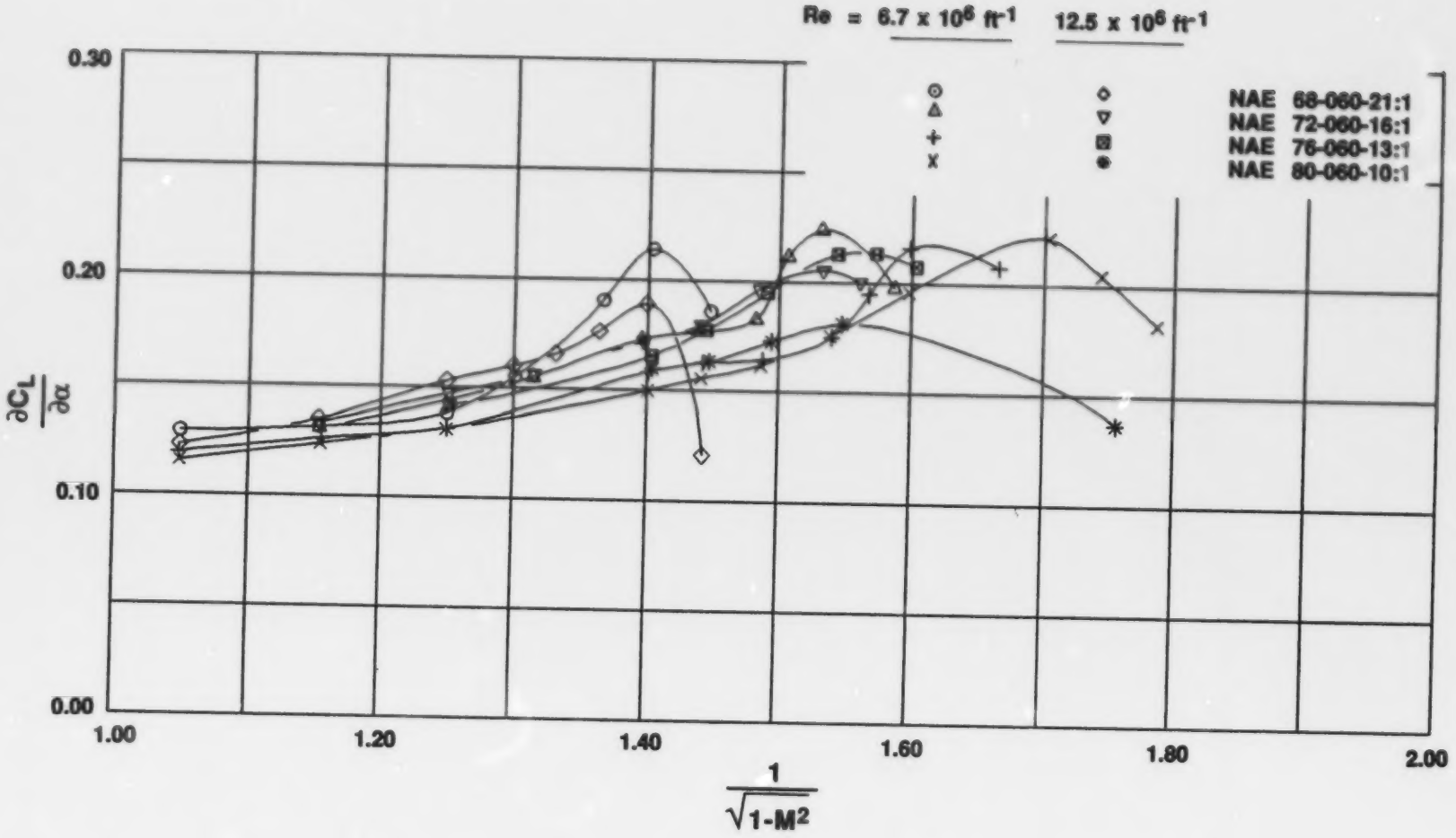


FIG. 7: LINEAR COMPRESSIBILITY $\frac{\partial C_L}{\partial \alpha}$ VERSUS $\frac{1}{\sqrt{1-M^2}}$ (FREE TRANSITION)

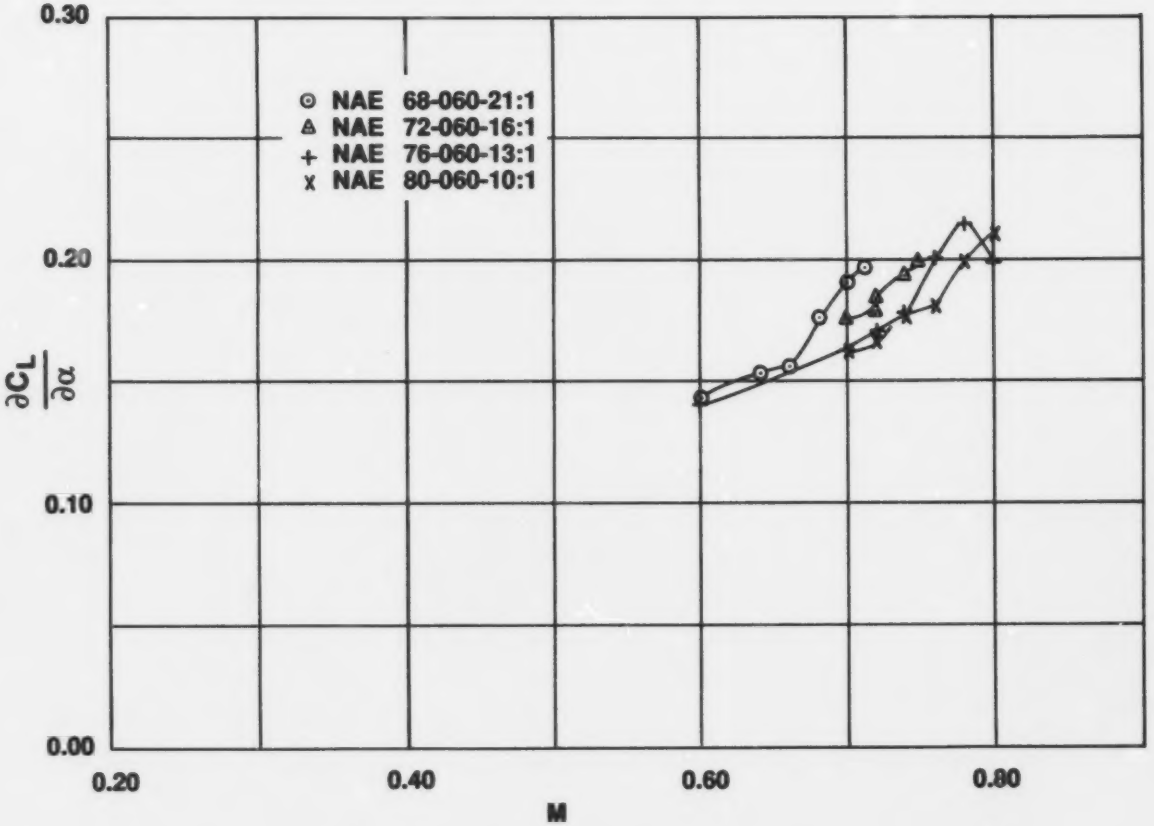


**FIG. 8: LIFT CURVE SLOPE VERSUS MACH NUMBER $\frac{\partial C_L}{\partial \alpha}$ VERSUS M, Re = 6.7 x $10^6$ (TRANSITION FIXED)**

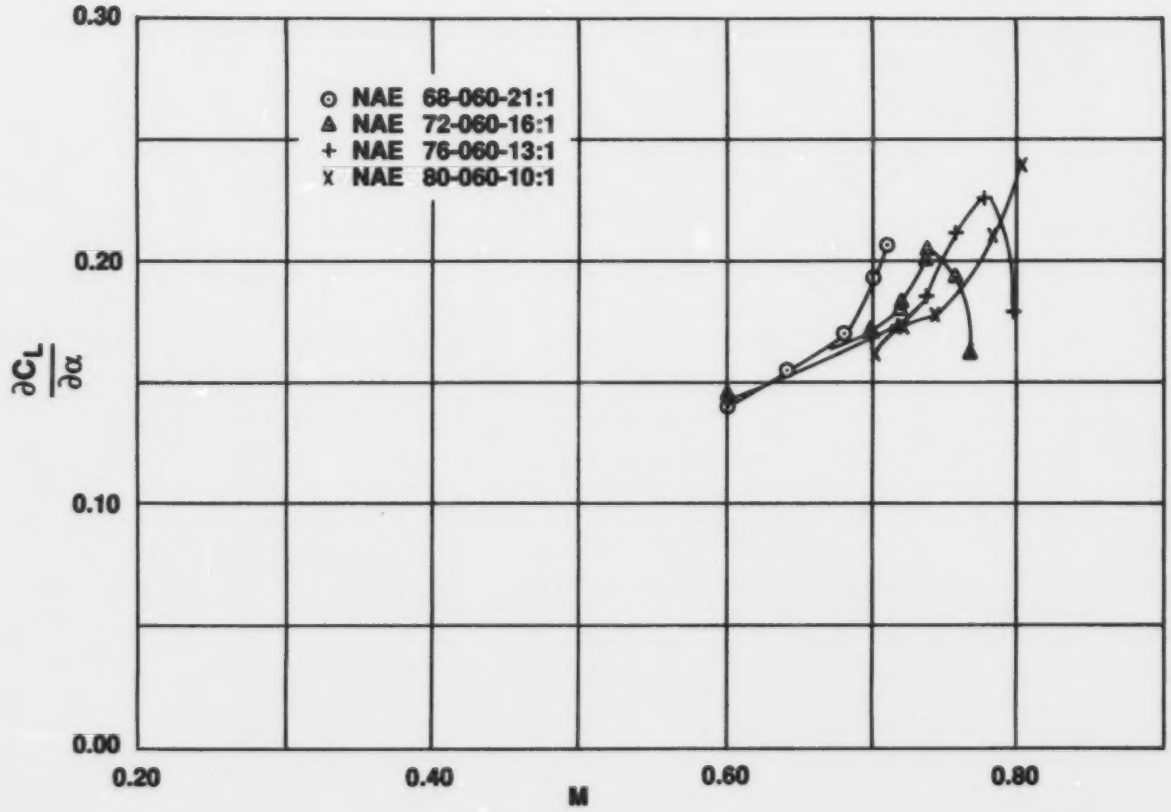


**FIG. 9: LIFT CURVE SLOPE VERSUS MACH NUMBER $\frac{\partial C_L}{\partial \alpha}$ VERSUS M, Re = 12.5 x $10^6$ (TRANSITION FIXED)**

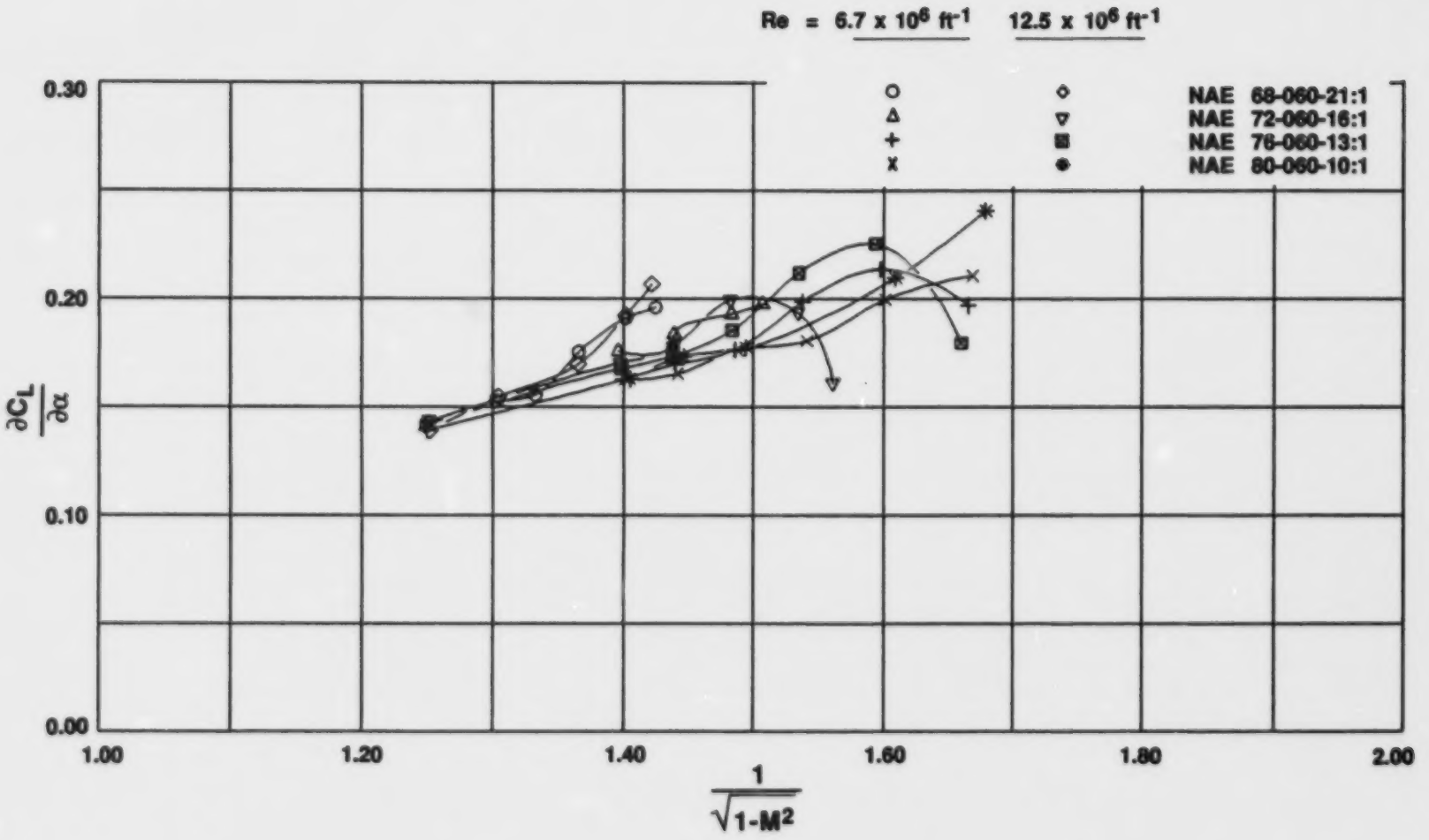


FIG. 10: LINEAR COMPRESSIBILITY $\frac{\partial C_L}{\partial \alpha}$ VERSUS $\frac{1}{\sqrt{1-M^2}}$ (TRANSITION FIXED)

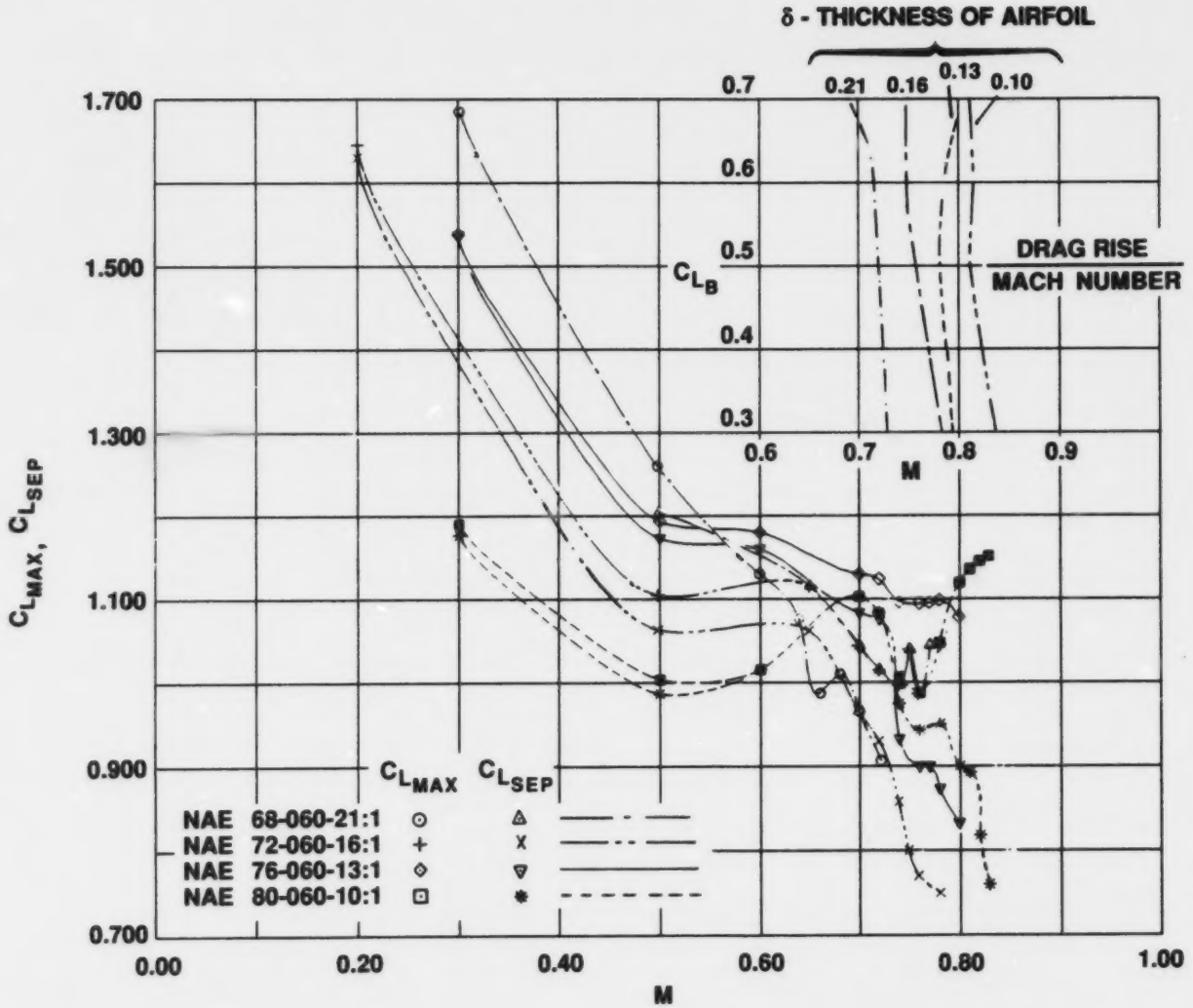


**FIG. 11: MAXIMUM LIFT AND LIFT AT SEPARATION VERSUS MACH NUMBER $C_{L_{MAX}}$, $C_{L_{SEP}}$ VERSUS M, Re = 6.7 x $10^6$ (FREE TRANSITION)**

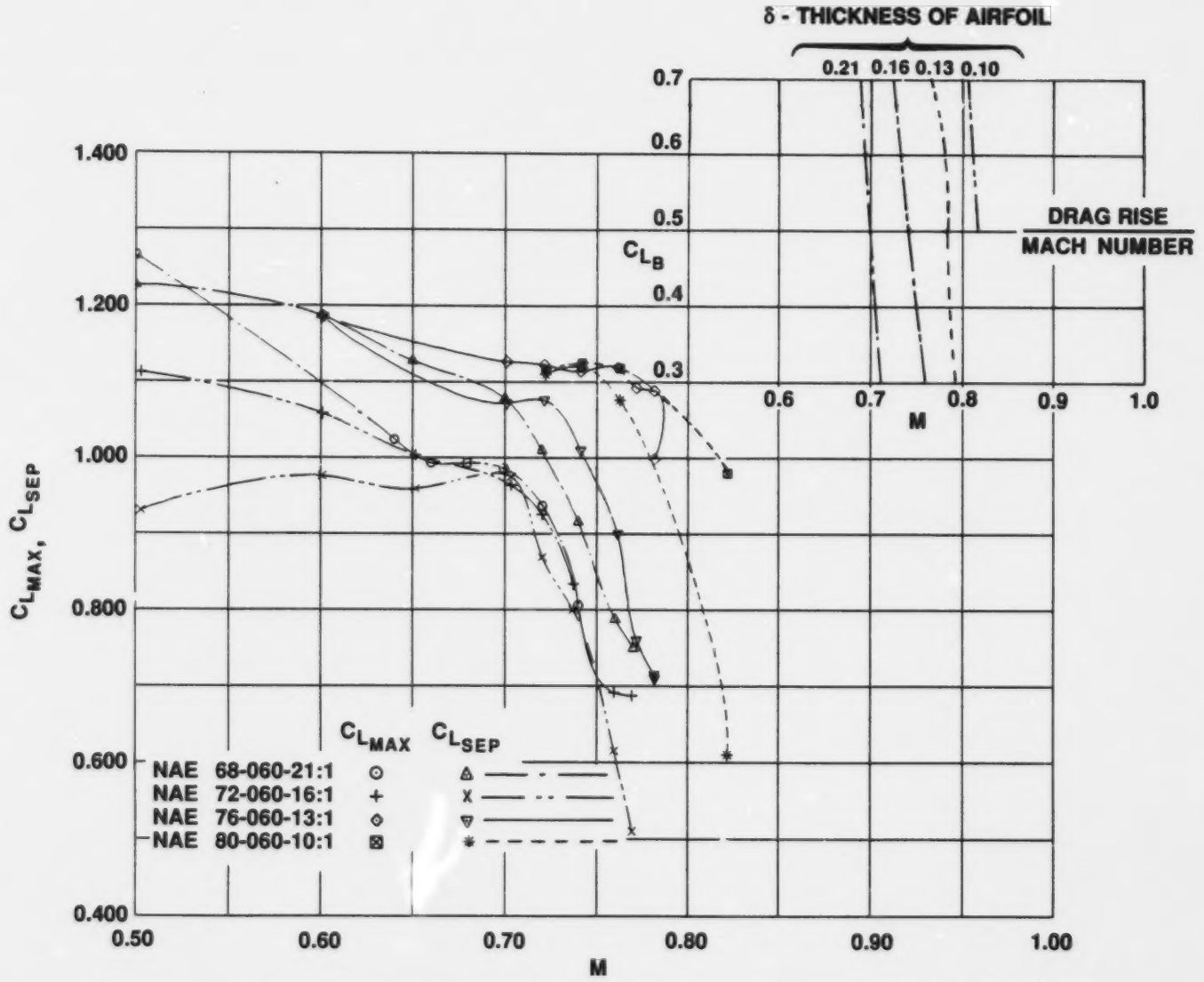


**FIG. 12: MAXIMUM LIFT AND LIFT AT SEPARATION VERSUS MACH NUMBER $C_{L_{MAX}}$, $C_{L_{SEP}}$ VERSUS M, Re = 12.5 x $10^6$ (FREE TRANSITION)**

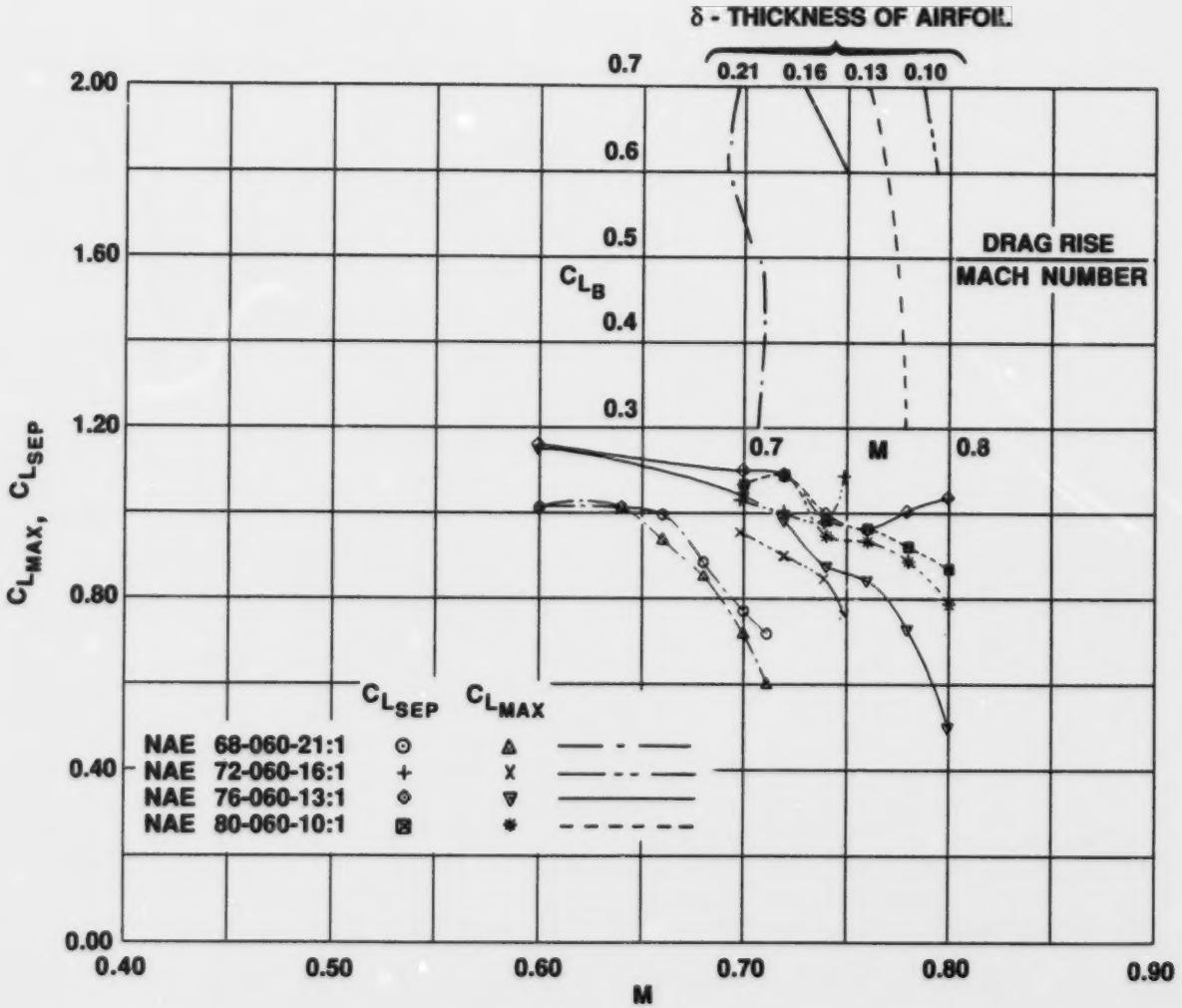


**FIG. 13: MAXIMUM LIFT AND LIFT AT SEPARATION VERSUS MACH NUMBER $C_{L_{MAX}}$, $C_{L_{SEP}}$ VERSUS M, Re = 6.7 x $10^6$ (TRANSITION FIXED)**

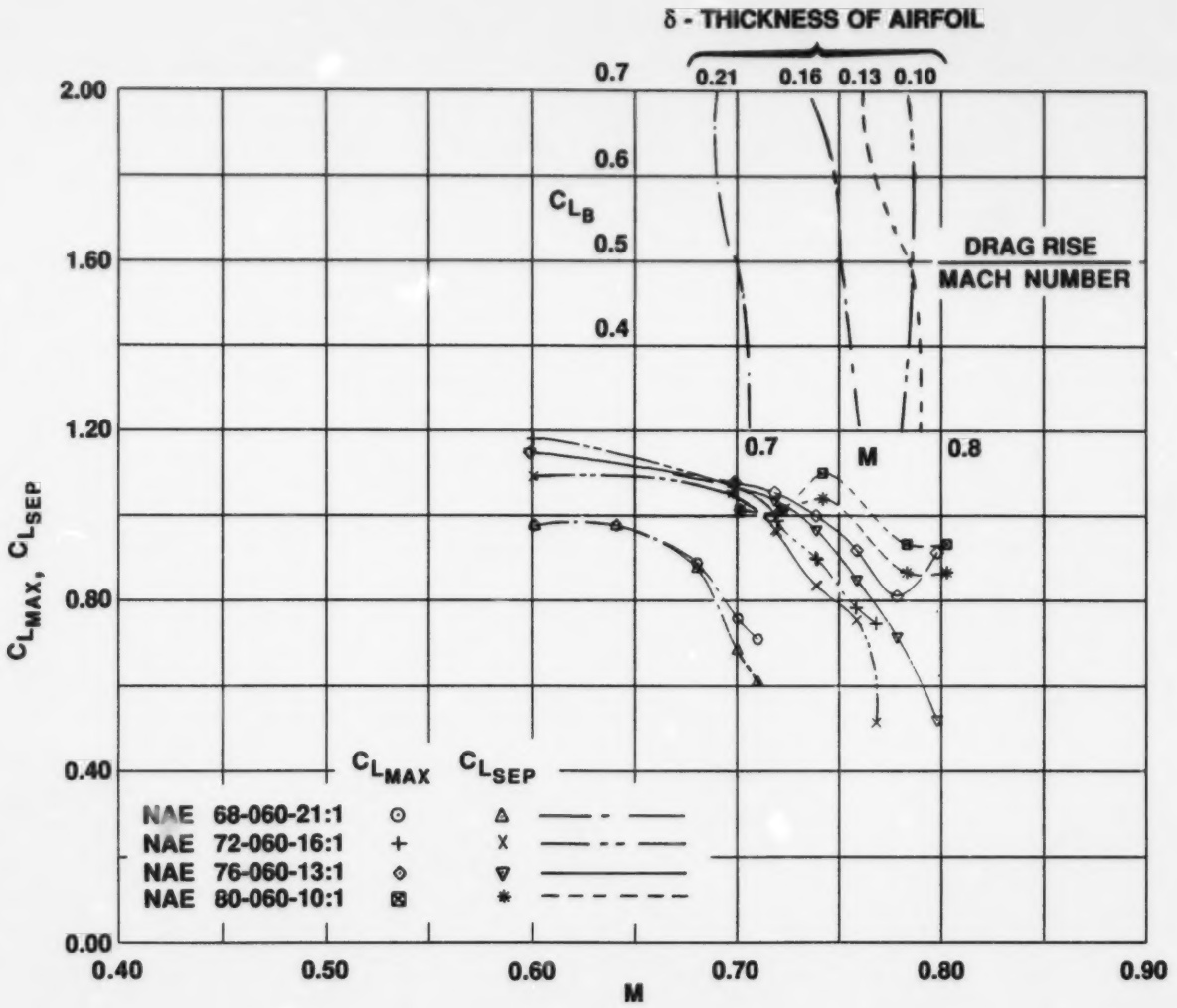


**FIG. 14: MAXIMUM LIFT AND LIFT AT SEPARATION VERSUS MACH NUMBER $C_{L_{MAX}}$, $C_{L_{SEP}}$ VERSUS M, Re = 12.5 x $10^6$ (TRANSITION FIXED)**

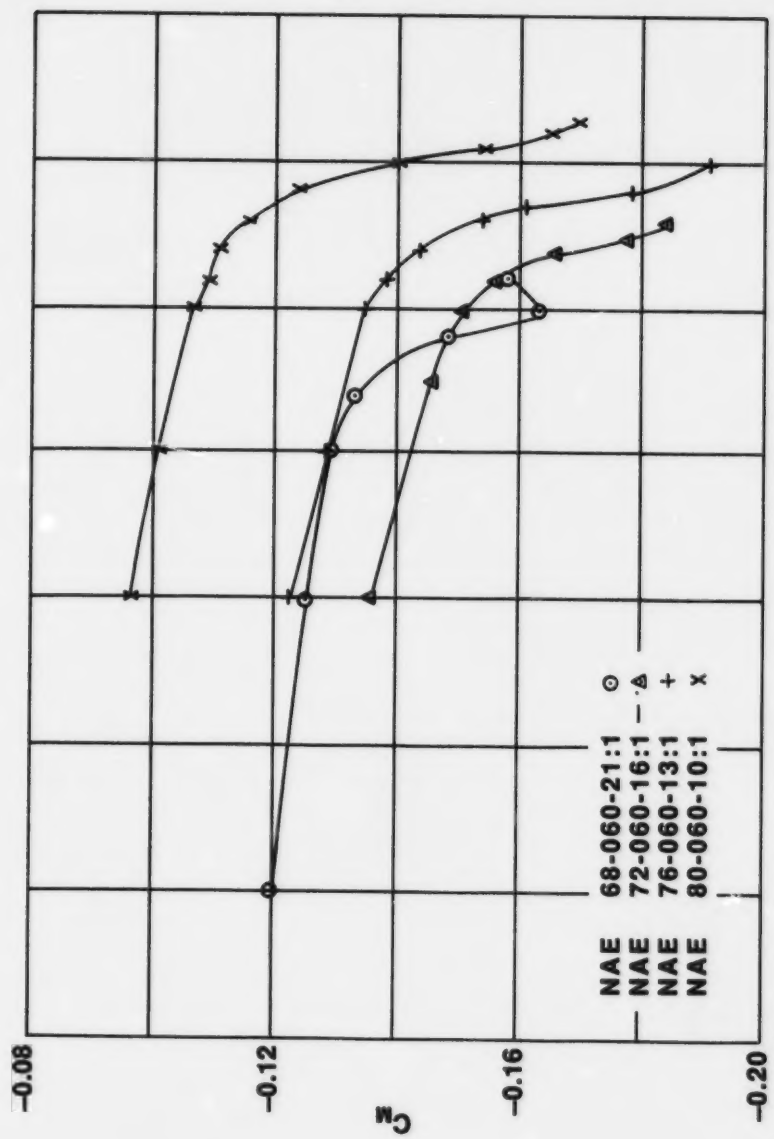


FIG. 15: PITCHING MOMENT $C_M$ VERSUS MACH NUMBER M,
$Re = 6.7 \times 10^6$, $C_{L_B} = 0.6$, (FREE TRANSITION)

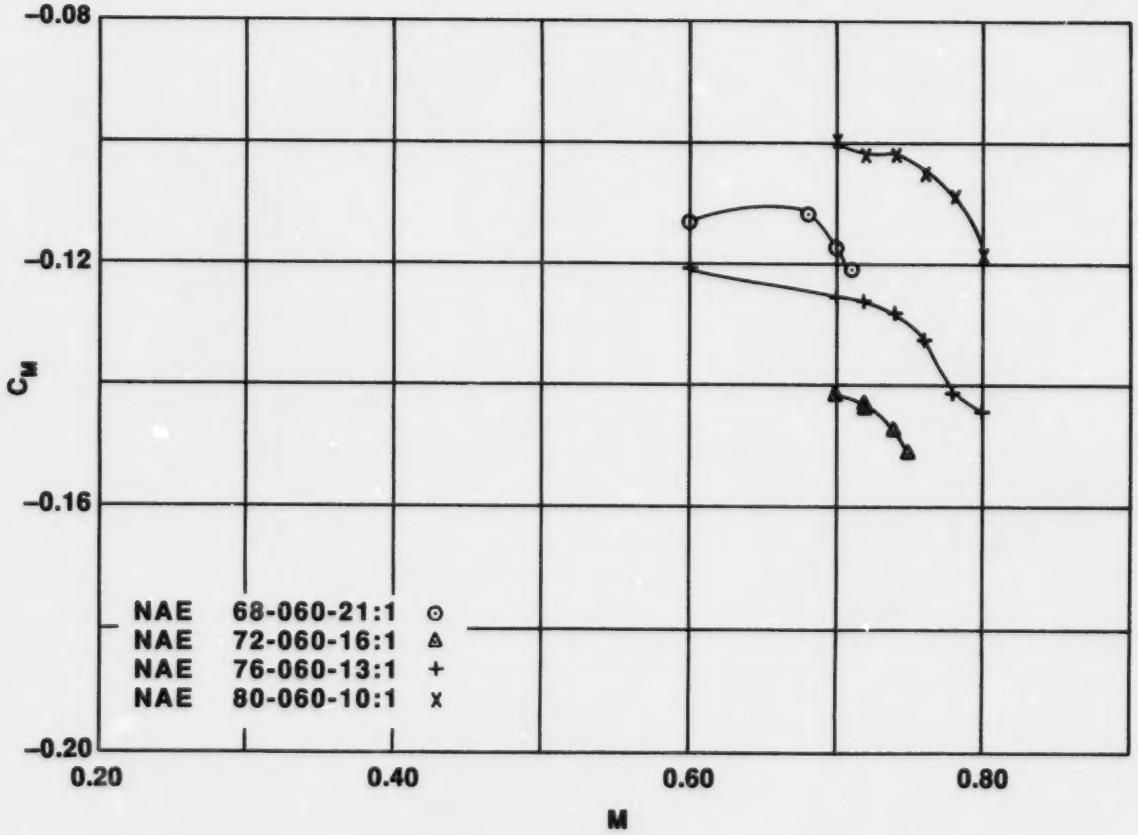


FIG. 16: PITCHING MOMENT $C_M$ VERSUS MACH NUMBER M, Re = 6.7 x $10^6$, $C_{L_B}$ = 0.6, (TRANSITION FIXED)

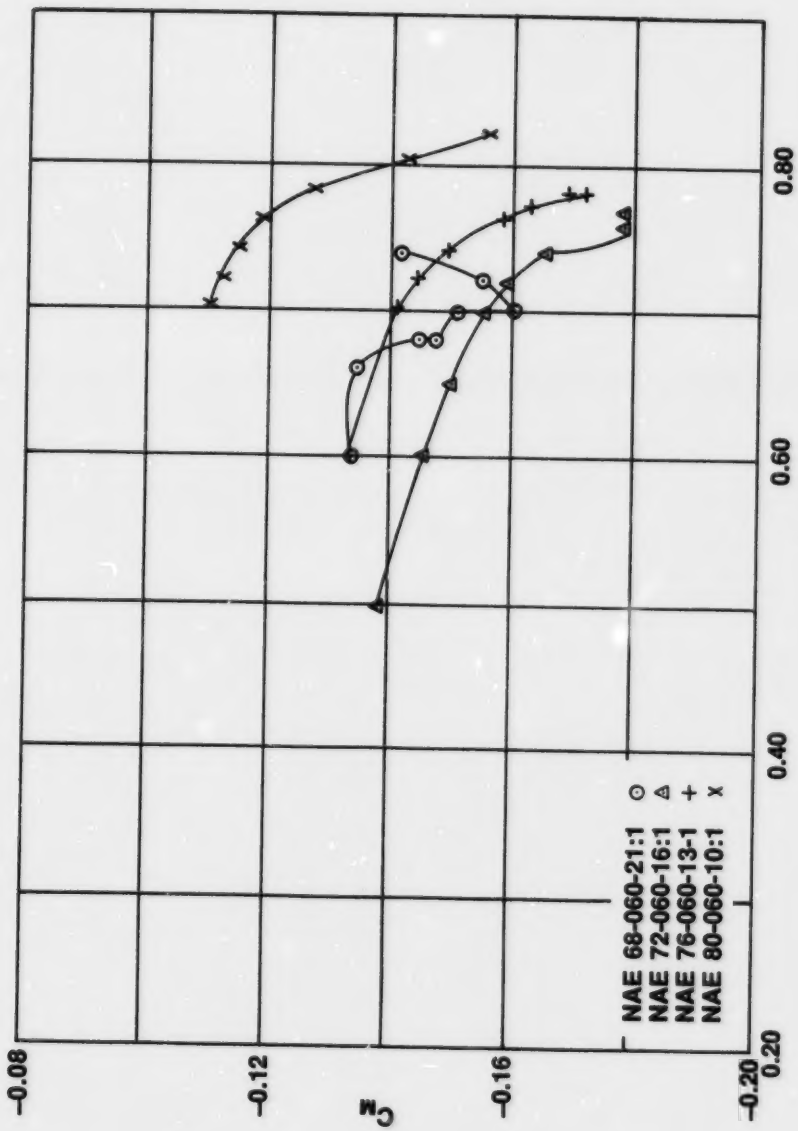


FIG. 17: PITCHING MOMENT $C_M$ VERSUS MACH NUMBER M, Re = 12.5 x $10^6$, $C_{L_B}$ = 0.6, (FREE TRANSITION)

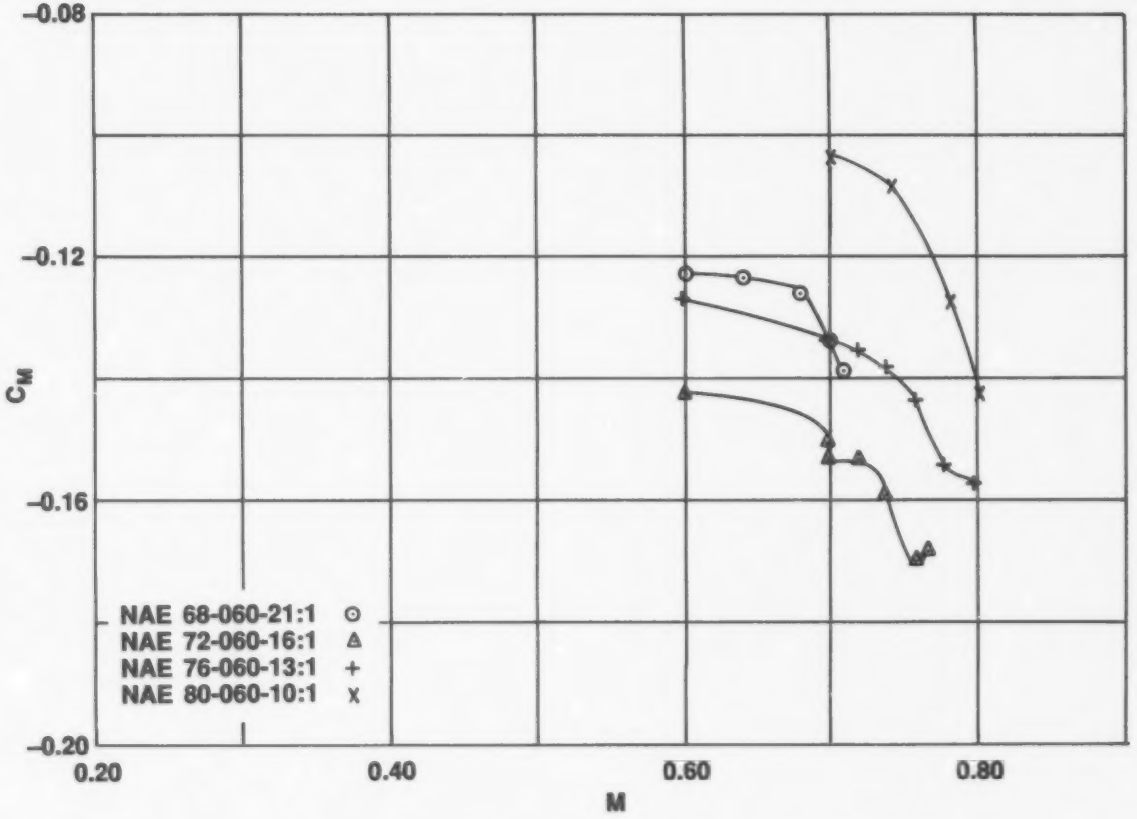


FIG. 18: PITCHING MOMENT $C_M$ VERSUS MACH NUMBER M, Re = 12.5 x $10^6$, $C_{L_B}$ = 0.6, (TRANSITION FIXED)

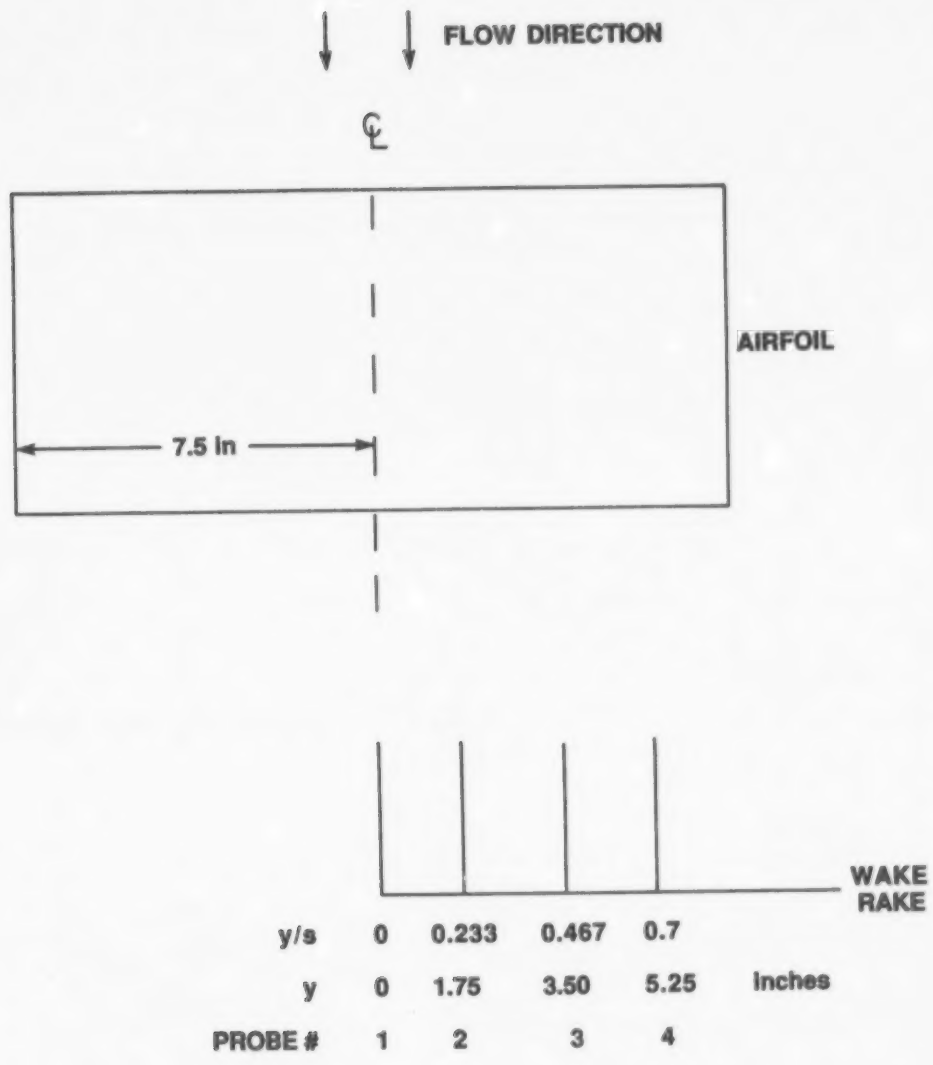


FIG. 19: THE WAKE RAKE PROBE LOCATIONS RELATIVE TO THE AIRFOIL

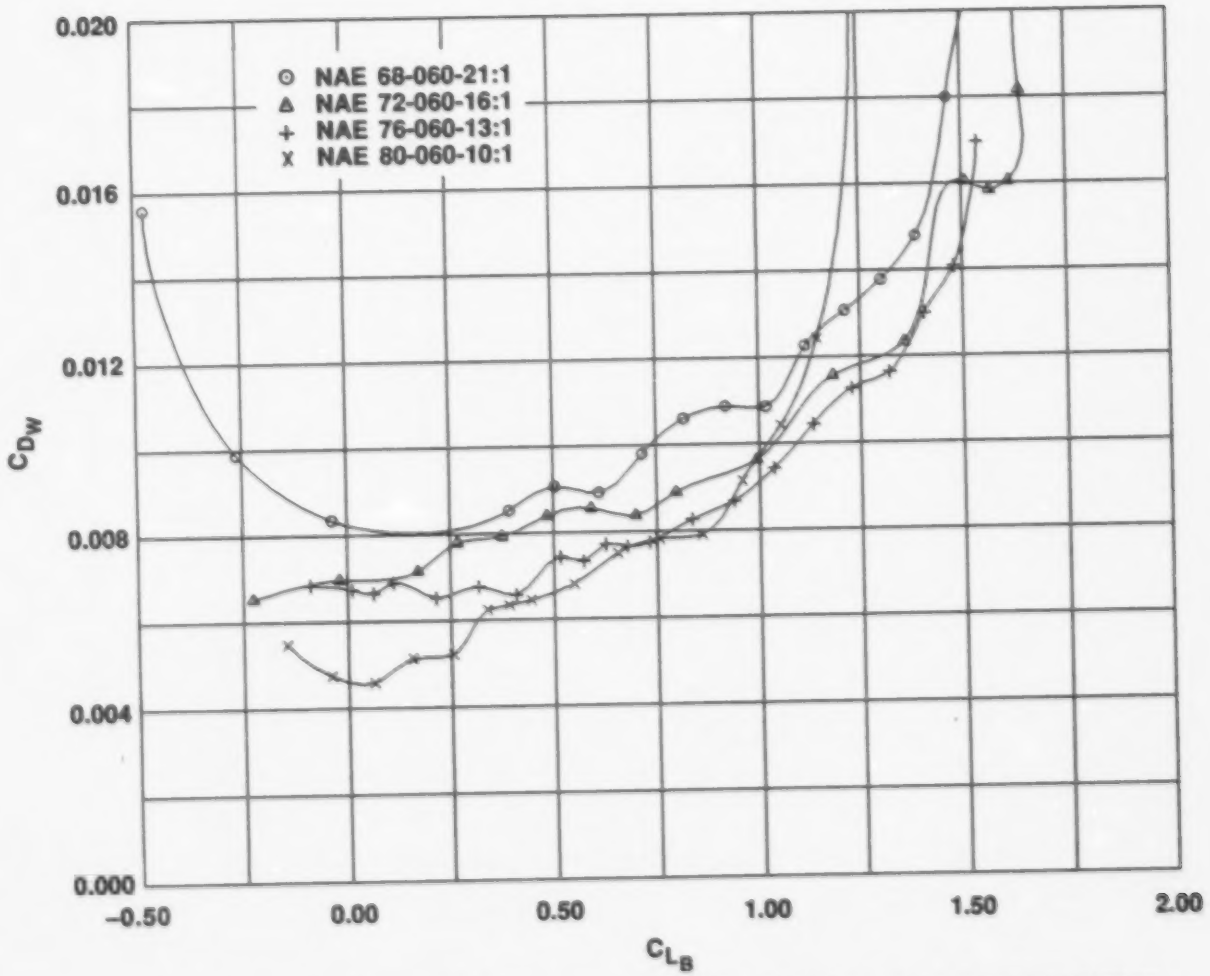


**FIG. 20: WAKE DRAG COEFFICIENT VERSUS LIFT COEFFICIENT, $C_{D_W}$ VERSUS $C_{L_B}$, (FREE TRANSITION)**

**Re = 6.7 x $10^6$, M = 0.2 & 0.3**

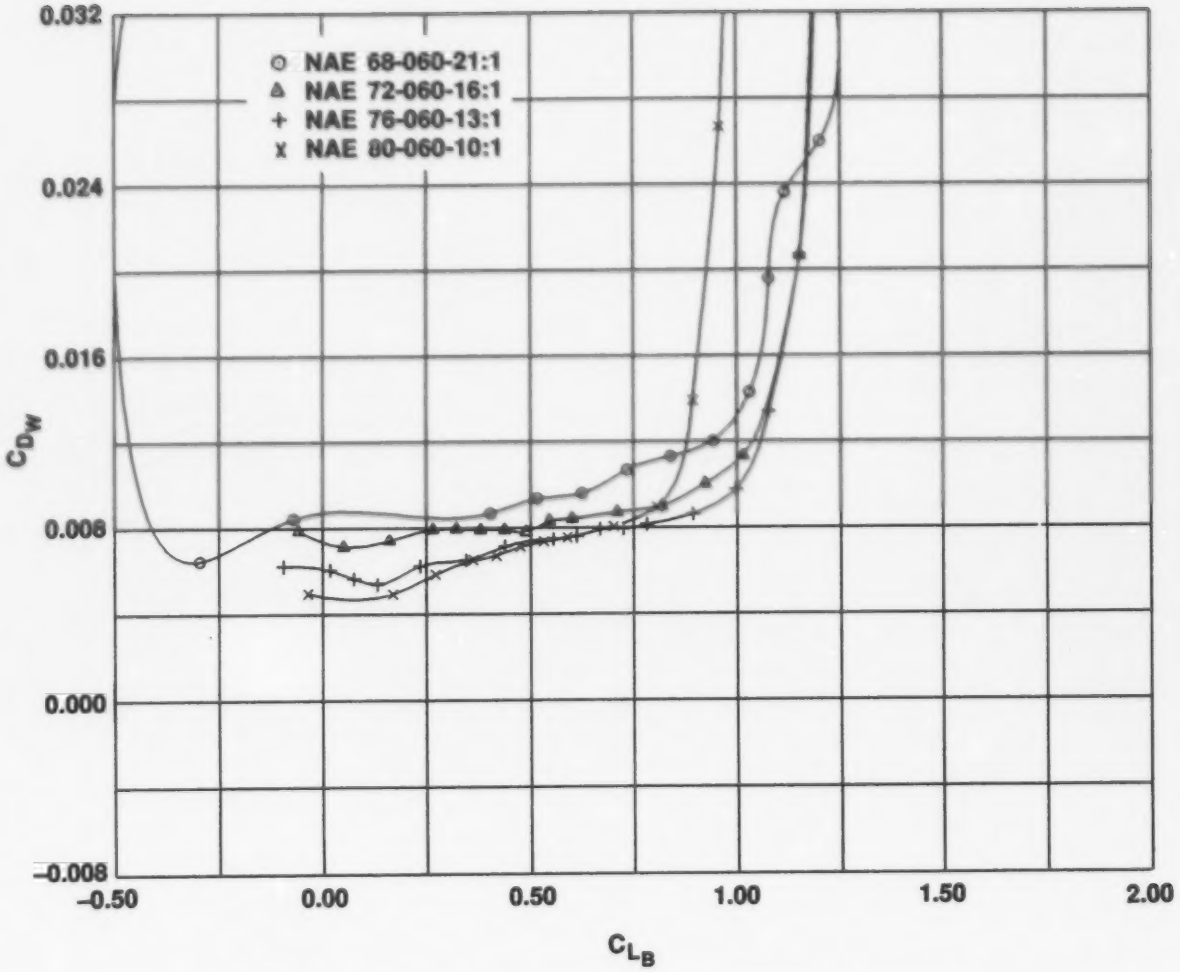


**FIG. 21: WAKE DRAG COEFFICIENT VERSUS LIFT COEFFICIENT, $C_{D_W}$ VERSUS $C_{L_B}$ (FREE TRANSITION)**

**Re = 6.7 x $10^6$, M = 0.5**

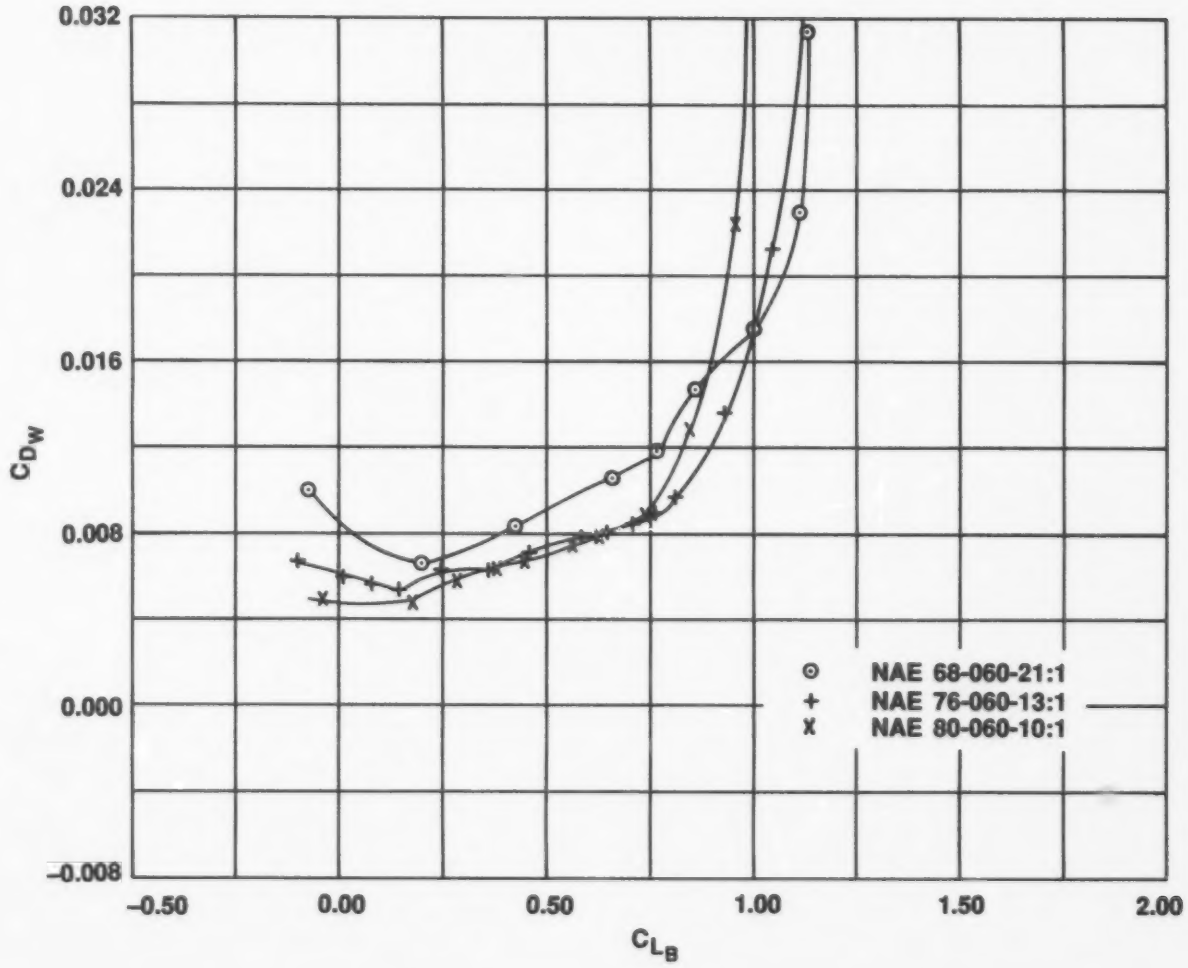


**FIG. 22: WAKE DRAG COEFFICIENT VERSUS LIFT COEFFICIENT $C_{L_W}$ VERSUS $C_{L_B}$, (FREE TRANSITION)**

**Re = 6.7 x $10^6$, M = 0.6**

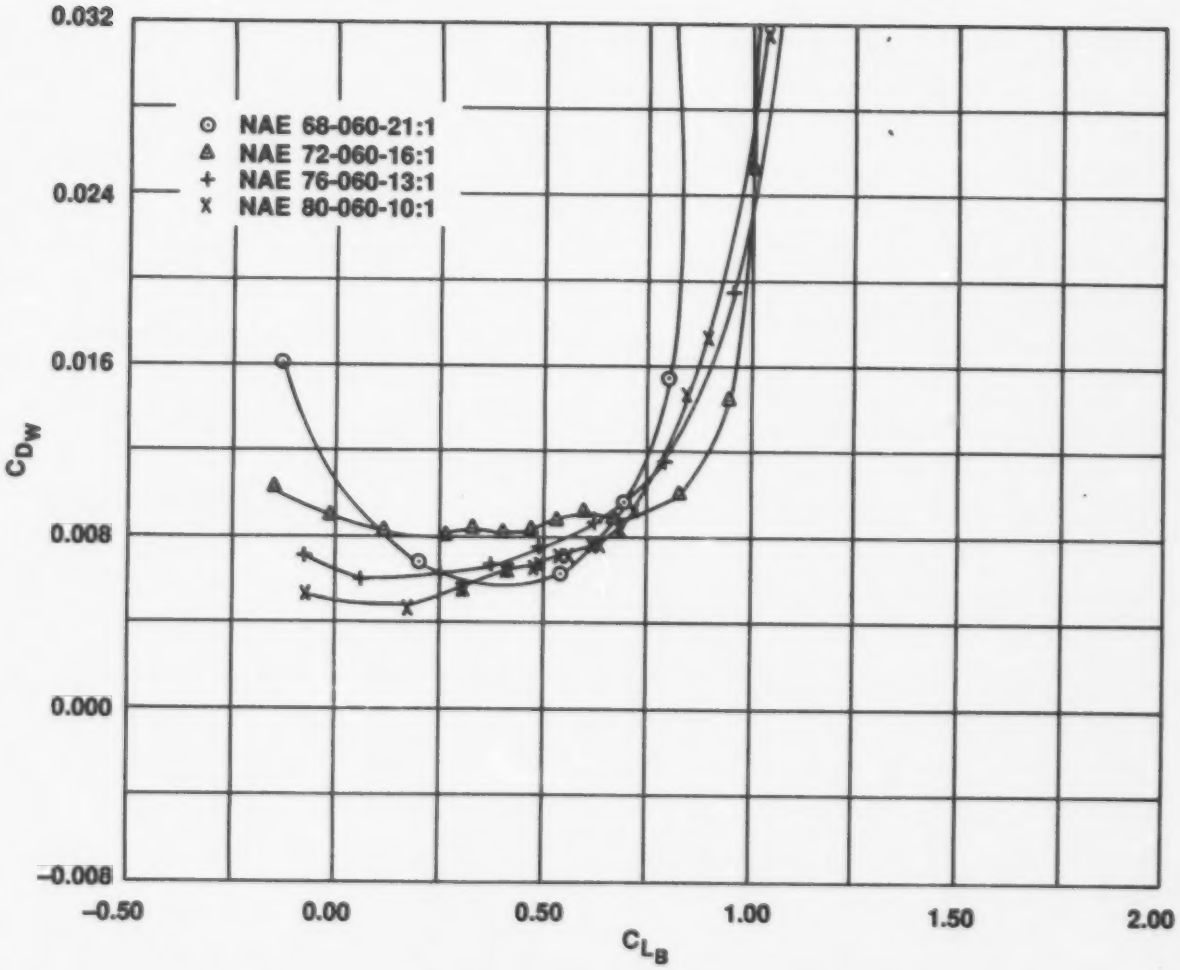


**FIG. 23: WAKE DRAG COEFFICIENT VERSUS LIFT COEFFICIENT $C_{D_W}$ VERSUS $C_{L_B}$ (FREE TRANSITION)**

**Re = 6.7 x $10^6$, M = 0.7**

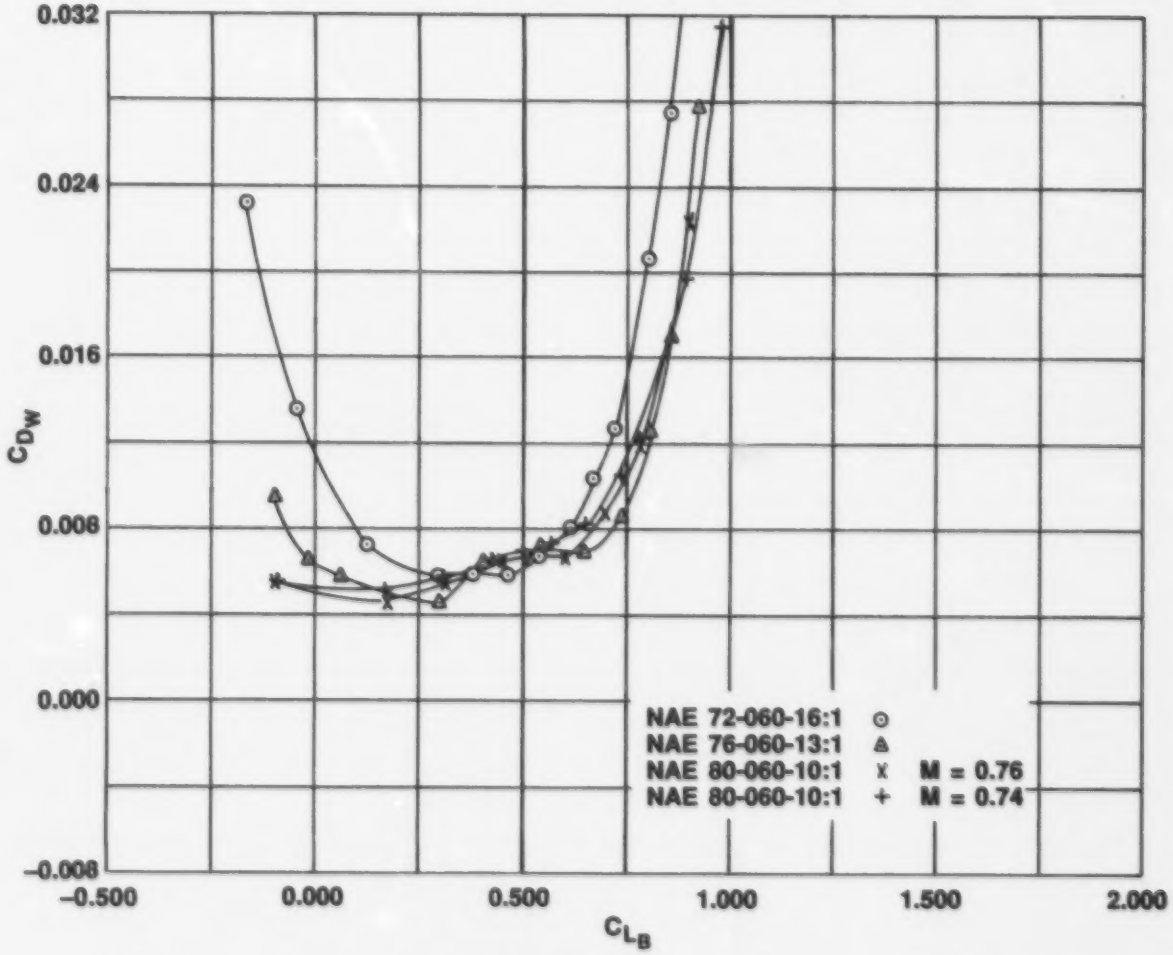


**FIG. 24: WAKE DRAG COEFFICIENT VERSUS LIFT COEFFICIENT $C_{D_W}$ VERSUS $C_{L_B}$, (FREE TRANSITION)**

**Re = 6.7 x $10^6$, M = 0.76, 0.74**

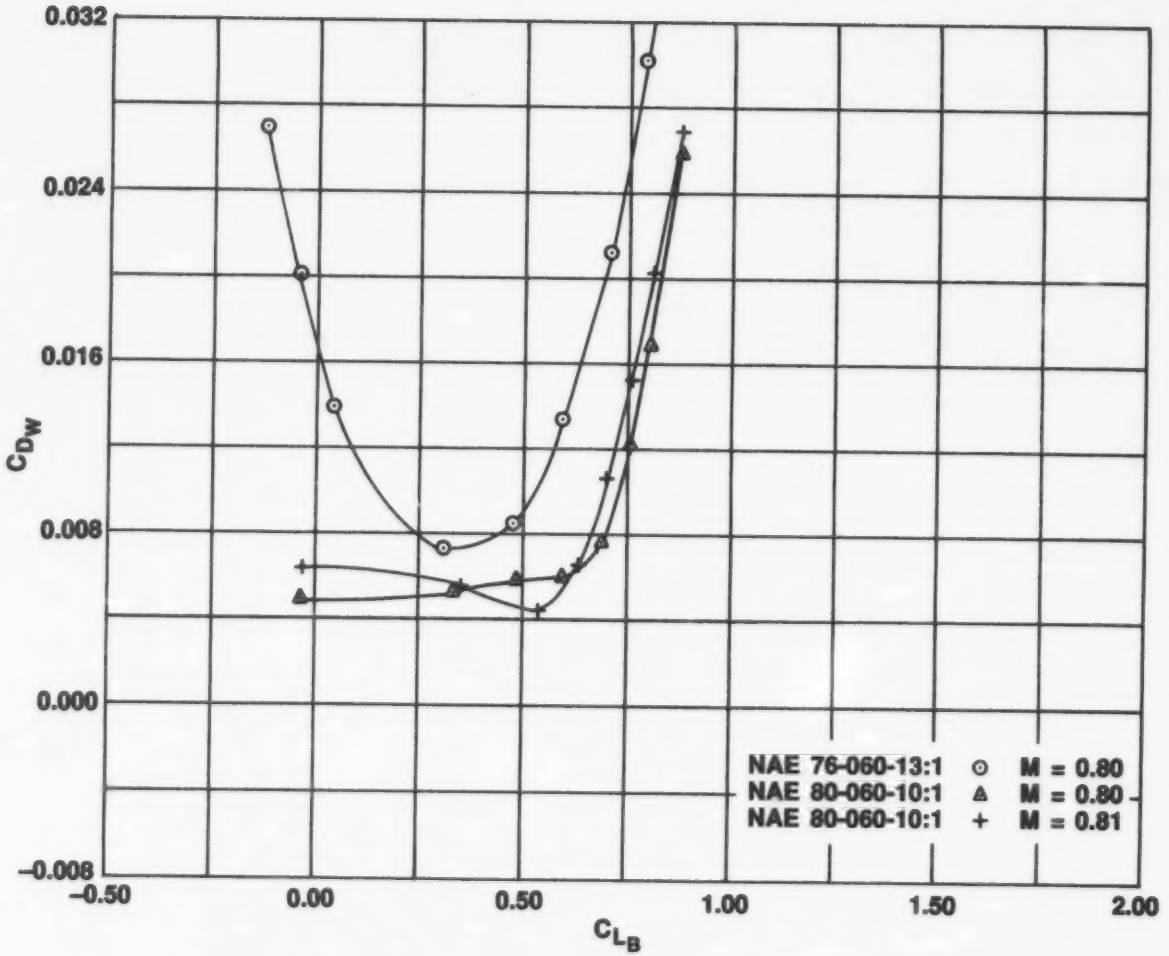


**FIG. 25: WAKE DRAG COEFFICIENT VERSUS LIFT COEFFICIENT $C_{D_W}$ VERSUS $C_{L_B}$, (FREE TRANSITION)**

**Re = 6.7 x $10^6$, M = 0.80, 0.81**

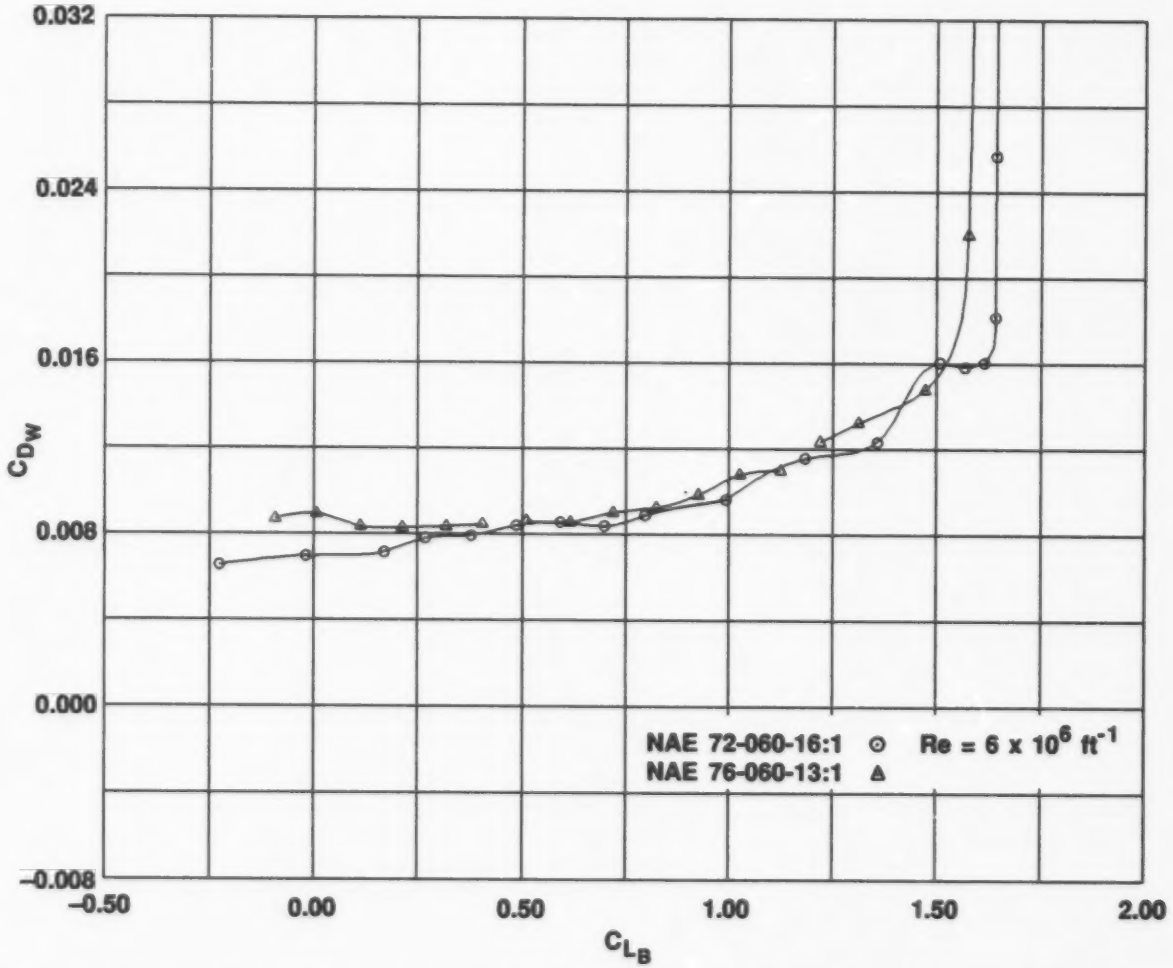


**FIG. 26: WAKE DRAG COEFFICIENT VERSUS LIFT COEFFICIENT $C_{D_W}$ VERSUS $C_{L_B}$ (TRANSITION FIXED)**

**Re = 6.7 x $10^6$, M = 0.2**

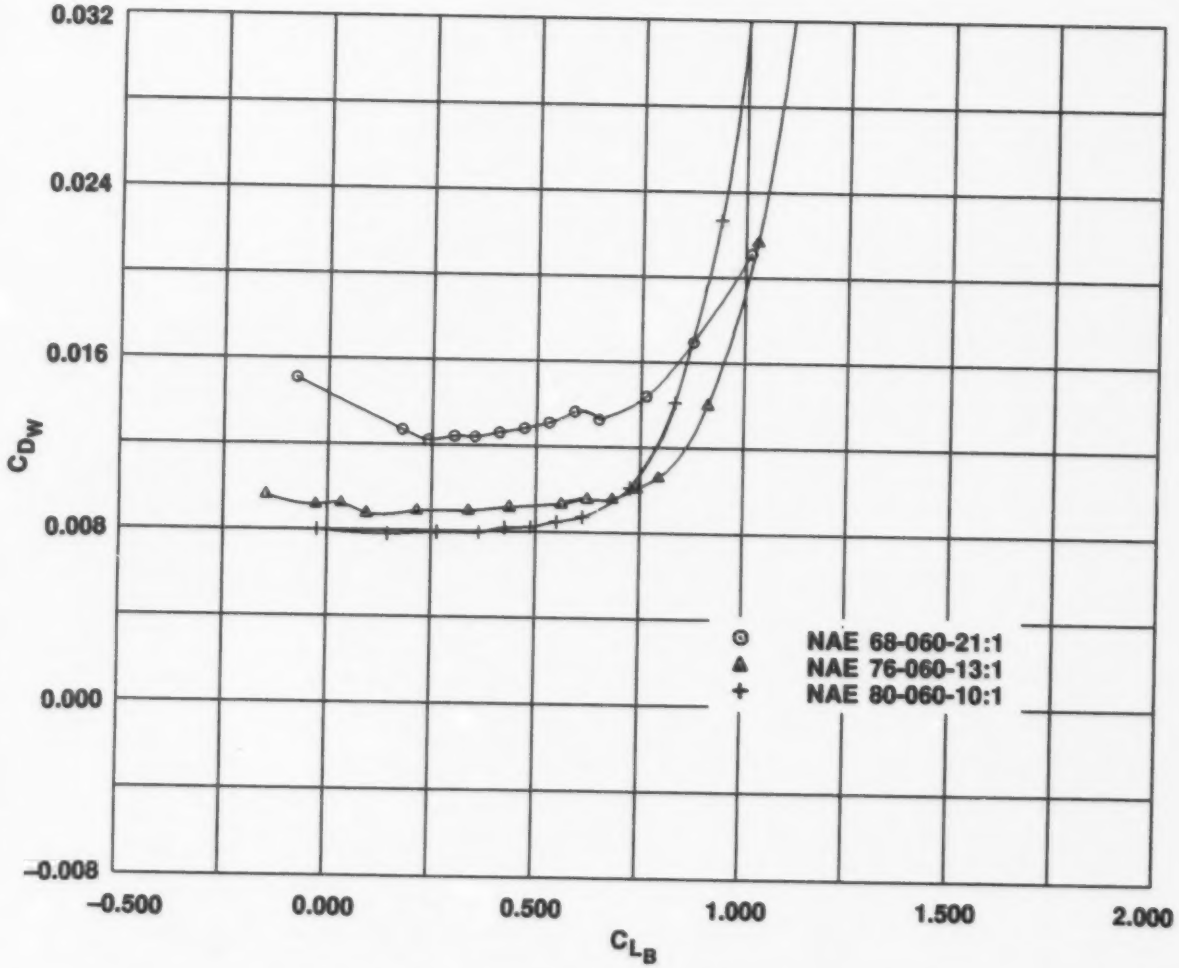


**FIG. 27: WAKE DRAG COEFFICIENT VERSUS LIFT COEFFICIENT $C_{D_W}$ VERSUS $C_{L_B}$ (TRANSITION FIXED)**

**Re = 6.7 x$10^6$, M = 0.6**

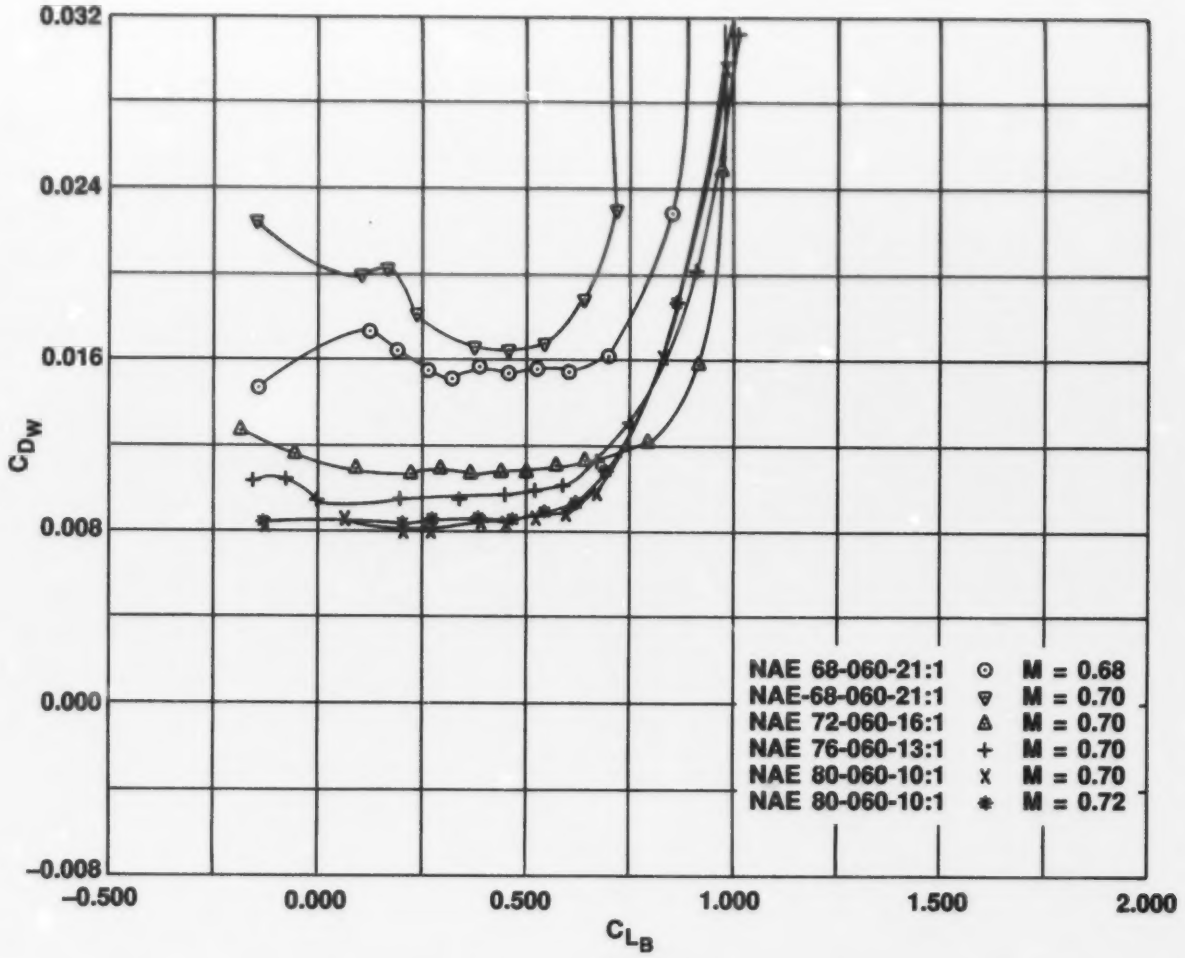


**FIG. 28: WAKE DRAG COEFFICIENT VERSUS LIFT COEFFICIENT $C_{D_W}$ VERSUS $C_{L_B}$ (TRANSITION FIXED)**

**Re = 6.7 x $10^6$, M = 0.68 – 0.72**

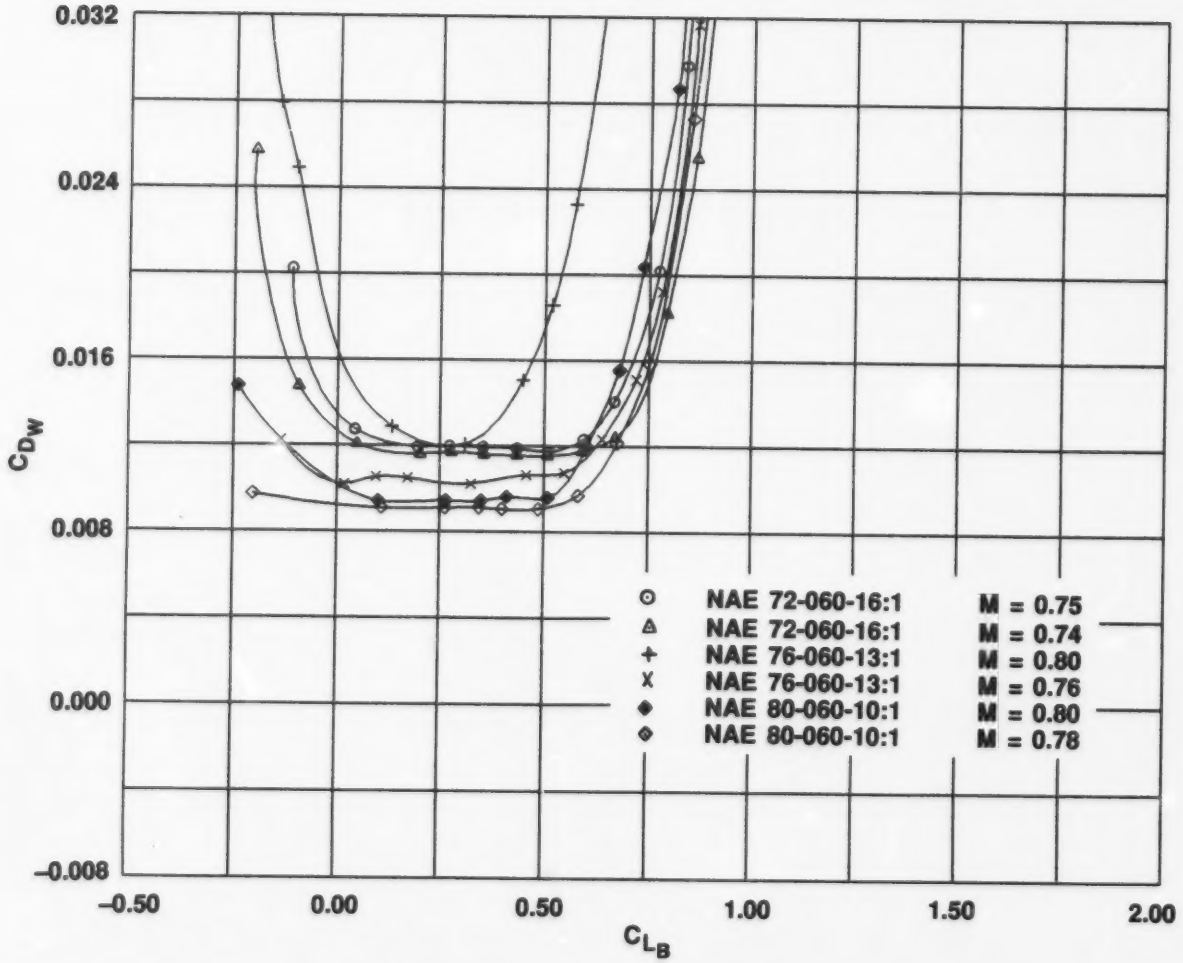


**FIG. 29: WAKE DRAG COEFFICIENT VERSUS LIFT COEFFICIENT $C_{D_W}$ VERSUS $C_{L_B}$, (TRANSITION FIXED)**

**Re = 6.7 x $10^6$, M = 0.74 – 0.80**

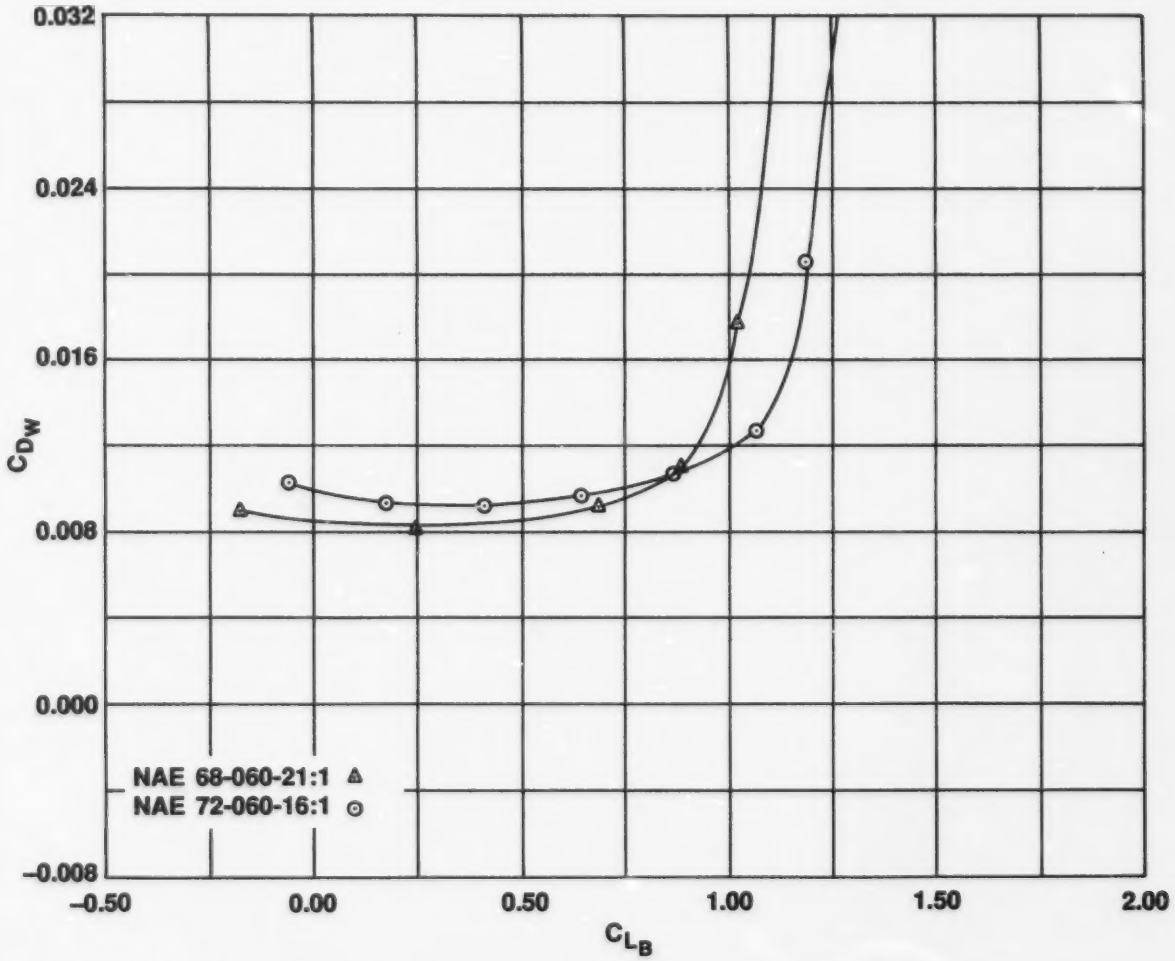


**FIG. 30: WAKE DRAG COEFFICIENT VERSUS LIFT COEFFICIENT $C_{D_W}$ VERSUS $C_{L_B}$, (FREE TRANSITION)**

**Re = 12.5 x $10^6$, M = 0.5**

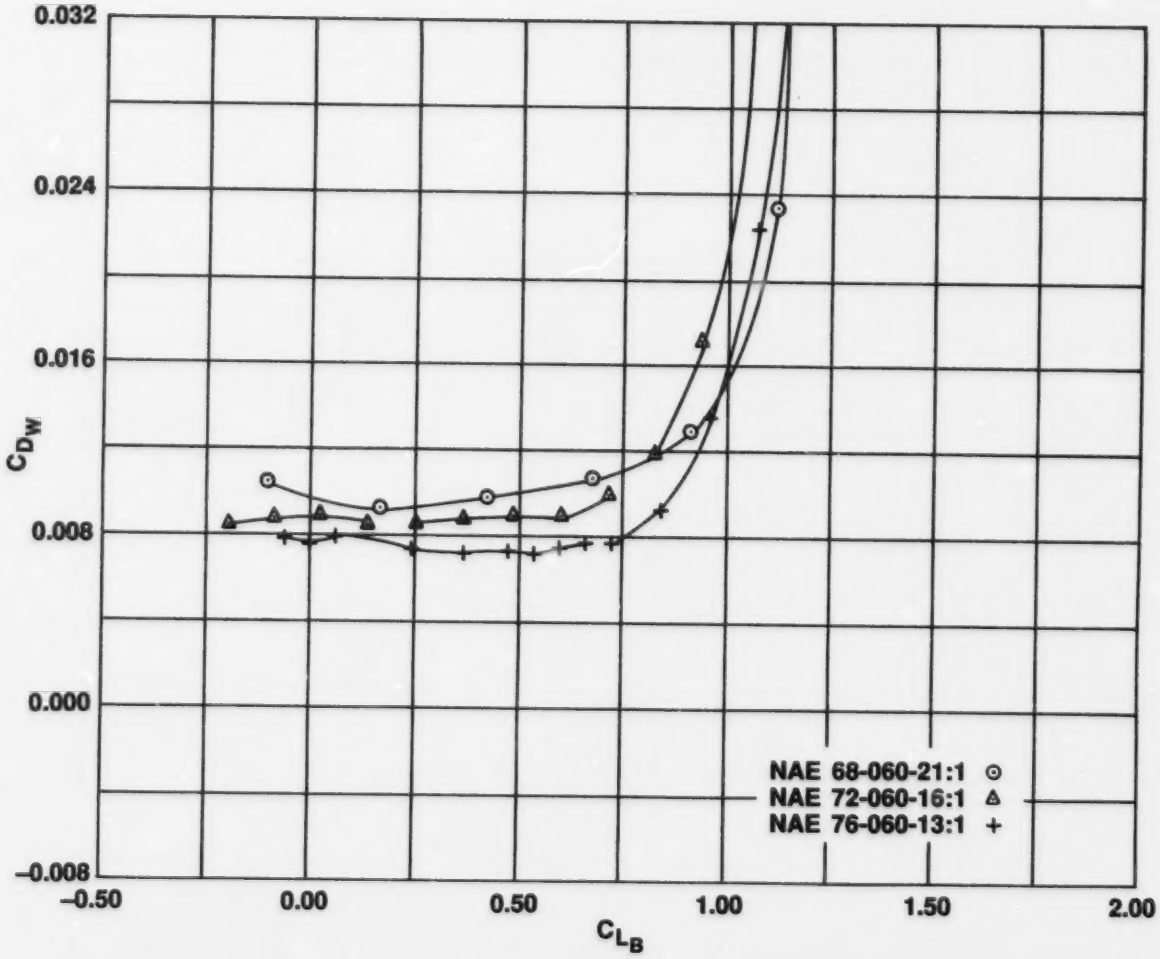


**FIG. 31: WAKE DRAG COEFFICIENT VERSUS LIFT COEFFICIENT $C_{D_W}$ VERSUS $C_{L_B}$, (FREE TRANSITION)**

**Re = 12.5 x $10^6$, M = 0.6**

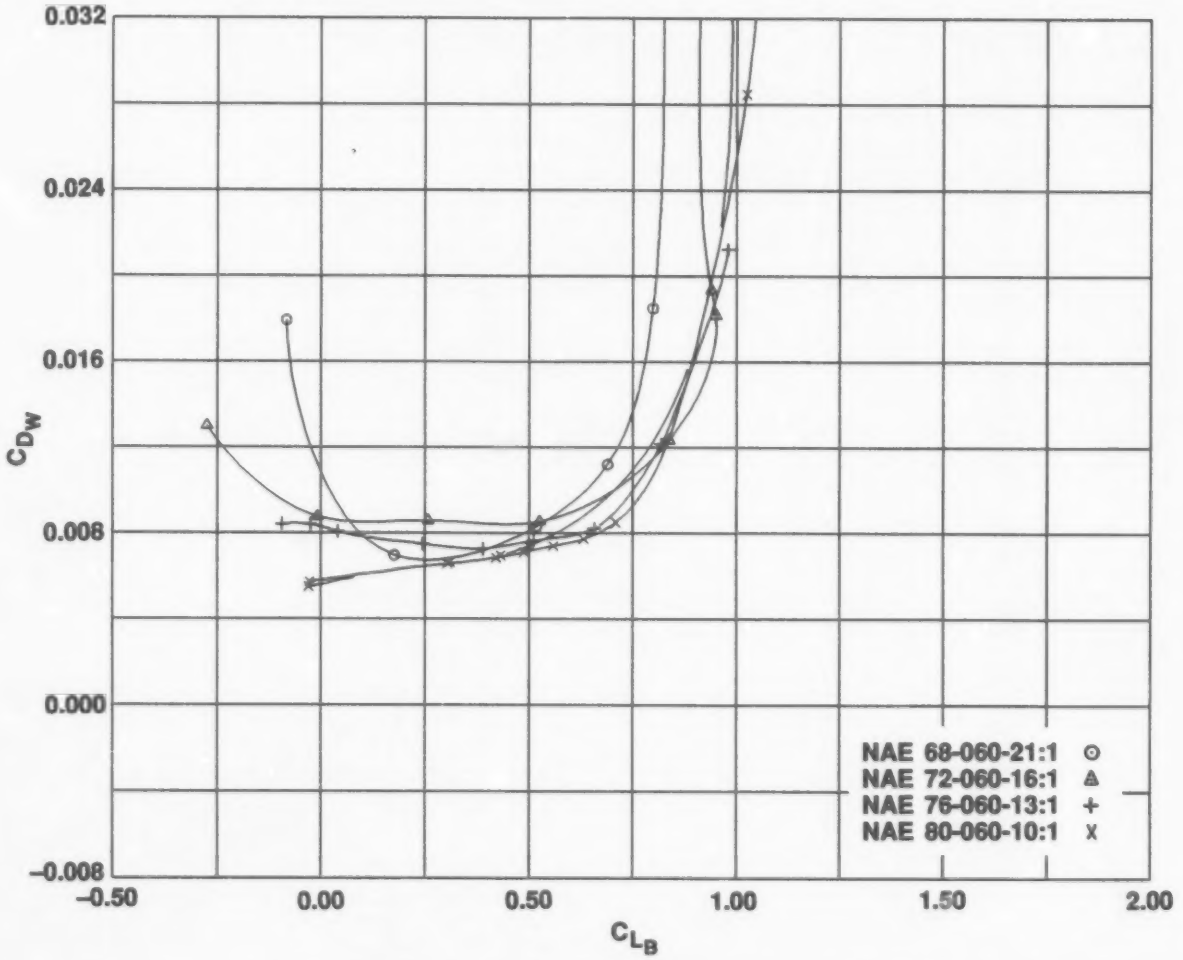


**FIG. 32: WAKE DRAG COEFFICIENT VERSUS LIFT COEFFICIENT $C_{D_W}$ VERSUS $C_{L_B}$, (FREE TRANSITION)**

**Re = 12.5 x $10^6$, M = 0.7**

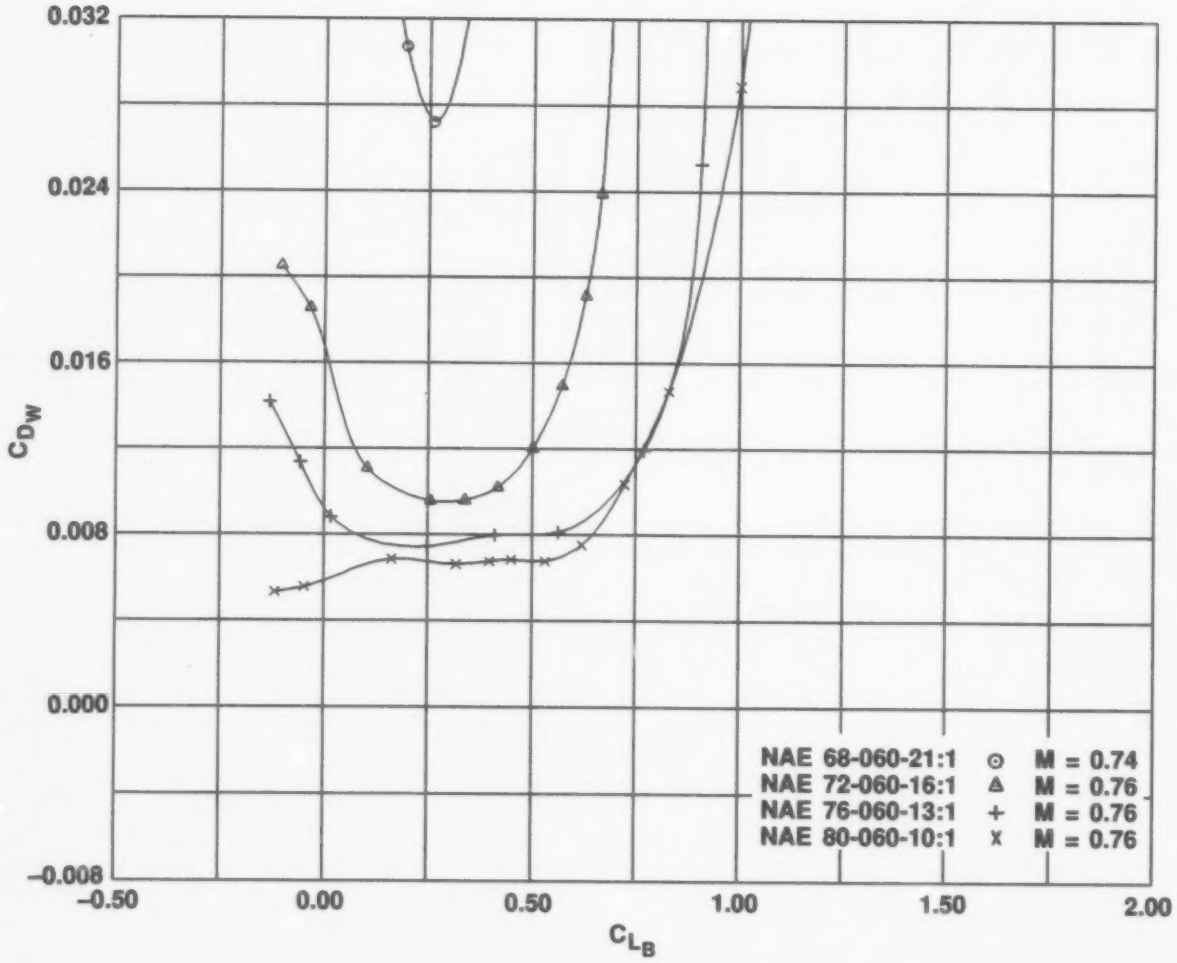


**FIG. 33: WAKE DRAG COEFFICIENT VERSUS LIFT COEFFICIENT $C_{D_W}$ VERSUS $C_{L_B}$, (FREE TRANSITION)**

**Re = 12.5 x $10^6$, M = 0.74 – 0.76**

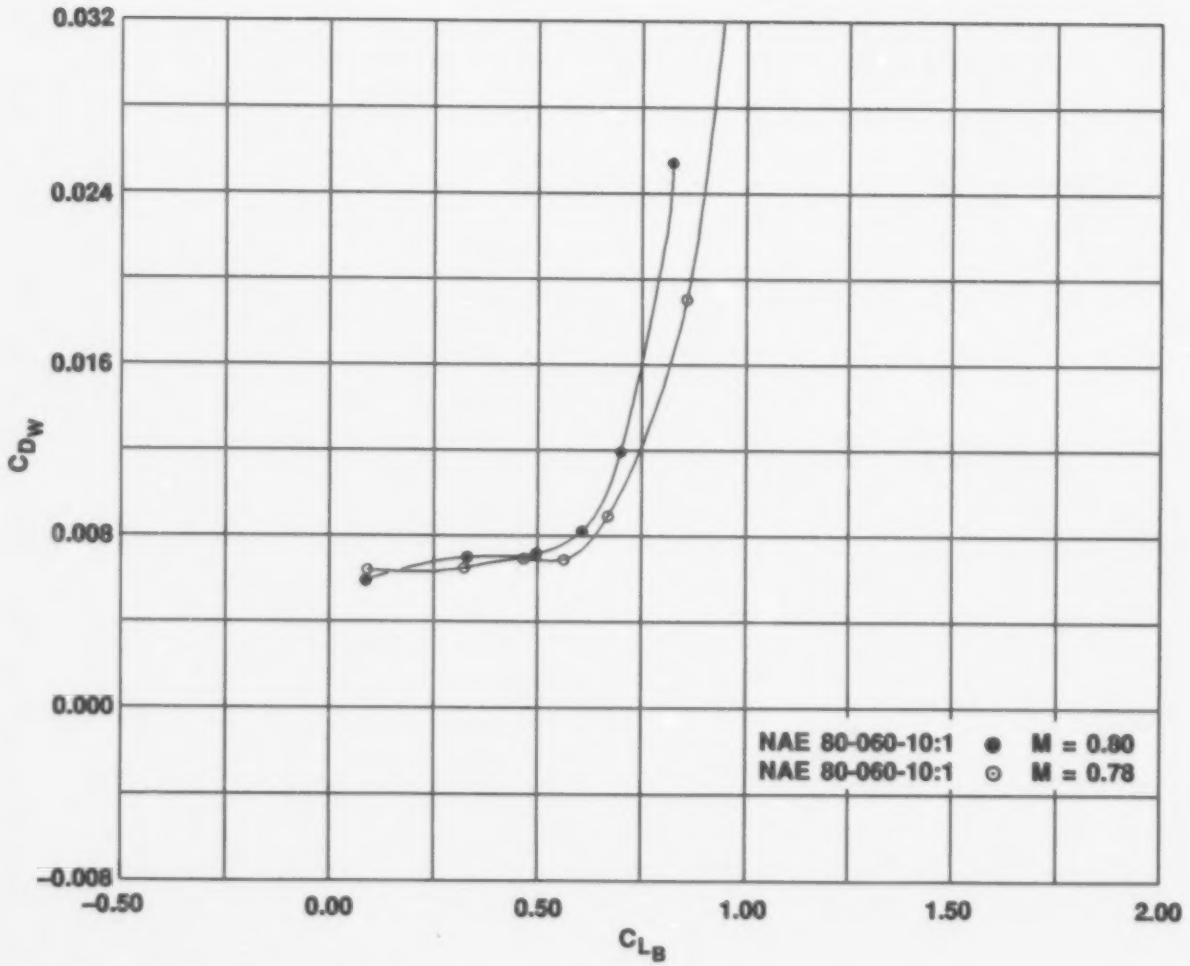


**FIG. 34: WAKE DRAG COEFFICIENT VERSUS LIFT COEFFICIENT $C_{D_W}$ VERSUS $C_{L_B}$, (FREE TRANSITION)**

**Re = 12.5 x $10^6$, M = 0.78, 0.80**

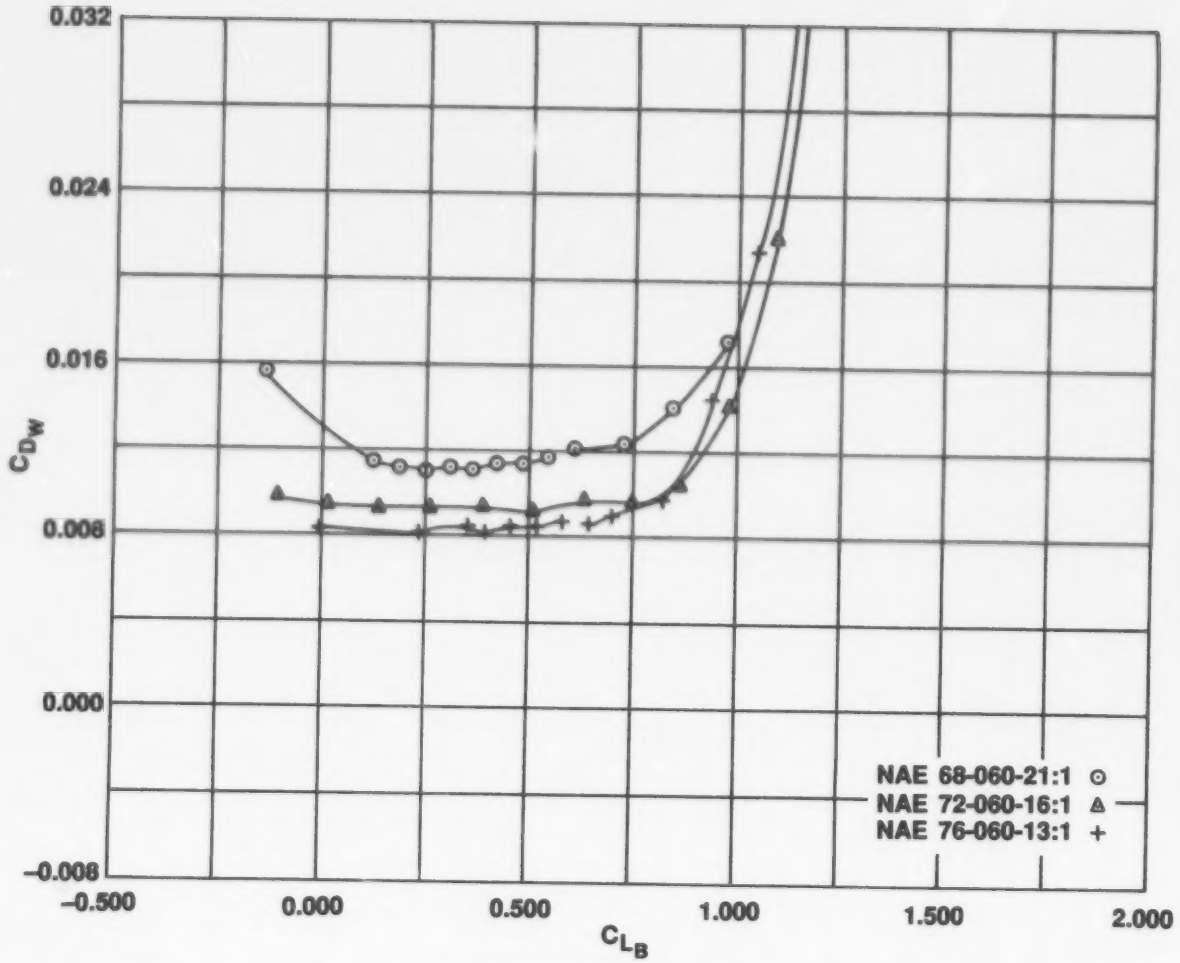


FIG. 35: WAKE DRAG COEFFICIENT VERSUS LIFT COEFFICIENT
$C_{D_W}$ VERSUS $C_{L_B}$, (TRANSITION FIXED)
Re = 12.5 x $10^6$, M = 0.6

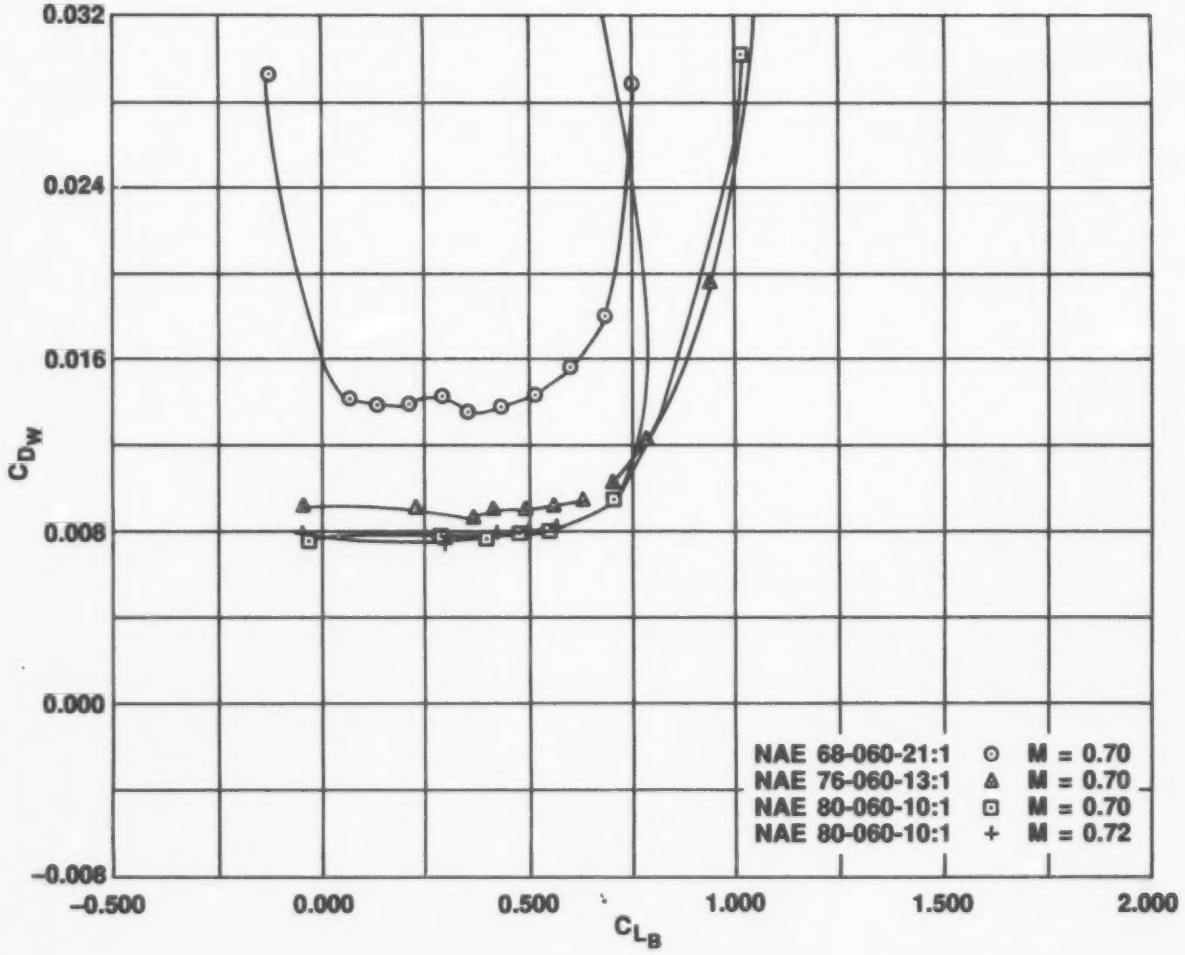


**FIG. 36: WAKE DRAG COEFFICIENT VERSUS LIFT COEFFICIENT $C_{D_W}$ VERSUS $C_{L_B}$, (TRANSITION FIXED)**

**Re = 12.5 x $10^6$, M = 0.70 – 0.72**

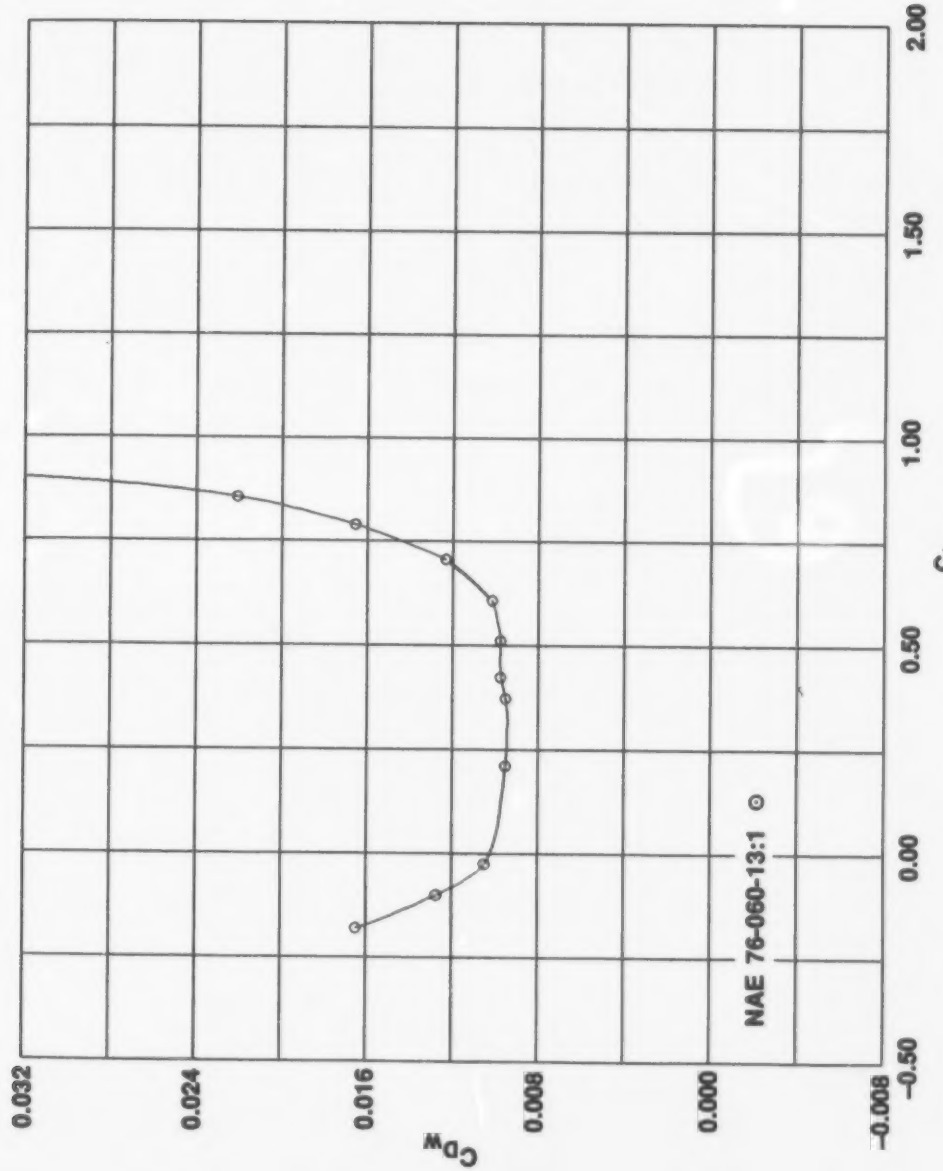


FIG. 37: WAKE DRAG COEFFICIENT VERSUS LIFT COEFFICIENT $C_{D_W}$ VERSUS $C_{L_B}$, (TRANSITION FIXED)
Re = 12.5 x $10^6$, M = 0.76

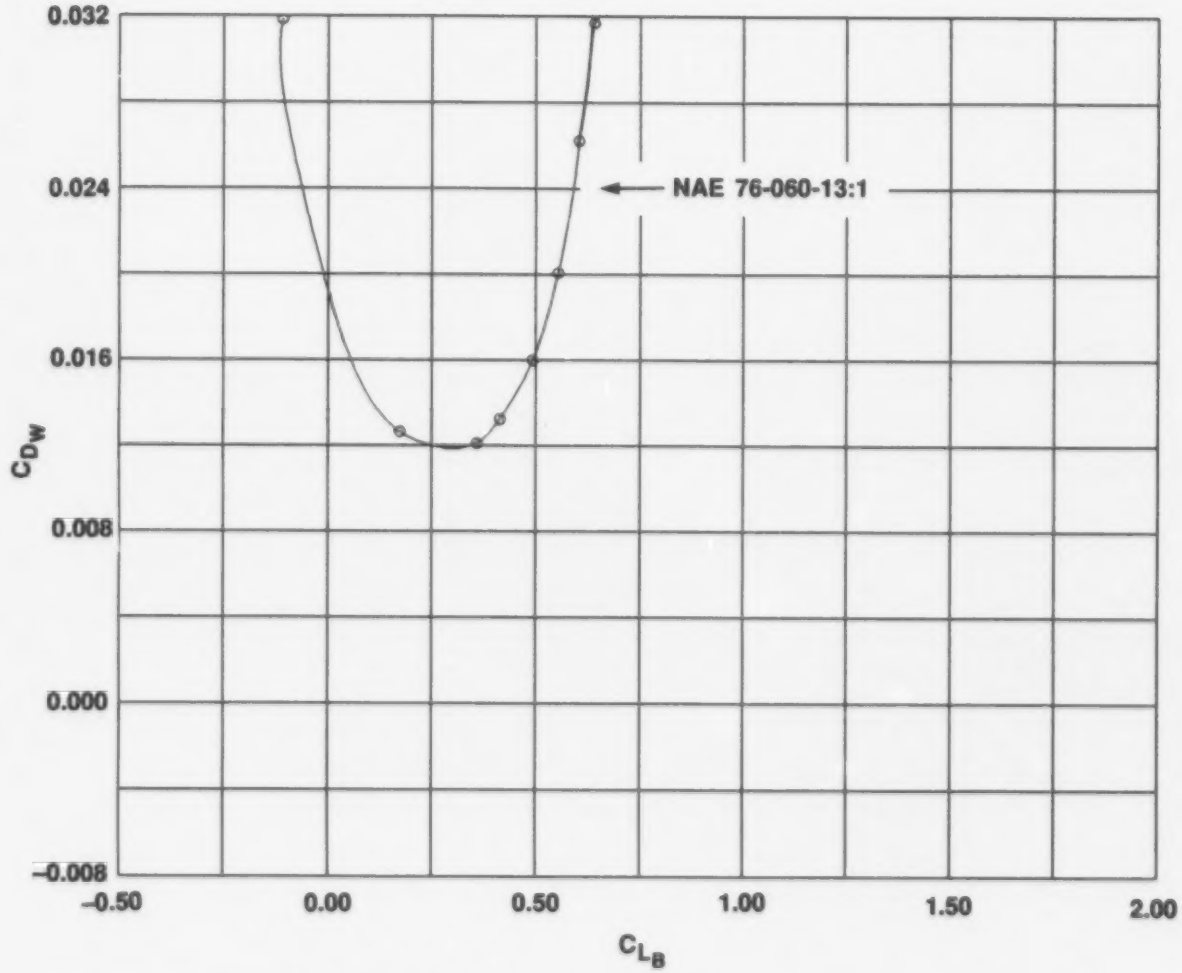


FIG. 38: WAKE DRAG COEFFICIENT VERSUS LIFT COEFFICIENT
$C_{D_W}$ VERSUS $C_{L_B}$, (TRANSITION FIXED)
Re = 12.5 x $10^6$, M = 0.80

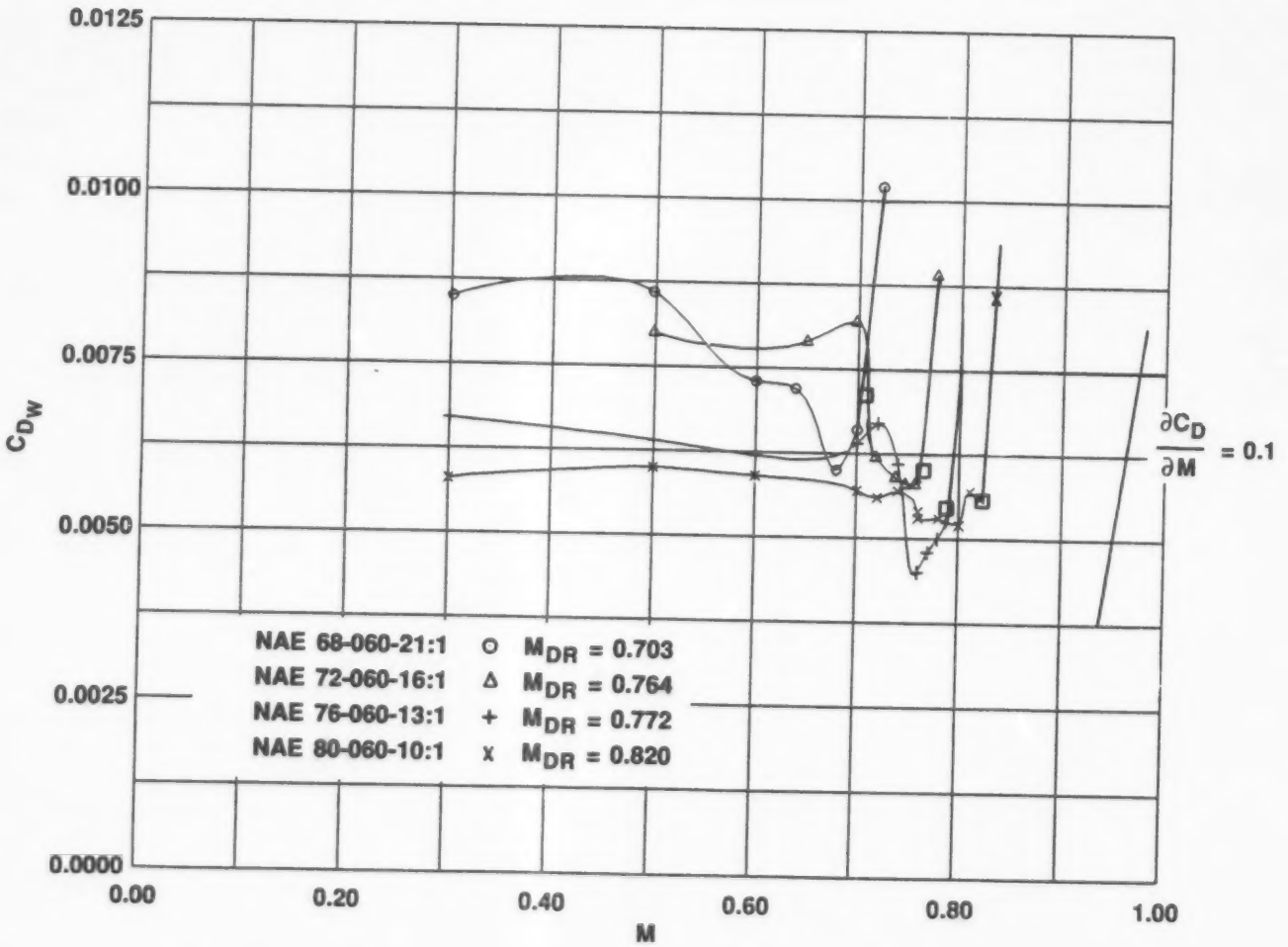


**FIG. 39: WAKE DRAG COEFFICIENT VERSUS MACH NUMBER**
**$C_{D_W}$ VERSUS M, (FREE TRANSITION)**
**$C_{L_B} = 0.3$, Re = $6.7 \times 10^6$**

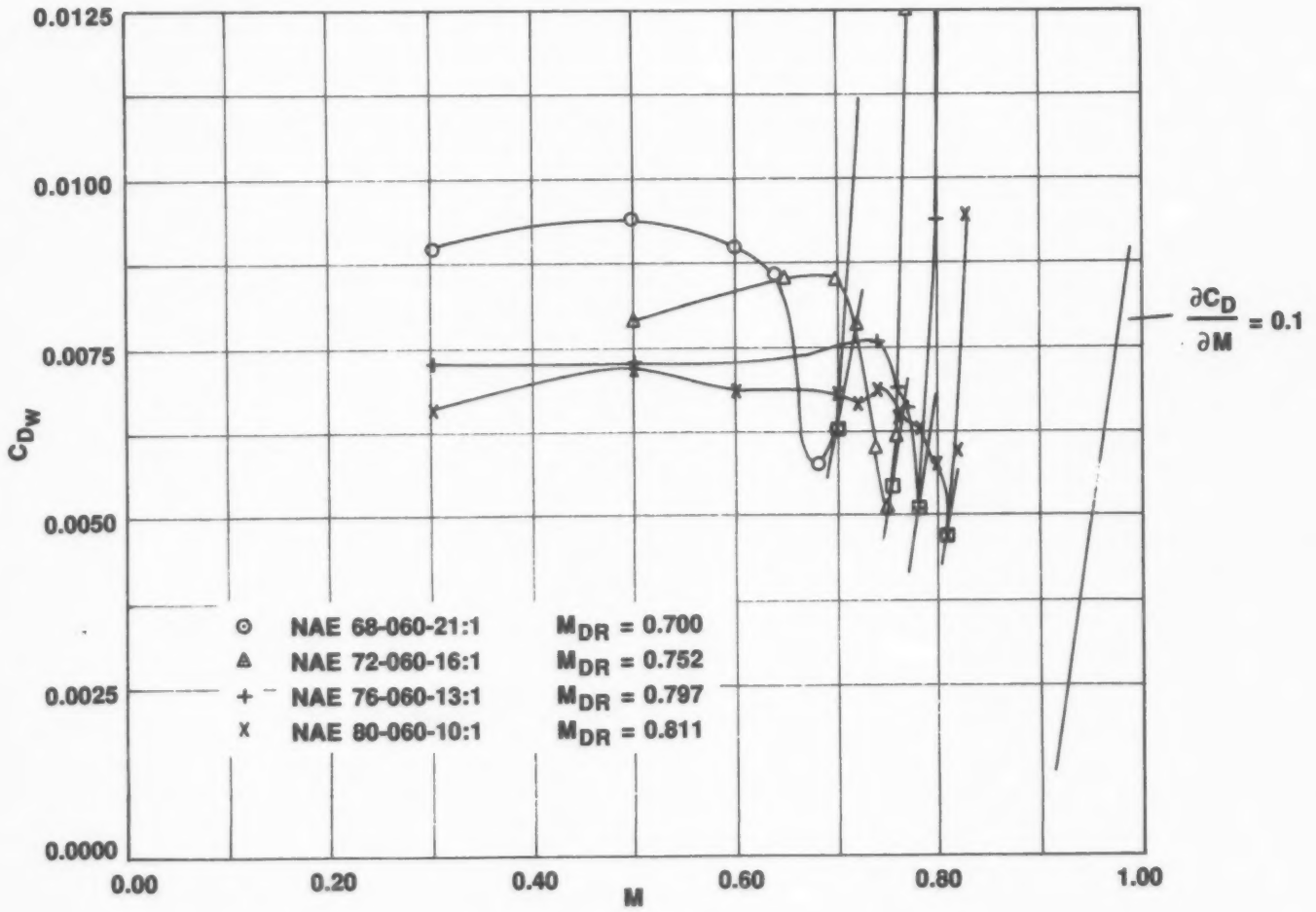


**FIG. 40: WAKE DRAG COEFFICIENT VERSUS MACH NUMBER**
**$C_{D_W}$ VERSUS M, (FREE TRANSITION)**
**$C_{L_B} = 0.5$, Re = $6.7 \times 10^6$**

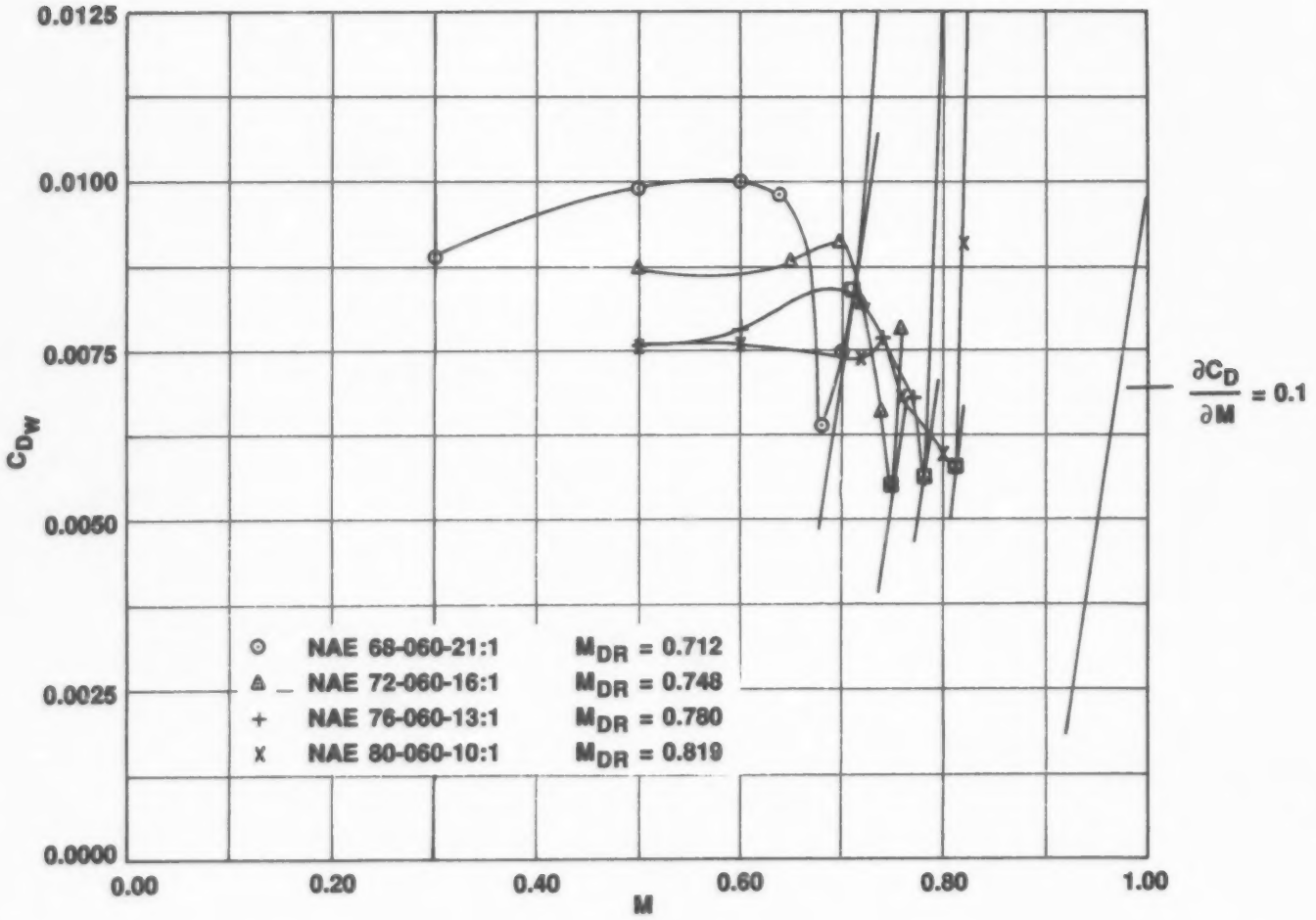


**FIG. 41: WAKE DRAG COEFFICIENT VERSUS MACH NUMBER $C_{D_W}$ VERSUS M, (FREE TRANSITION)**

**$C_{L_B}$ = 0.6, Re = 6.7 x $10^6$**

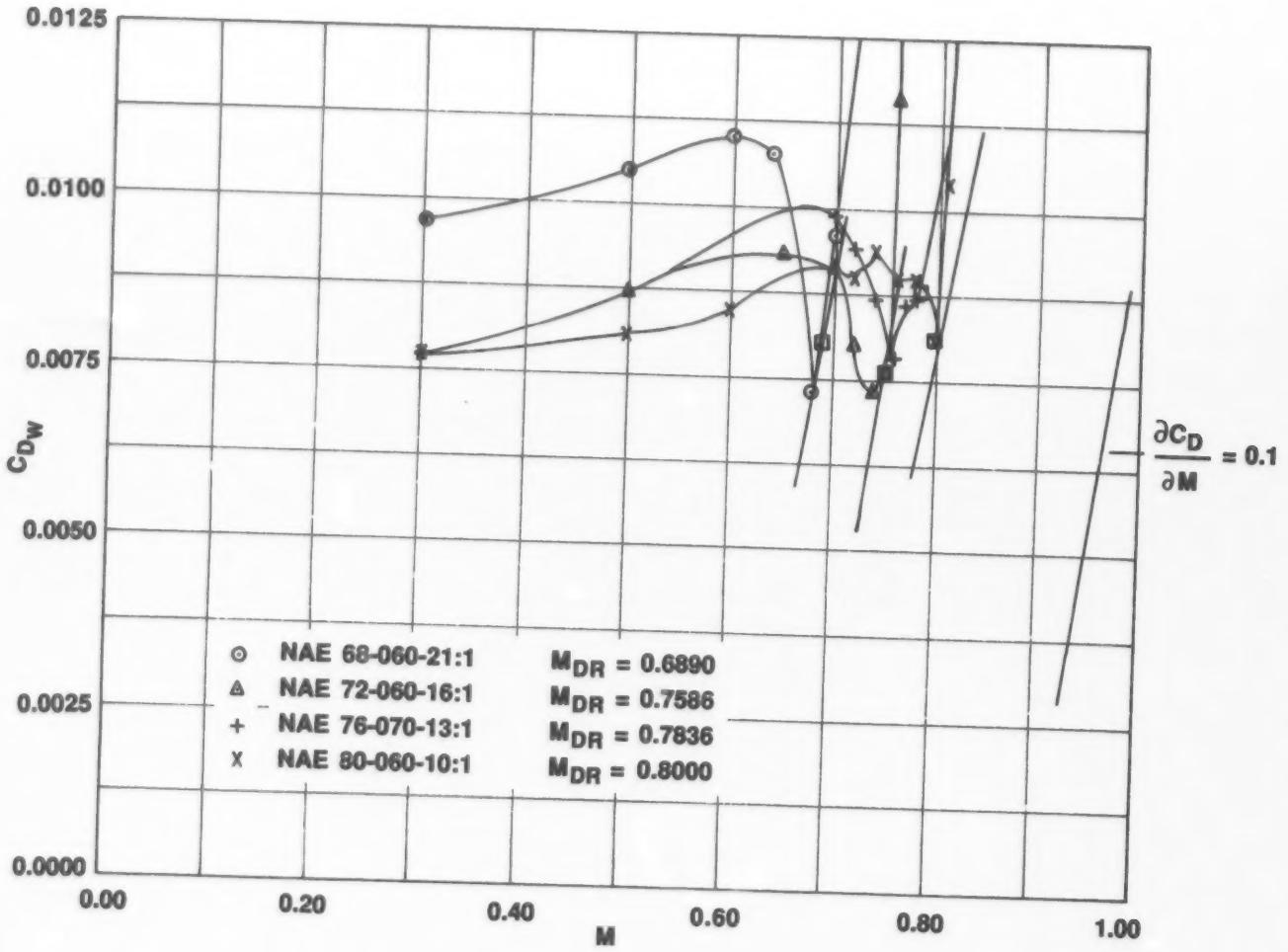


**FIG. 42: WAKE DRAG COEFFICIENT VERSUS MACH NUMBER**
**$C_{D_W}$ VERSUS M, (FREE TRANSITION)**
**$C_{L_B} = 0.7$, Re = $6.7 \times 10^6$**

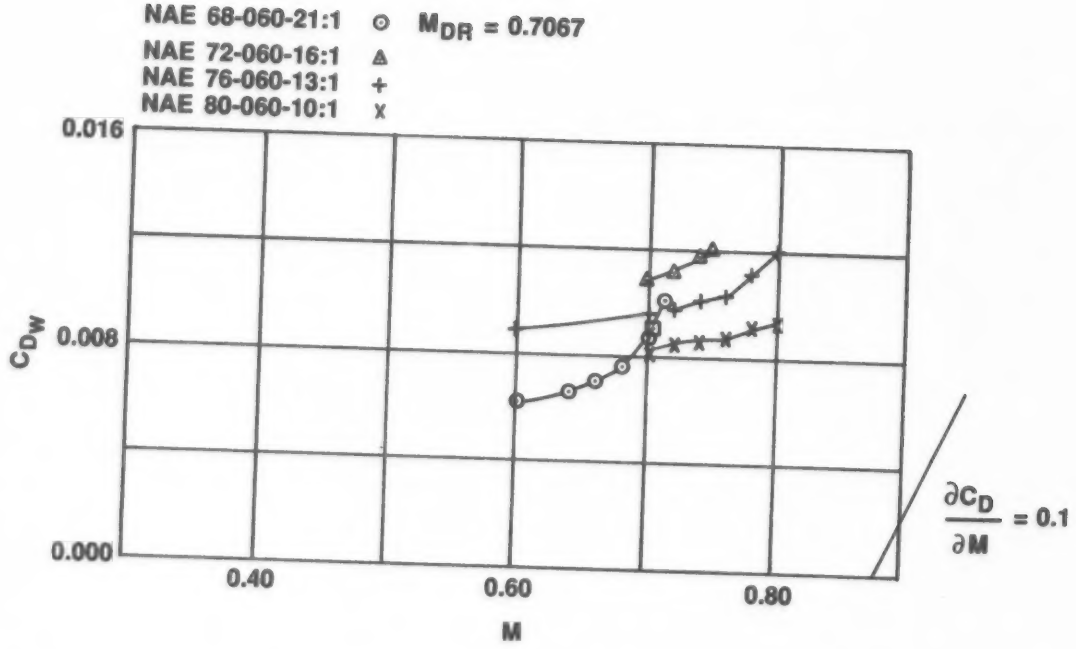


FIG. 43: WAKE DRAG COEFFICIENT VERSUS MACH NUMBER
$C_{D_W}$ VERSUS M, (TRANSITION FIXED)
$C_{L_B}$ = 0.3, Re = 6.7 x $10^6$

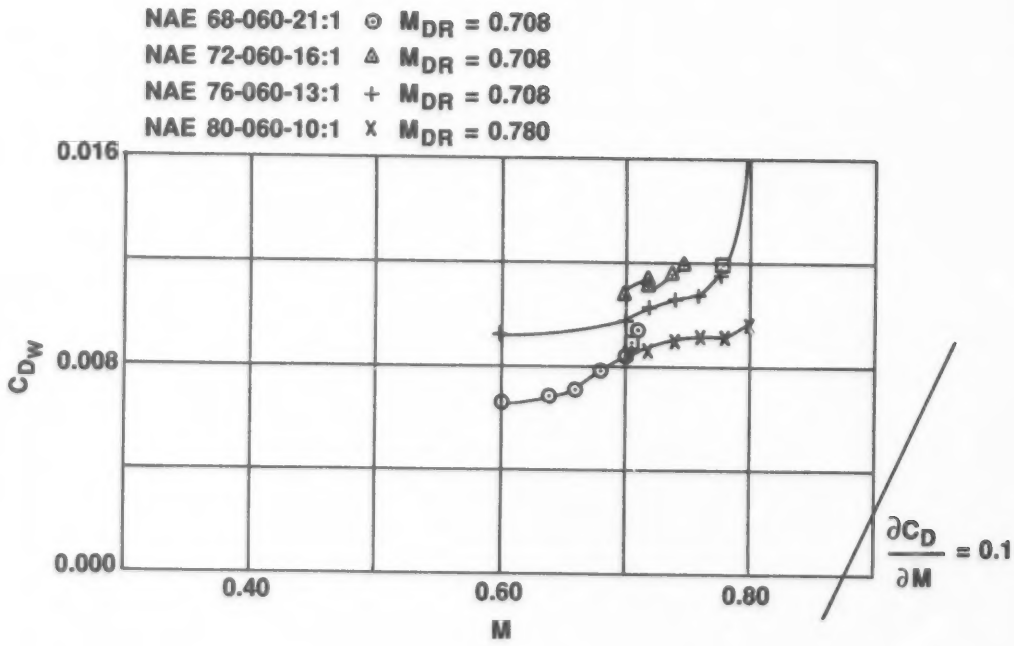


**FIG. 44: WAKE DRAG COEFFICIENT VERSUS MACH NUMBER**
**$C_{D_W}$ VERSUS M, (TRANSITION FIXED)**
**$C_{L_B}$ = 0.5, Re = 6.7 x $10^6$**

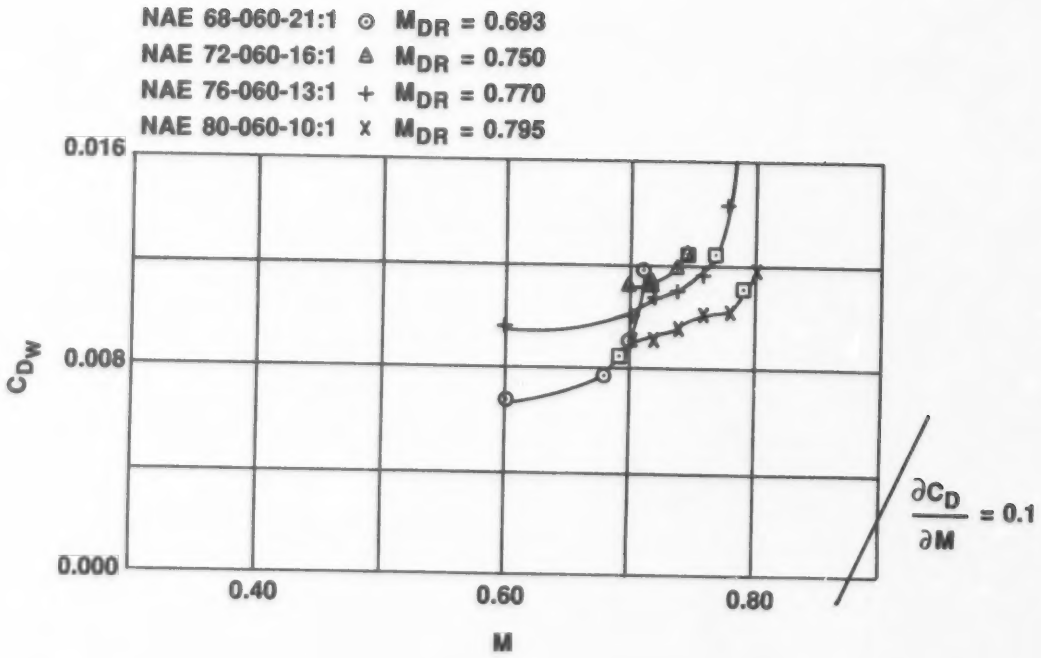


**FIG. 45: WAKE DRAG COEFFICIENT VERSUS MACH NUMBER**
**$C_{D_W}$ VERSUS M, (TRANSITION FIXED)**
**$C_{L_B}$ = 0.6, Re = 6.7 x $10^6$**

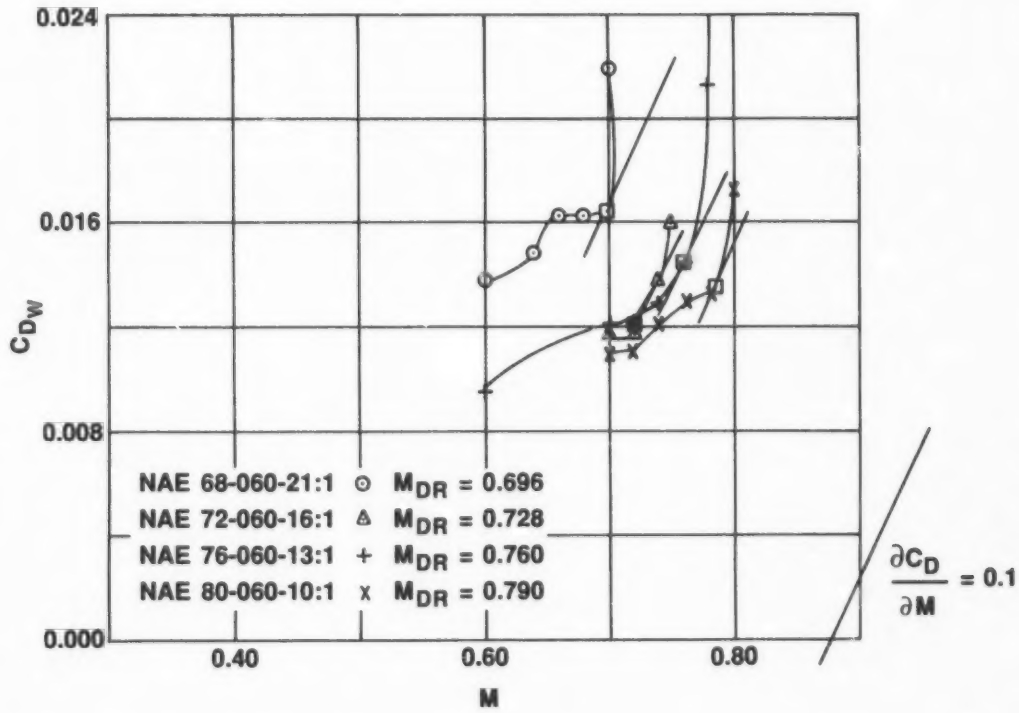


**FIG. 46: WAKE DRAG COEFFICIENT VERSUS MACH NUMBER $C_{D_W}$ VERSUS M, (TRANSITION FIXED)**

**$C_{L_B}$ = 0.7, Re = 6.7 x $10^6$**

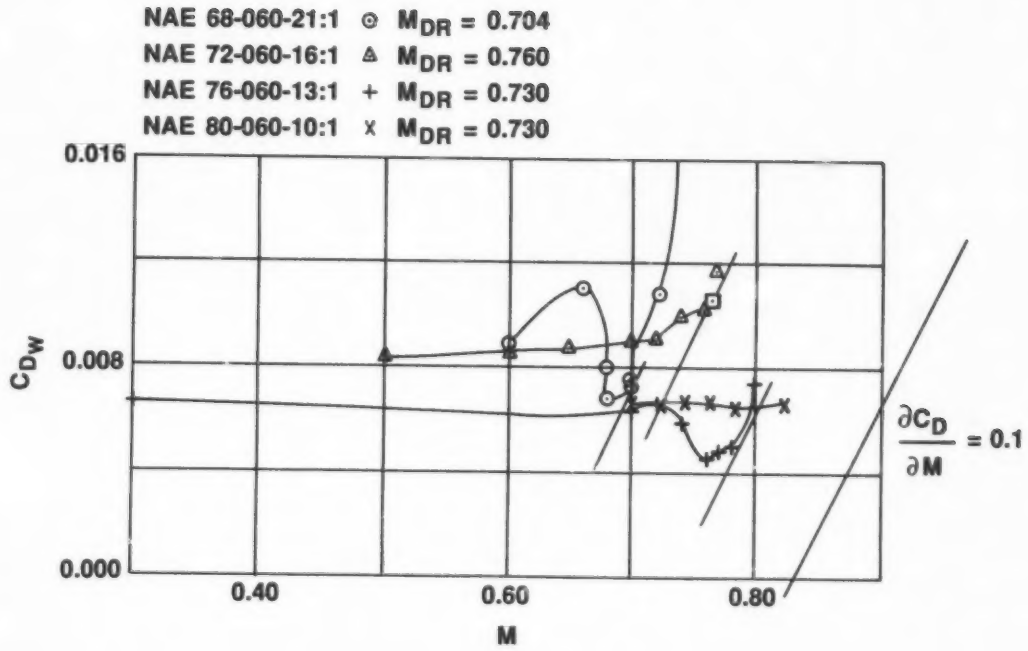


**FIG. 47: WAKE DRAG COEFFICIENT VERSUS MACH NUMBER**
**$C_{D_W}$ VERSUS M, (FREE TRANSITION)**
**$C_{L_B}$ = 0.3, Re = 12.5 x $10^6$**

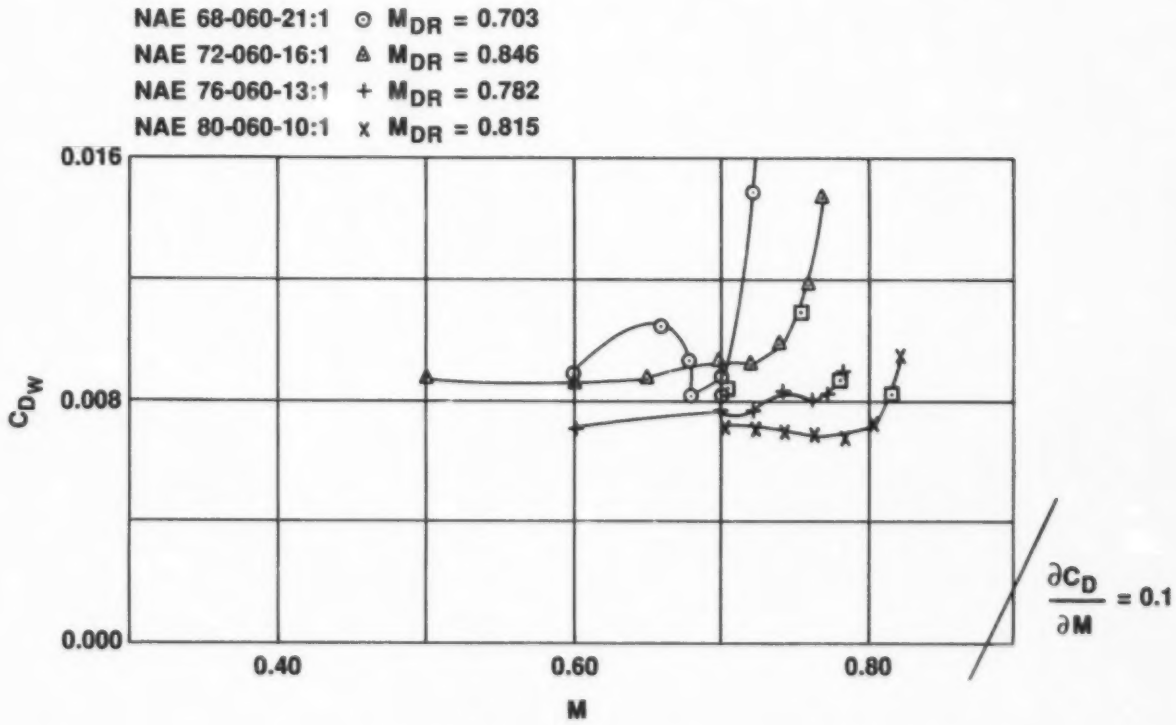


FIG. 48: WAKE DRAG COEFFICIENT VERSUS MACH NUMBER
$C_{D_W}$ VERSUS M, (FREE TRANSITION)
$C_{L_B}$ = 0.5, Re = 12.5 x $10^6$

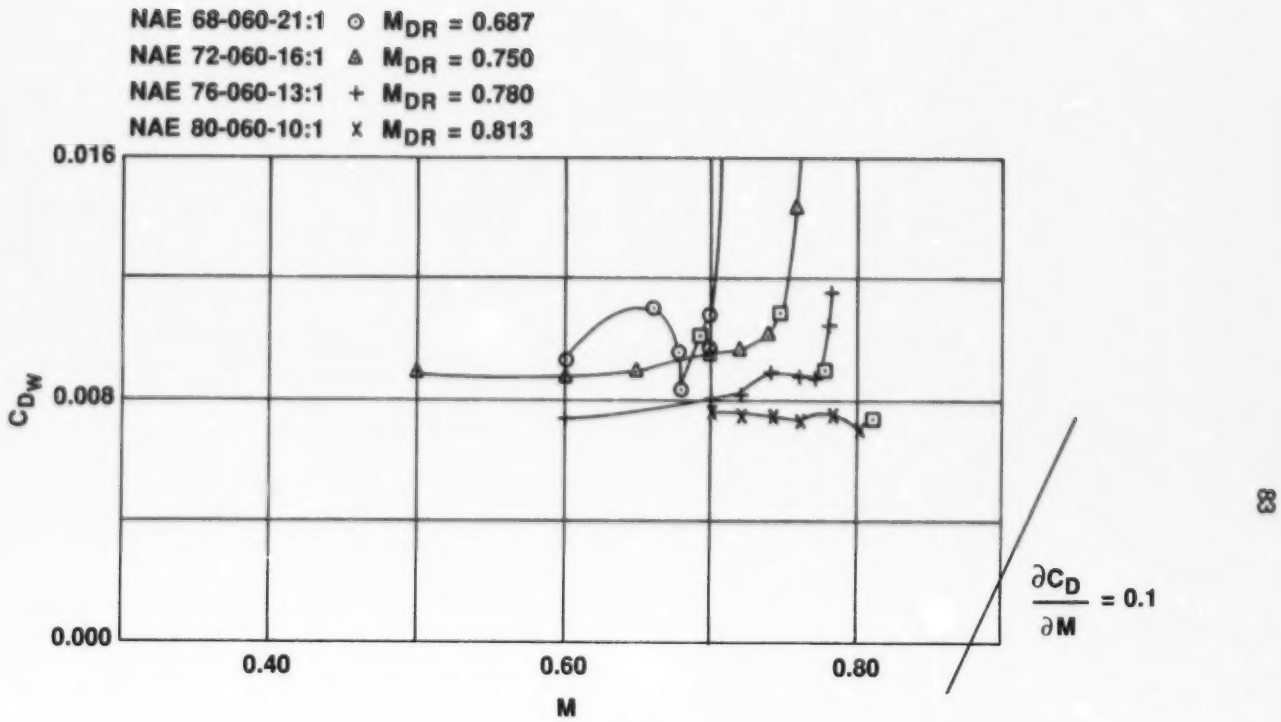


**FIG. 49: WAKE DRAG COEFFICIENT VERSUS MACH NUMBER**
**$C_{D_W}$ VERSUS M, (FREE TRANSITION)**
**$C_{L_B}$ = 0.6, Re = 12.5 x $10^6$**

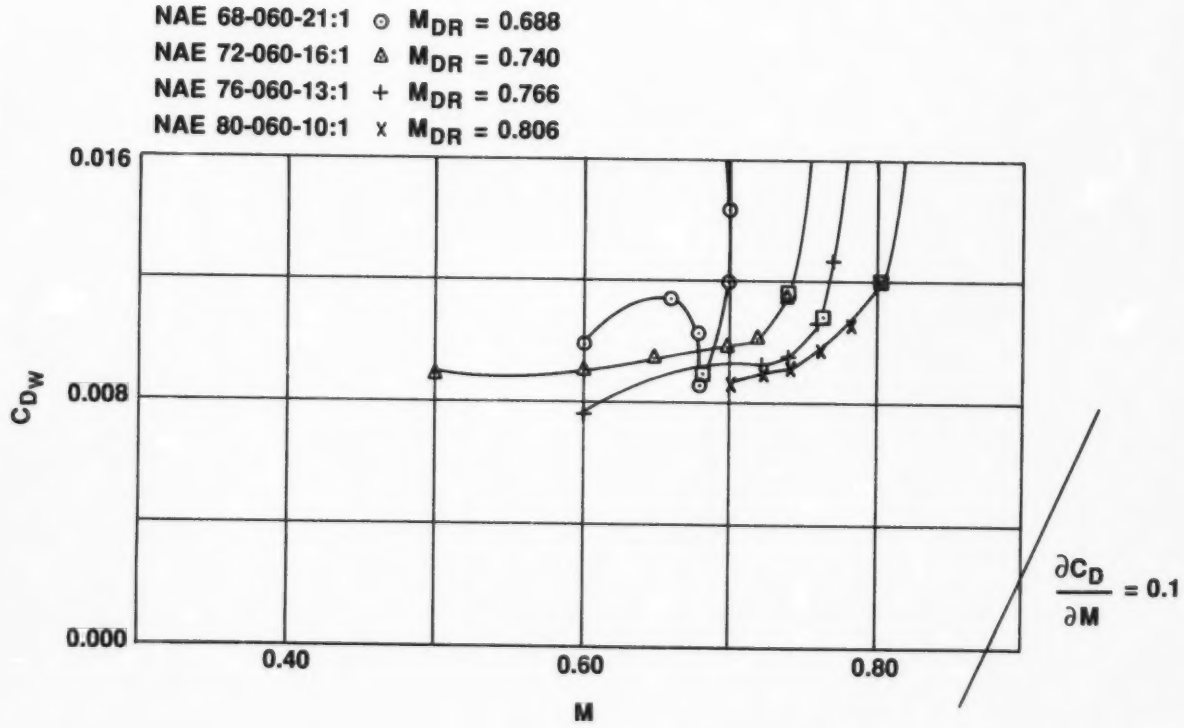


**FIG. 50: WAKE DRAG COEFFICIENT VERSUS MACH NUMBER**
**$C_{D_W}$ VERSUS M, (FREE TRANSITION)**
**$C_{L_B}$ = 0.7, Re = 12.5 x $10^6$**

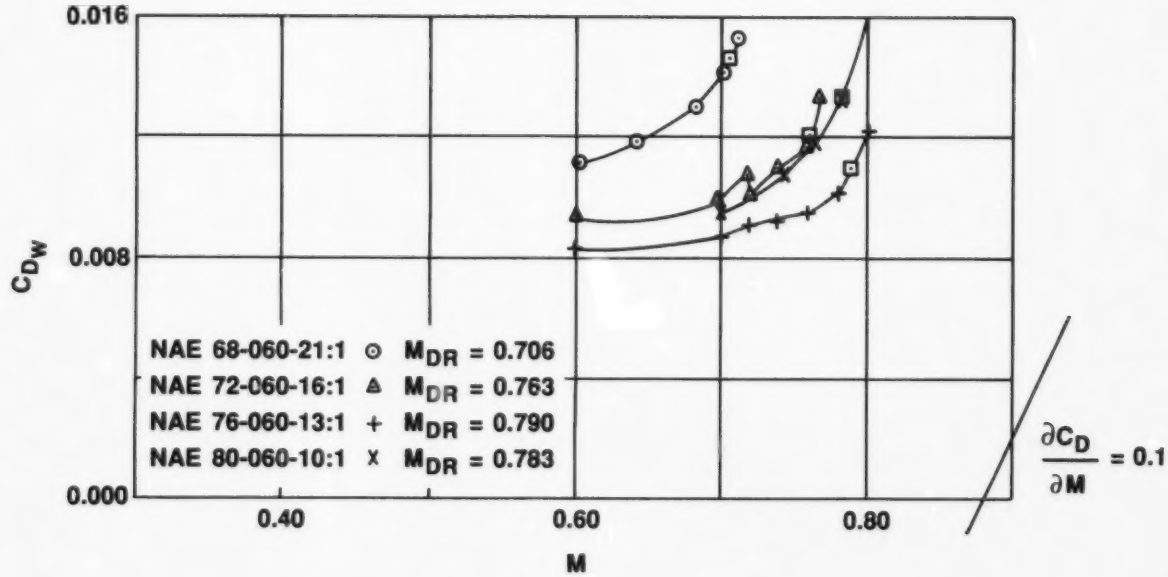


**FIG. 51: WAKE DRAG COEFFICIENT VERSUS MACH NUMBER**
**$C_{D_W}$ VERSUS M, (TRANSITION FIXED)**
**$C_{L_B}$ = 0.3, Re = 12.5 x $10^6$**

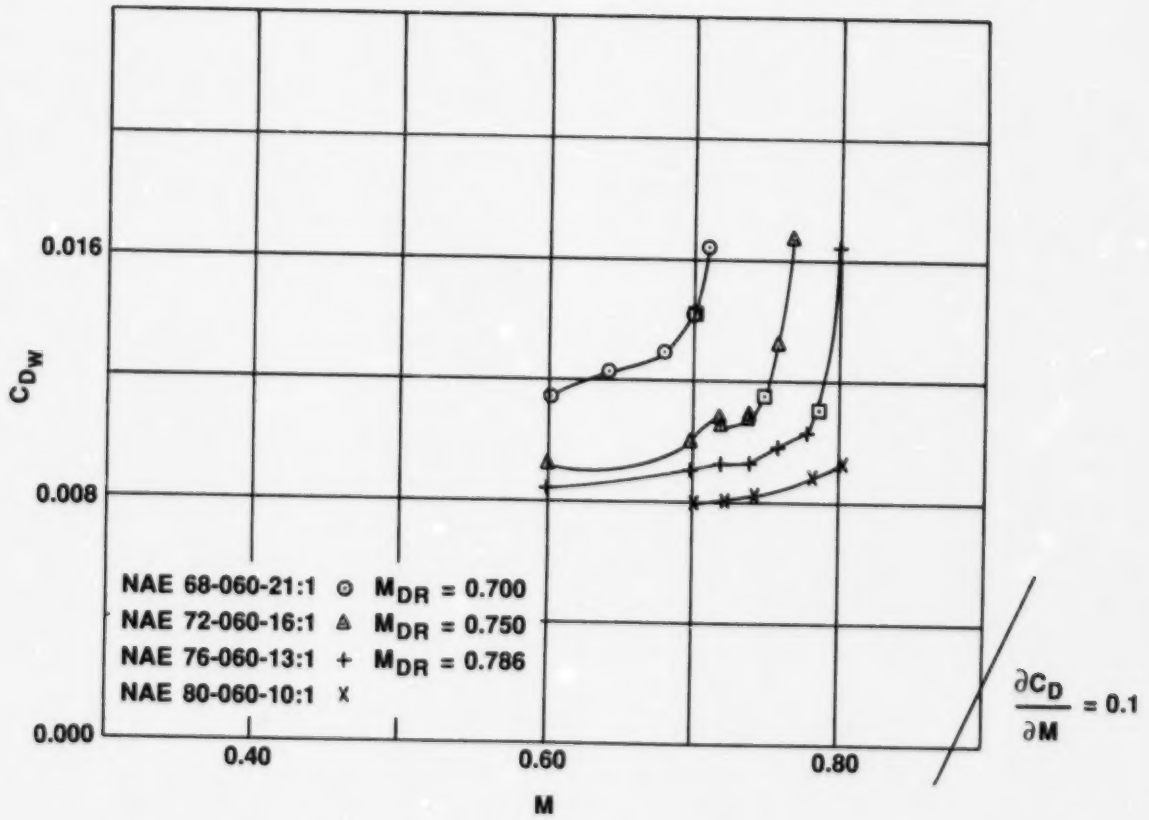


**FIG. 52: WAKE DRAG COEFFICIENT VERSUS MACH NUMBER**
**$C_{D_W}$ VERSUS M, (TRANSITION FIXED)**
**$C_{L_B}$ = 0.5, Re = 12.5 x $10^6$**

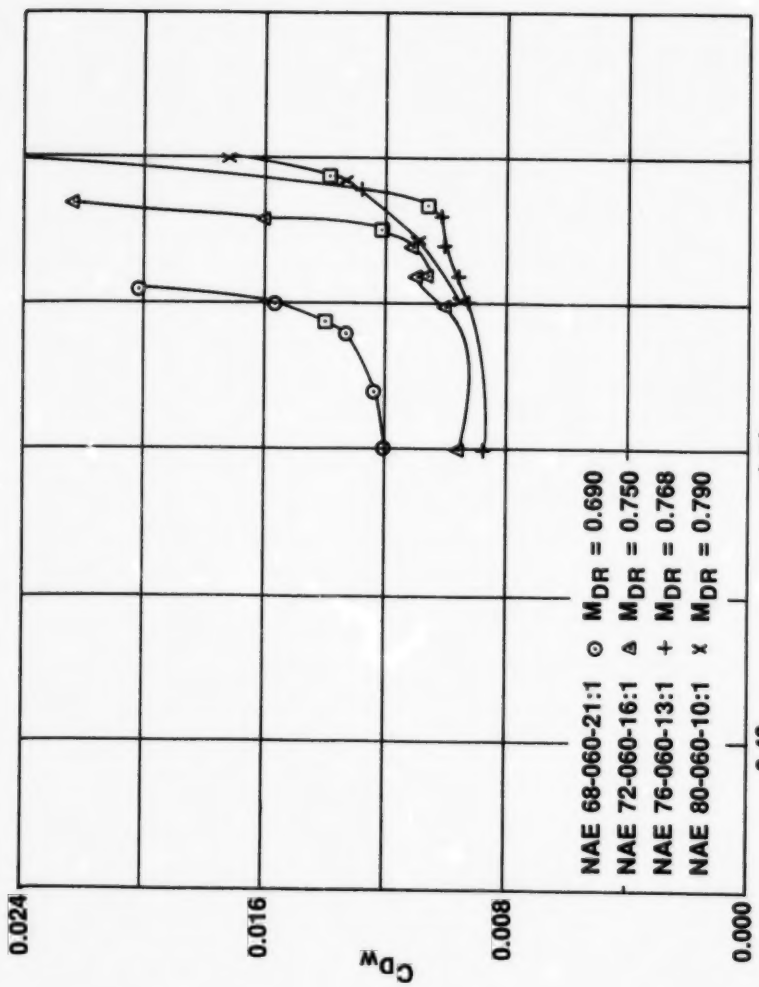


FIG. 53: WAKE DRAG COEFFICIENT VERSUS MACH NUMBER
$C_{D_W}$ VERSUS M, (TRANSITION FIXED)
$C_{L_B}$ = 0.6, Re = 12.5 x $10^6$

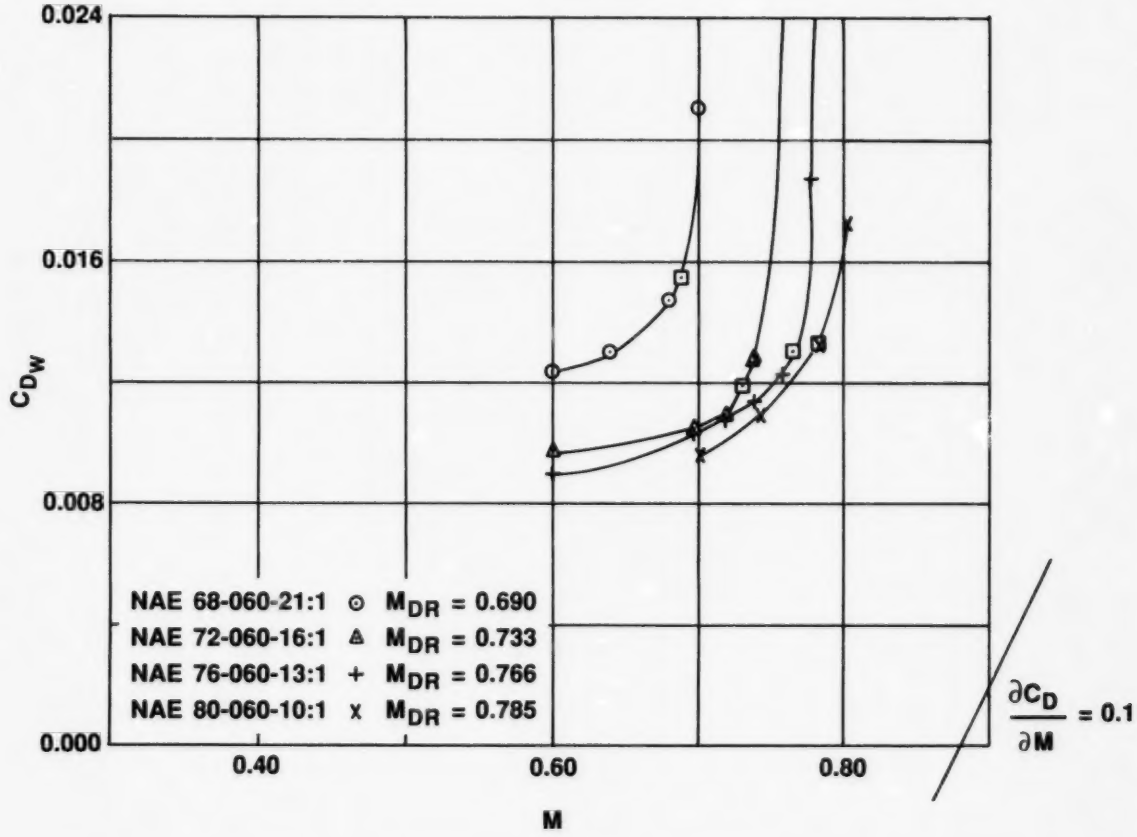


**FIG. 54: WAKE DRAG COEFFICIENT VERSUS MACH NUMBER $C_{D_W}$ VERSUS M, (TRANSITION FIXED)**

**$C_{L_B}$ = 0.7, Re = 12.5 x $10^6$**

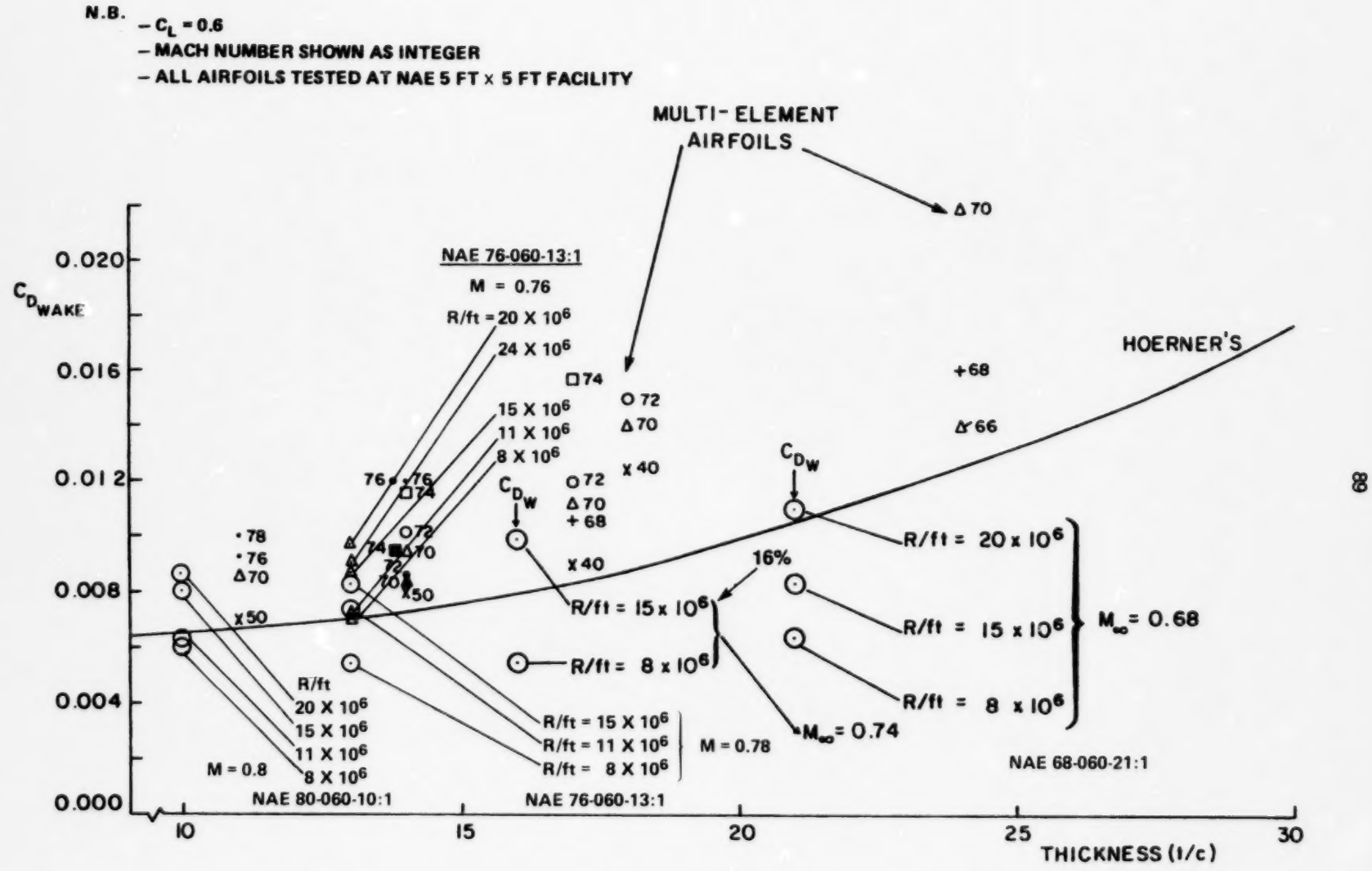


**FIG. 55: DRAG COMPARISONS WITH OTHER AIRFOILS USING $C_{D_W}$**

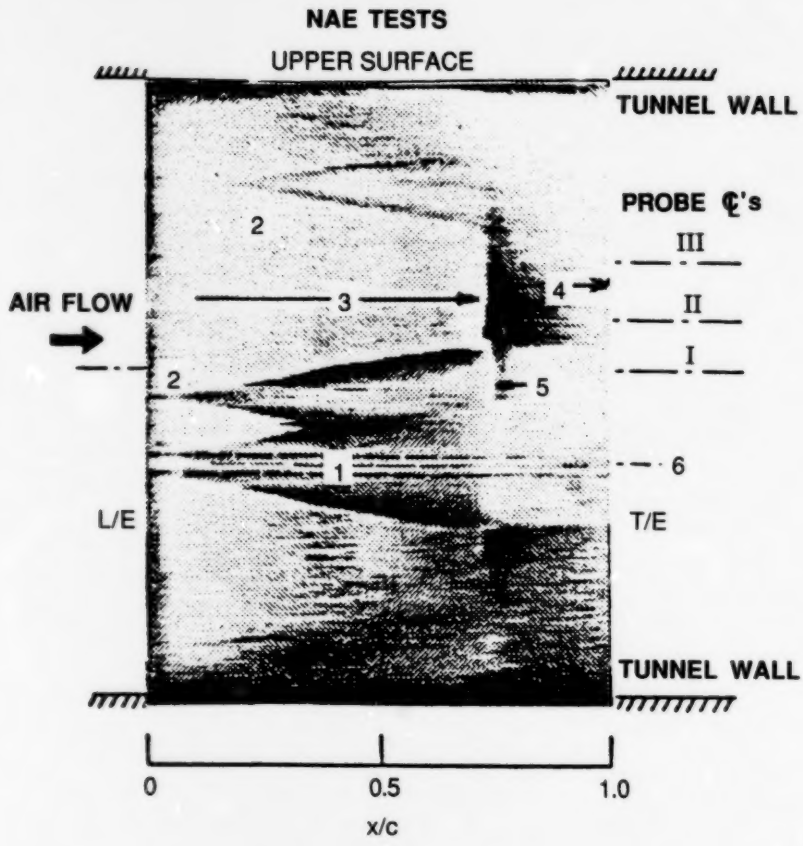


1 TRANSITION WEDGE DUE TO LINE OF PRESSURE TAPS

2 TRANSITION WEDGES DUE TO SPECKS OF DIRT

3 LAMINAR RUN BACK TO 70% CHORD

4 TURBULENT FLOW IN PRESSURE RECOVERY REGION

5 SHOCK LOCATION IN TURBULENT FLOW

6 PRESSURE TAPPINGS OFFSET TO REDUCE EFFECTS OF TRANSITION ON PROBE NO. 1

**FIG. 56: FLOW VISUALIZATION OF NAE 72-060-16:1 AT Re = 8 MILLION; M = 0.75, AND $C_L$ = 0.6**

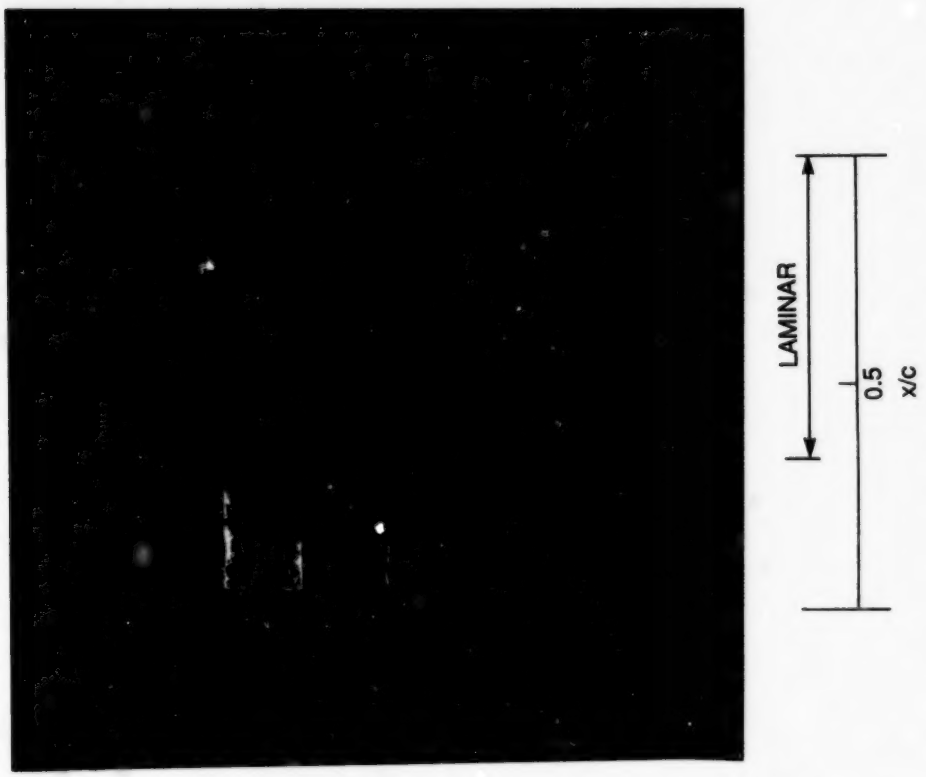


**FIG. 57: FLOW VISUALIZATION OF NAE 78-060-13:1 AT M = 0.78, Re = 6.7 x $10^6$, $\alpha$ = 0.33**

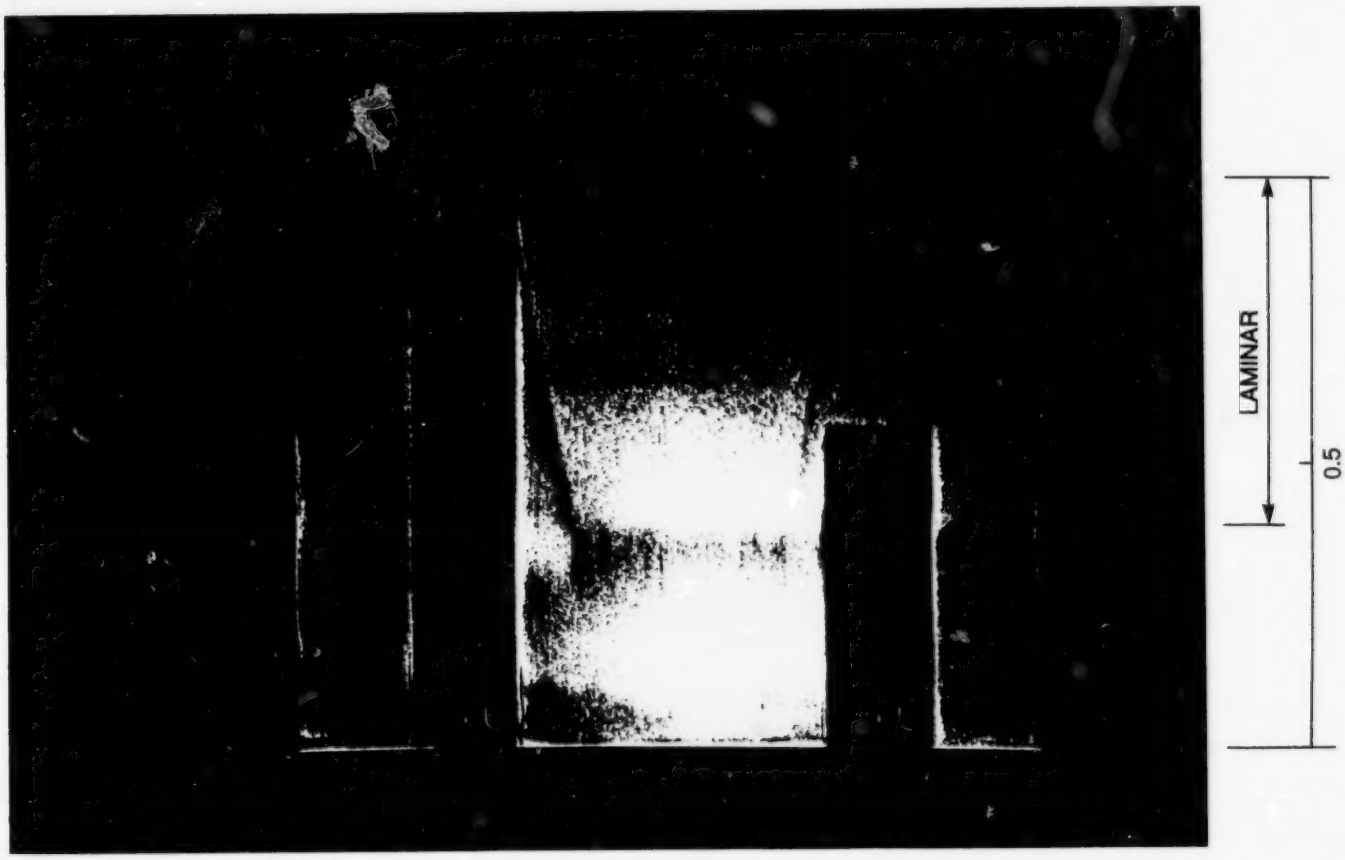


**FIG. 58: FLOW VISUALIZATION OF NAE 80-060-10:1 AT M = 0.8, Re = 6.7 x $10^6$, $\alpha$ = 1.39**

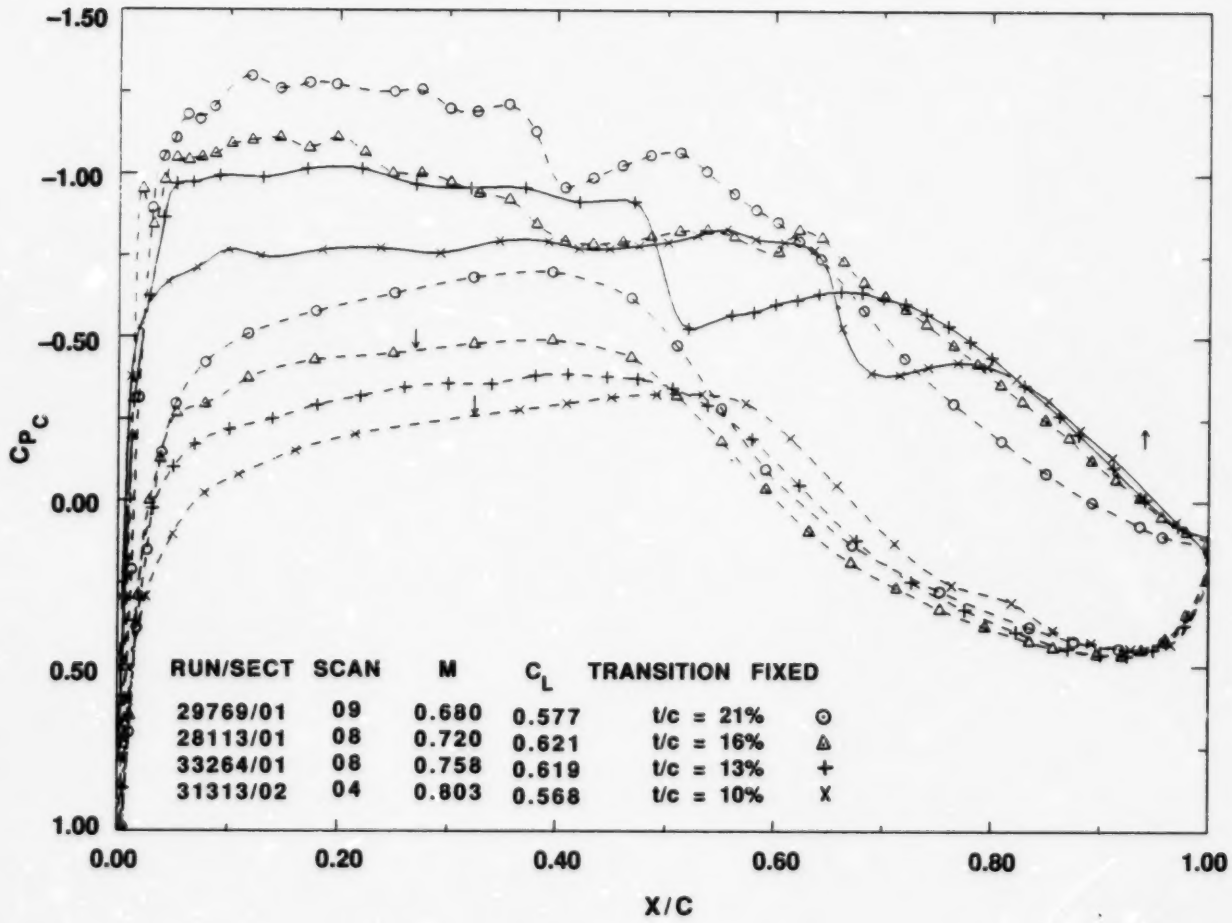


**FIG. 59a: PRESSURE DISTRIBUTION AT THE DESIGN CONDITIONS, Re/c = 12.5 x $10^6$**

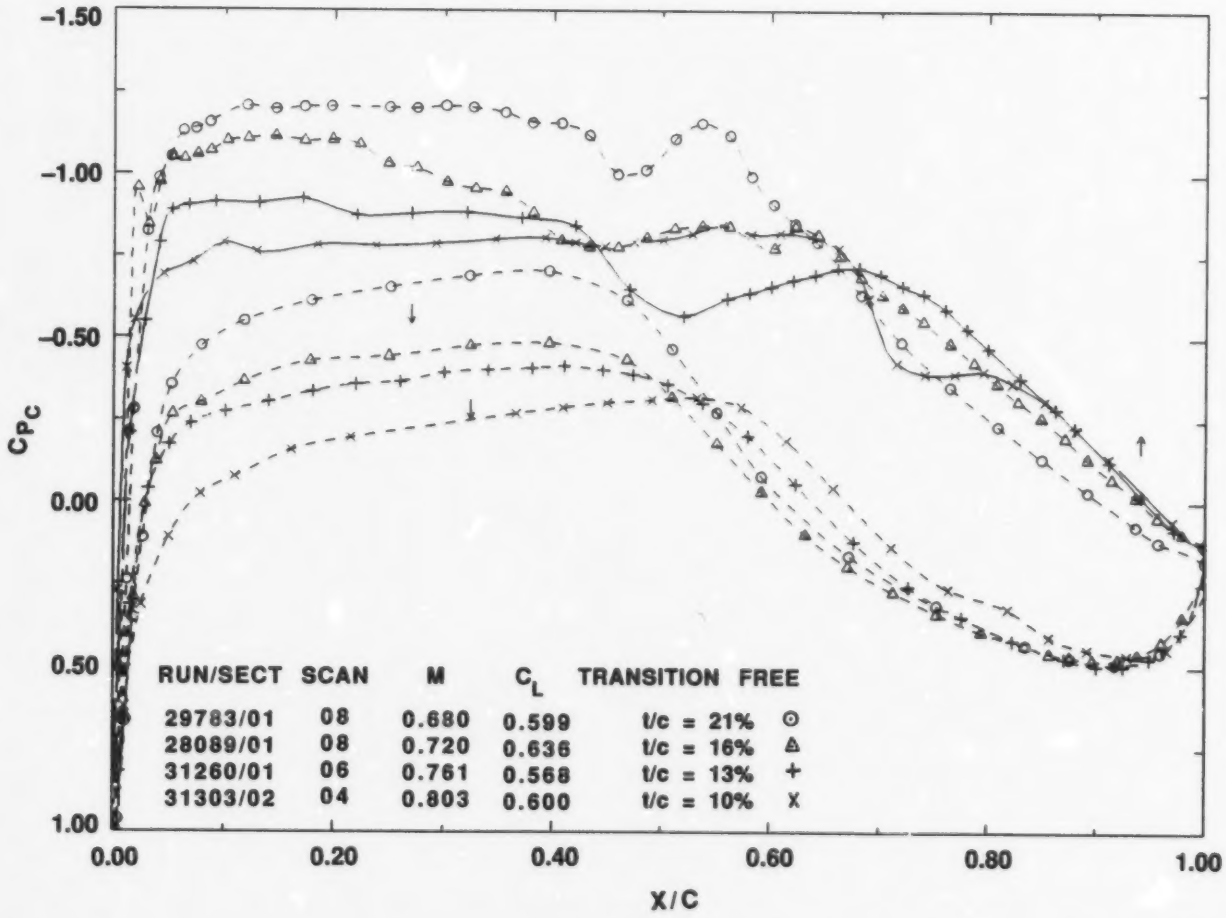


**FIG. 59b: PRESSURE DISTRIBUTION UNDER FREE TRANSITION CONDITIONS, Re/c = 12.5 x $10^6$**

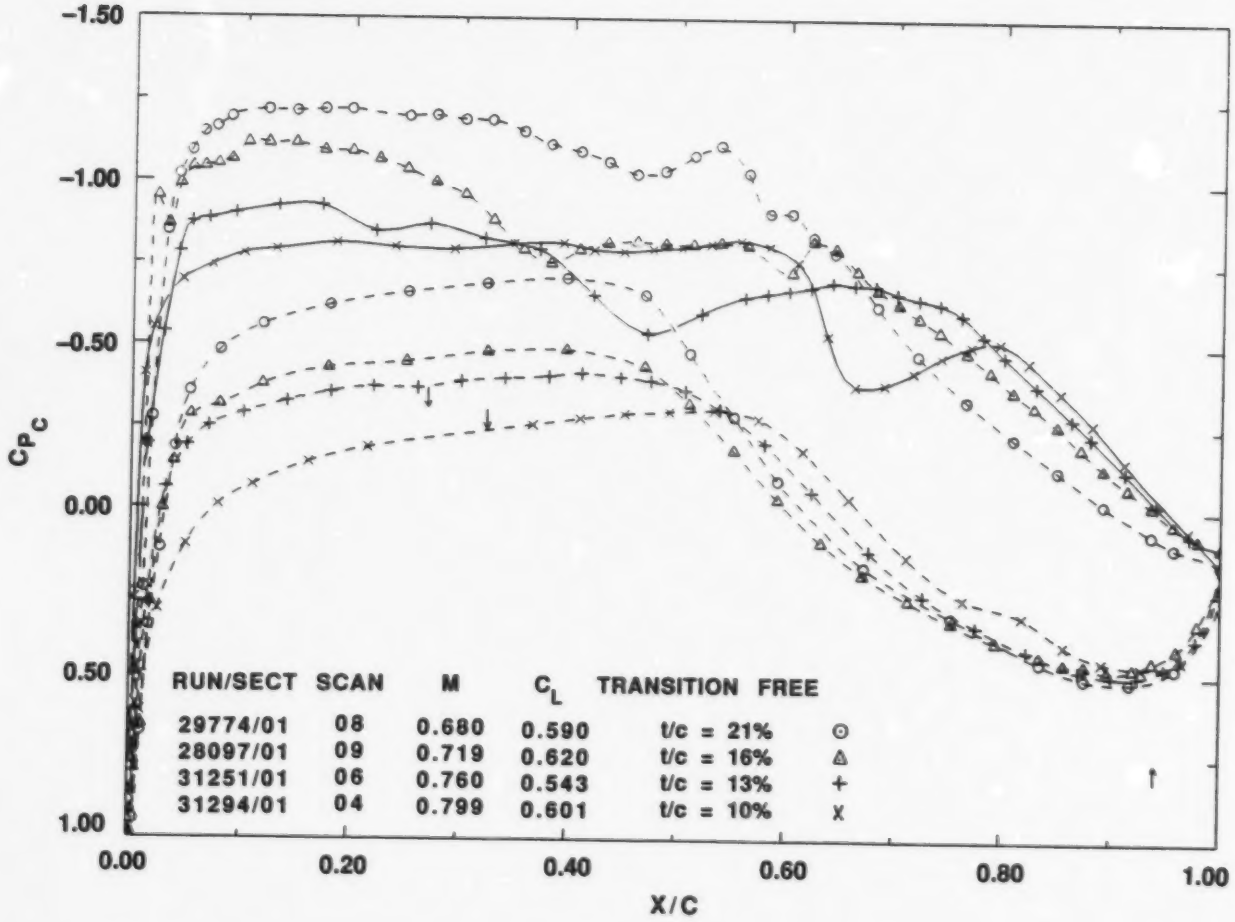


**FIG. 60: PRESSURE DISTRIBUTION UNDER FREE TRANSITION CONDITIONS, Re/c = 6.7 x $10^6$**

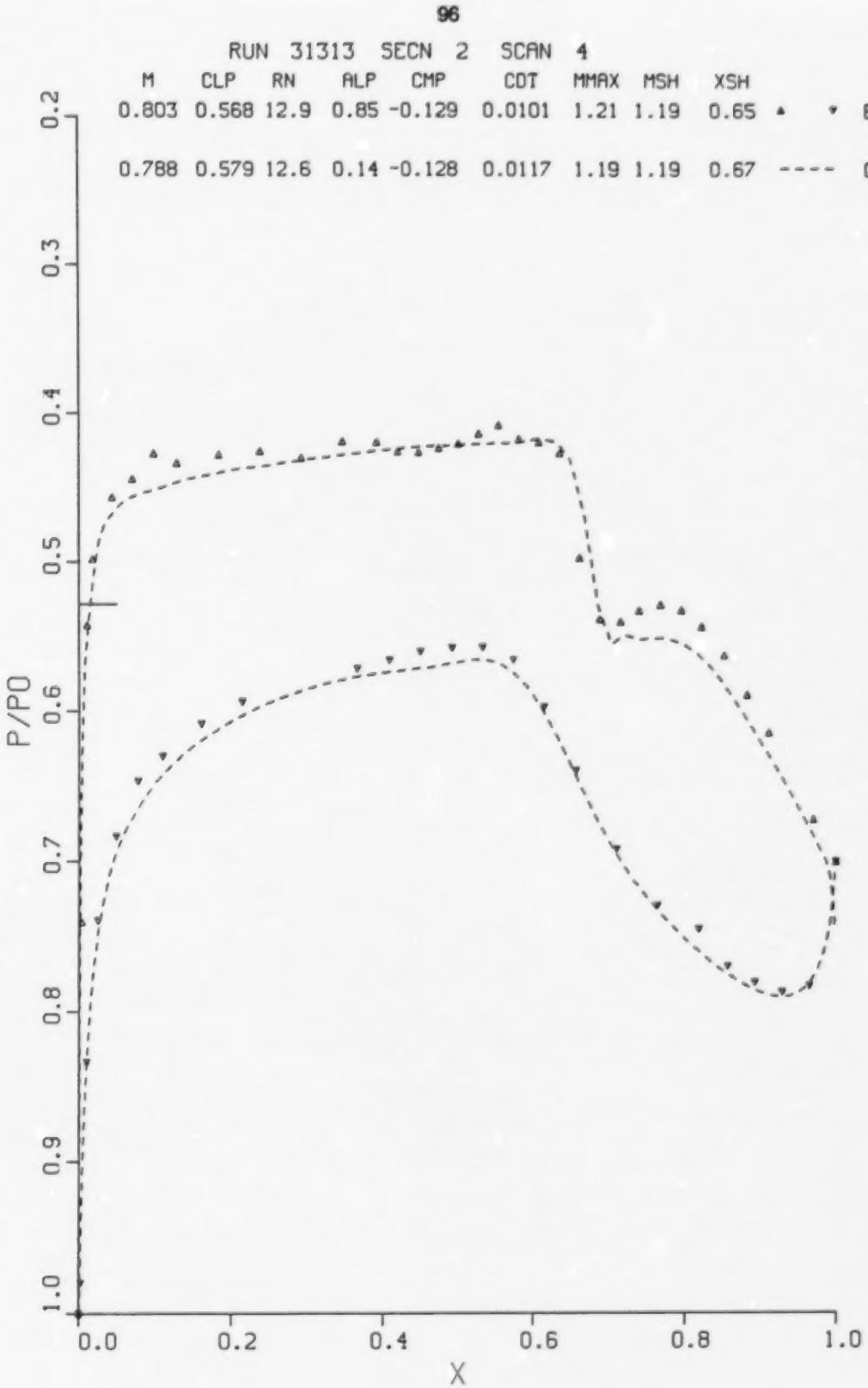


**FIG. 61a: GRUMFOIL VERSUS EXPERIMENT. 'SIDEWALL' CORRECTION OF –0.015 APPLIED. TRANSITION FIXED 10% AIRFOIL**

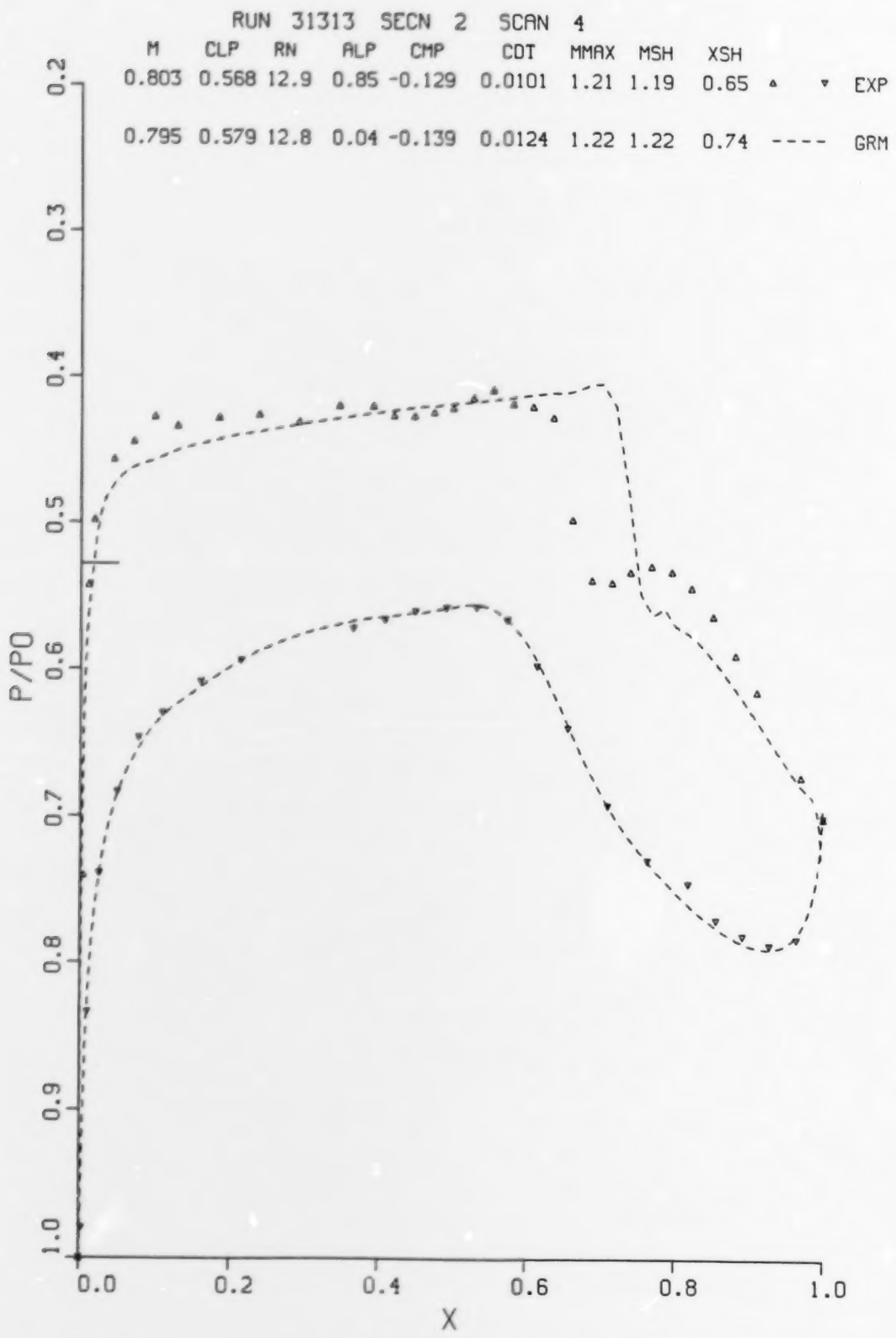


**FIG. 61b: GRUMFOIL VERSUS EXPERIMENT. 'SIDEWALL' CORRECTION OF –0.008 APPLIED. TRANSITION FIXED 10% AIRFOIL**

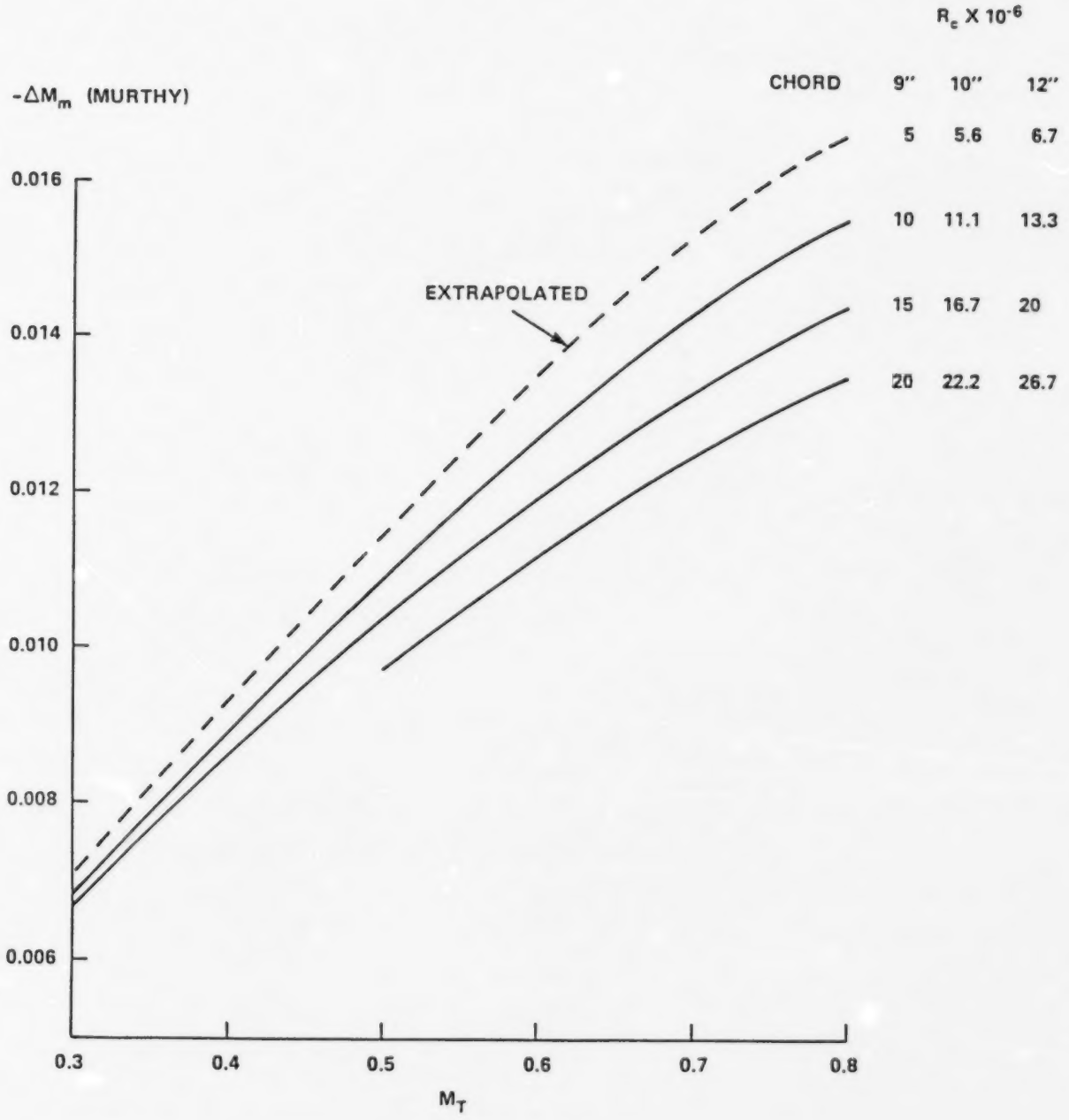


**FIG. 62: SIDEWALL CORRECTION COMPUTED ACCORDING TO MURTHY USING TUNNEL MEASURED VALUES OF $\delta^*$**

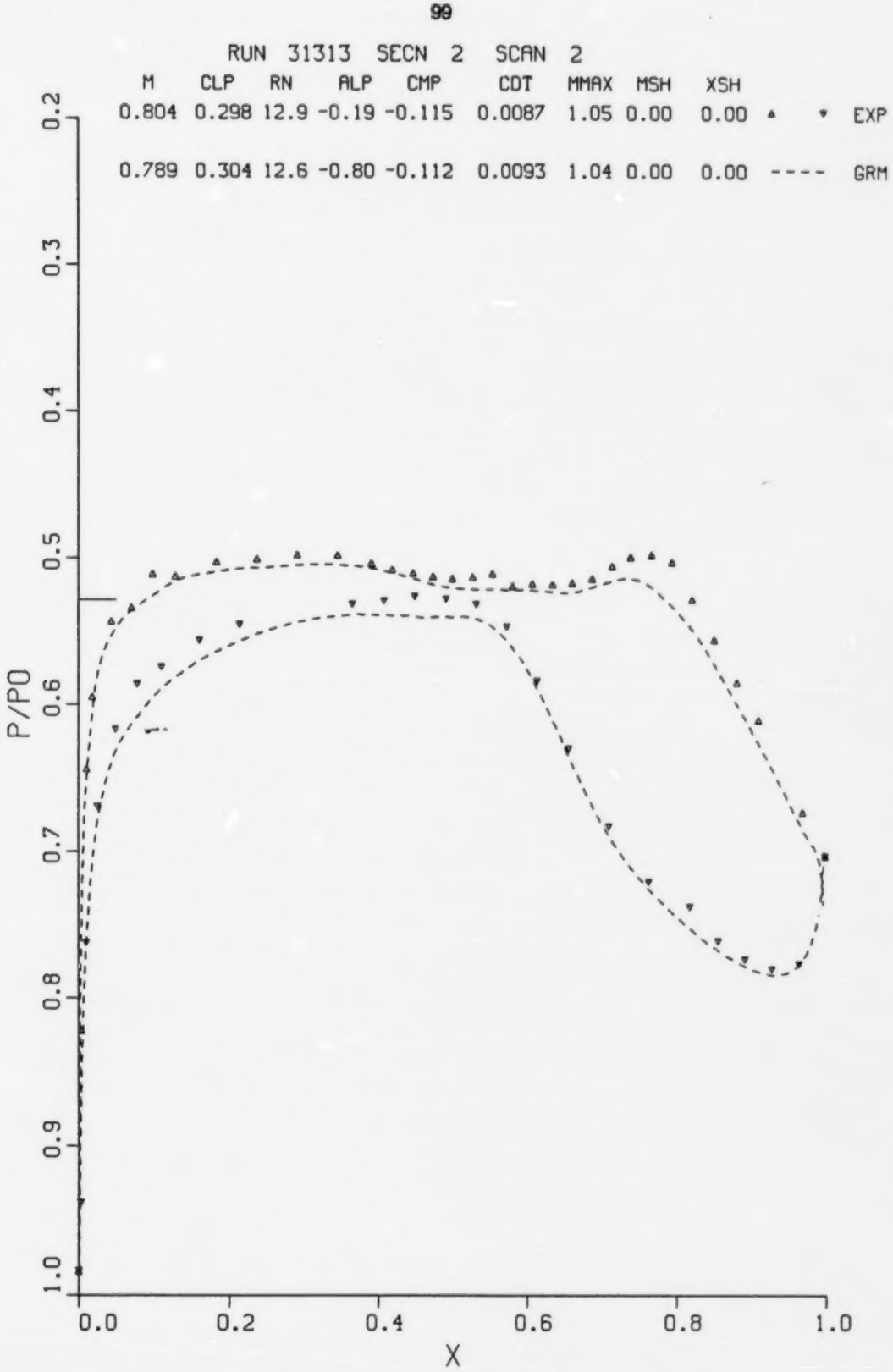


**FIG. 63a: COMPARISON OF GRUMFOIL AND EXPERIMENT, TRANSTION FIXED. 10% AIRFOIL. $C_L$ = 0.298**

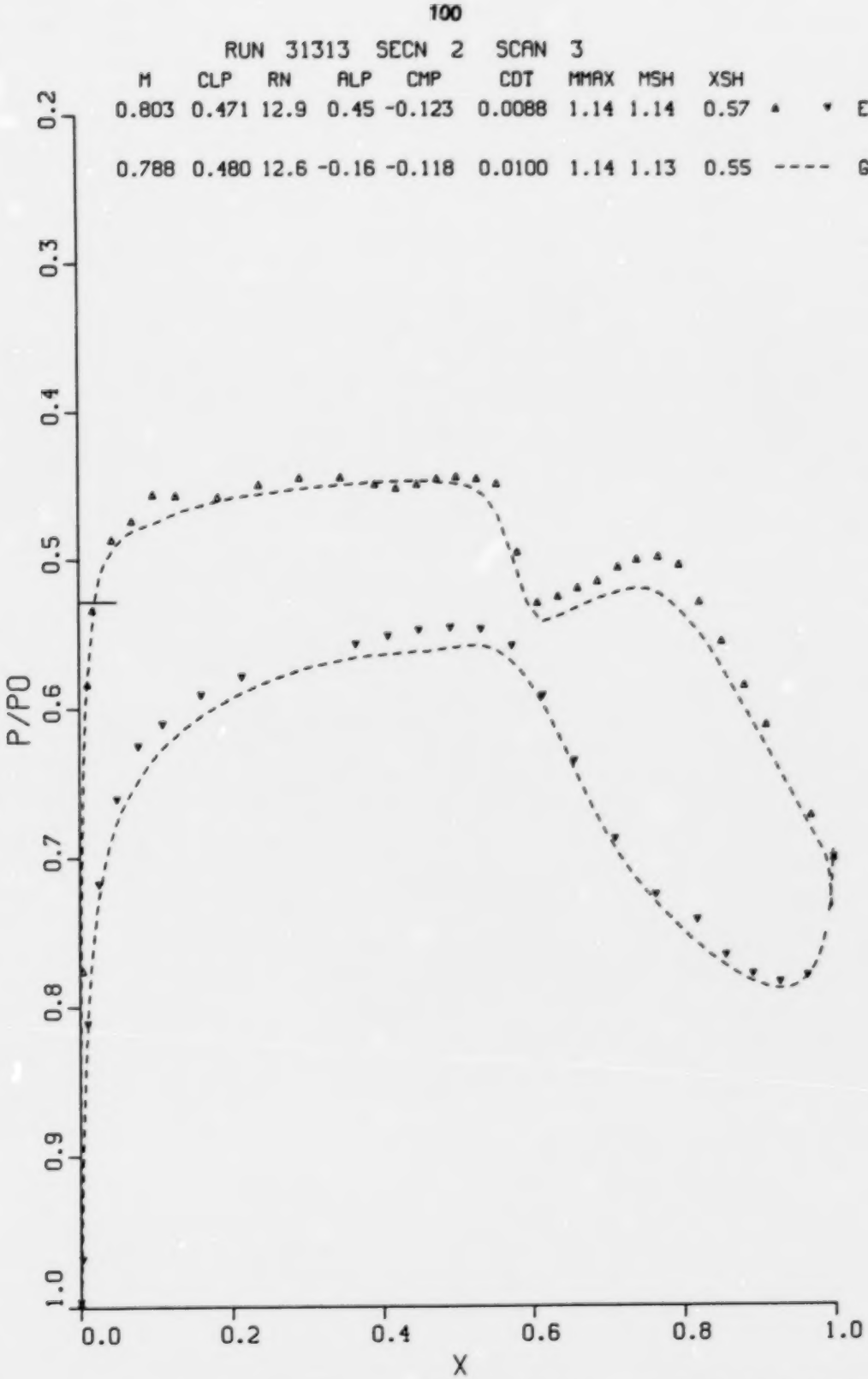


**FIG. 63b: COMPARISON OF GRUMFOIL AND EXPERIMENT, TRANSITION FIXED. 10% AIRFOIL. $C_L \approx 0.471$**

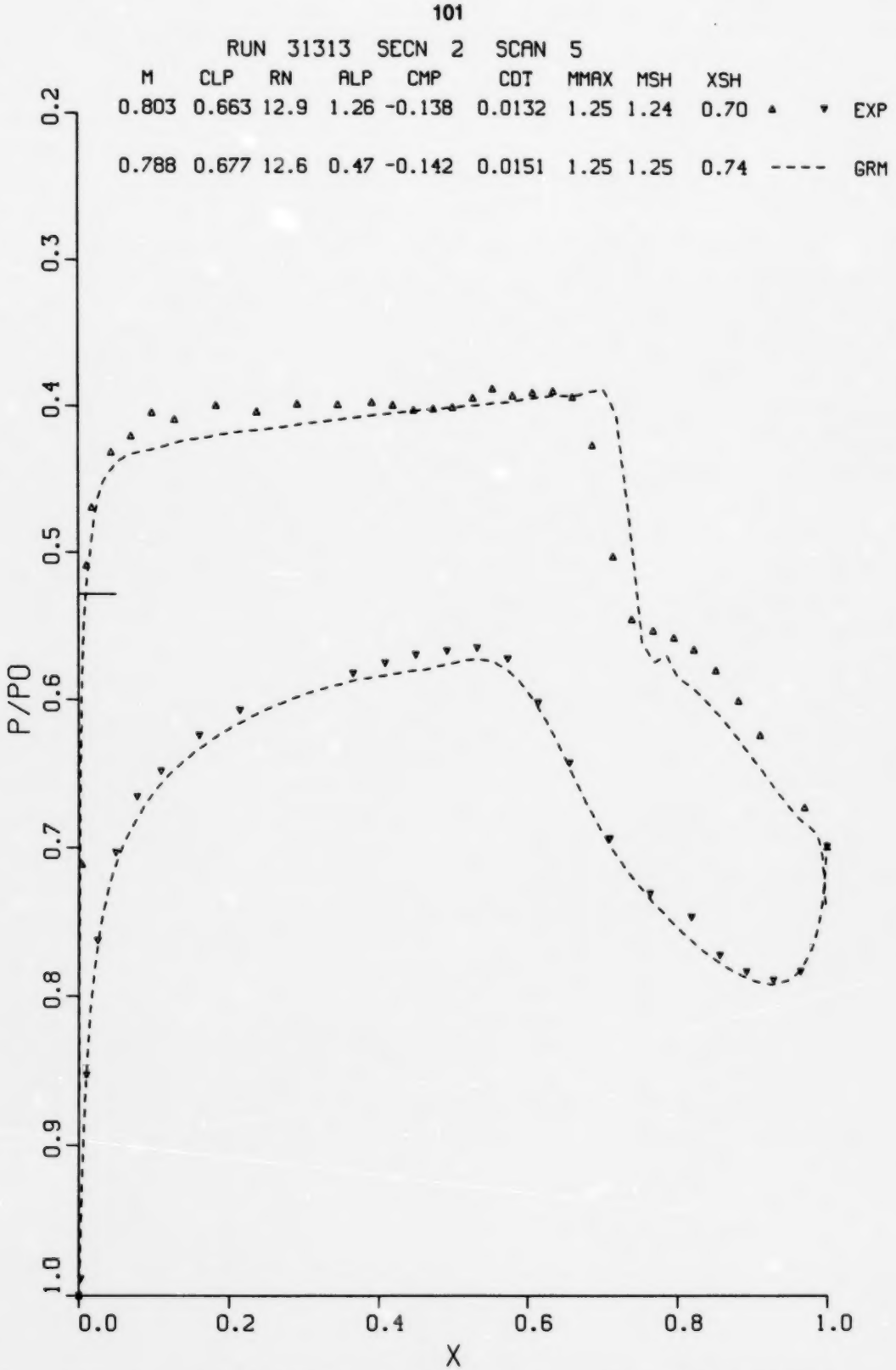


**FIG. 63c: COMPARISON OF GRUMFOIL AND EXPERIMENT, TRANSITION FIXED. 10% AIRFOIL. $C_L \approx 0.663$**

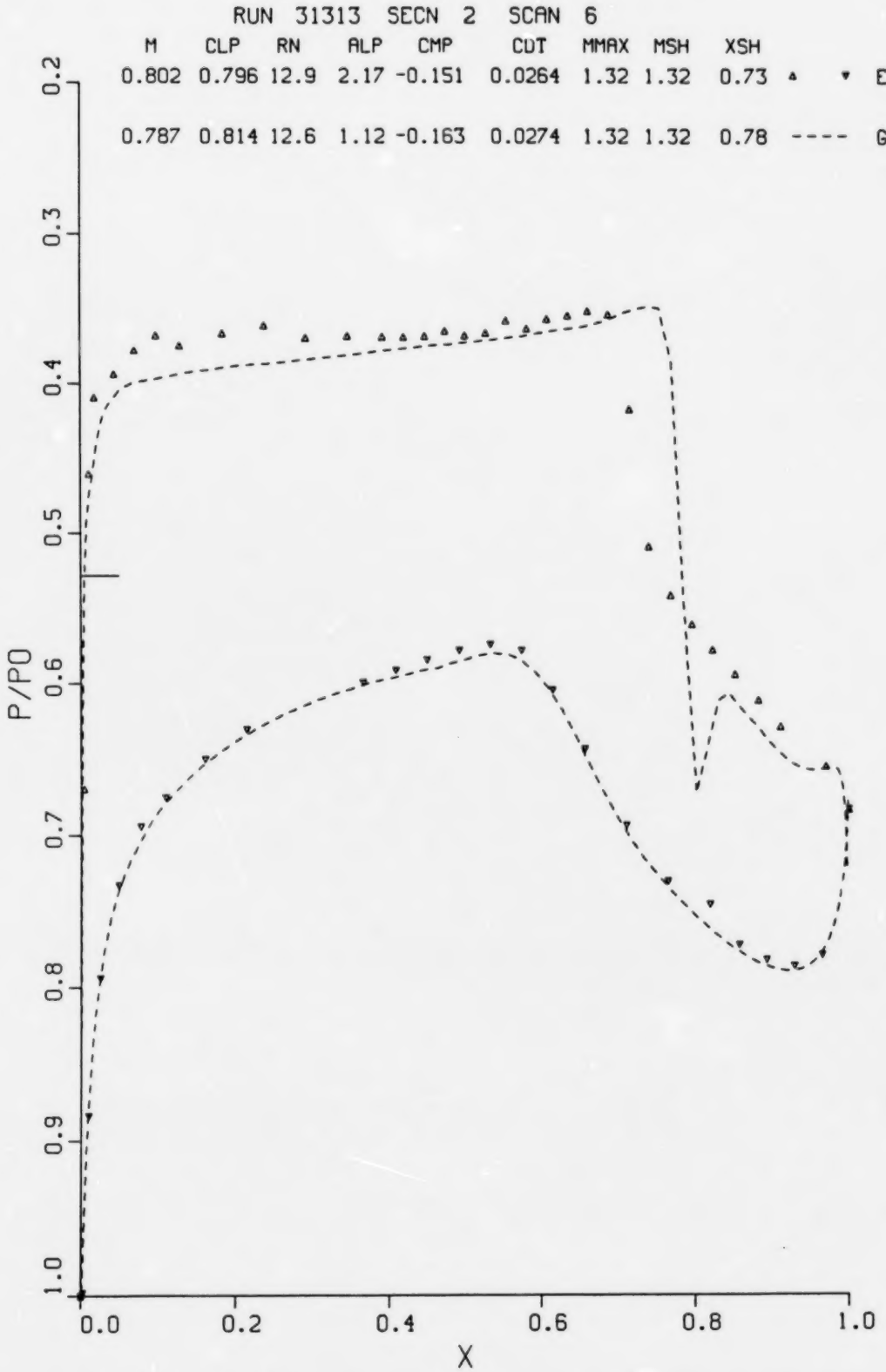


**FIG. 63d: COMPARISON OF GRUMFOIL AND EXPERIMENT, TRANSITION FIXED. 10% AIRFOIL. $C_L \approx 0.796$**

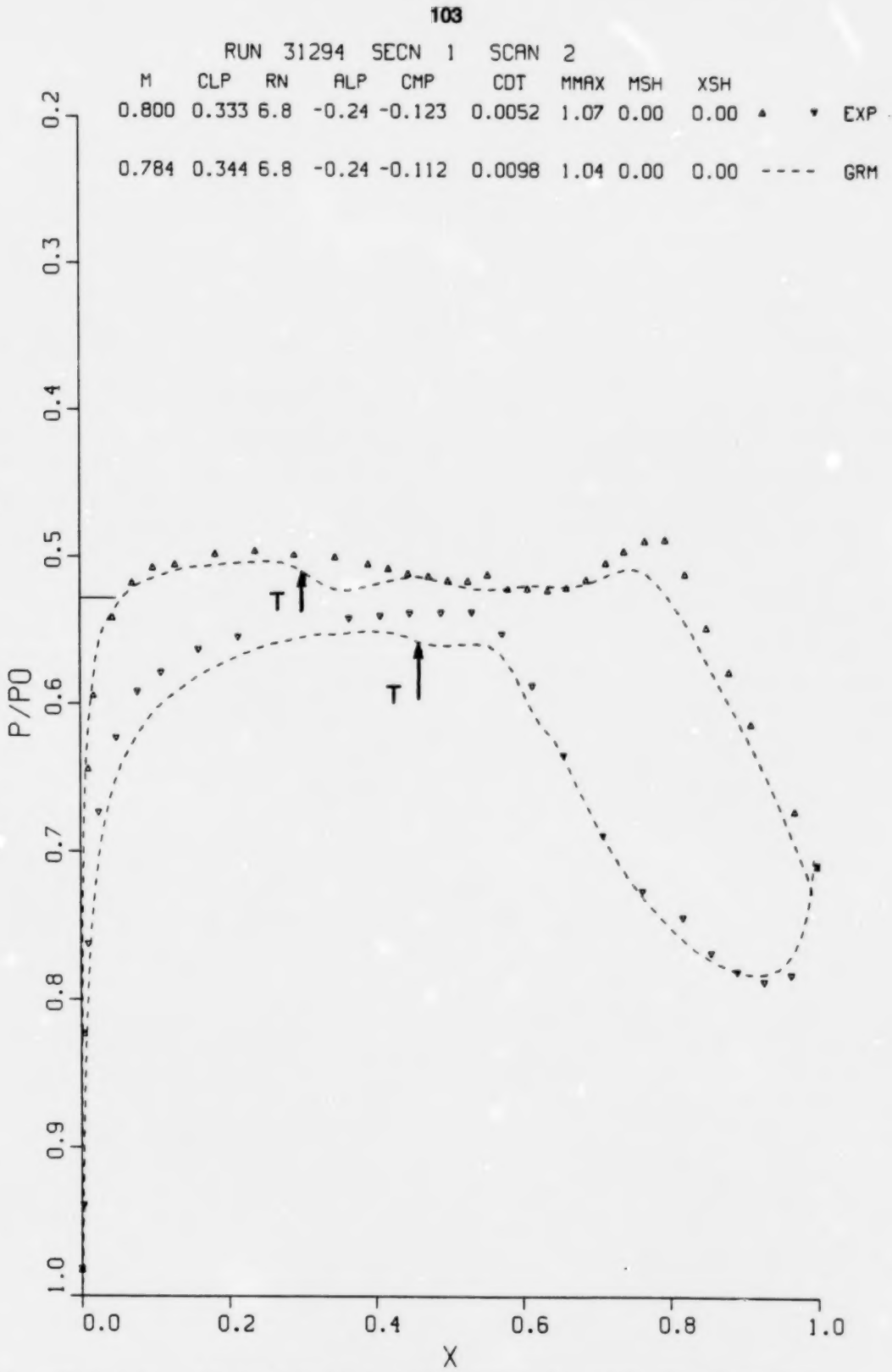


**FIG. 64a: COMPARISON OF GRUMFOIL AND EXPERIMENT, TRANSITION FREE. 10% AIRFOIL. $C_L$ = 0.333**

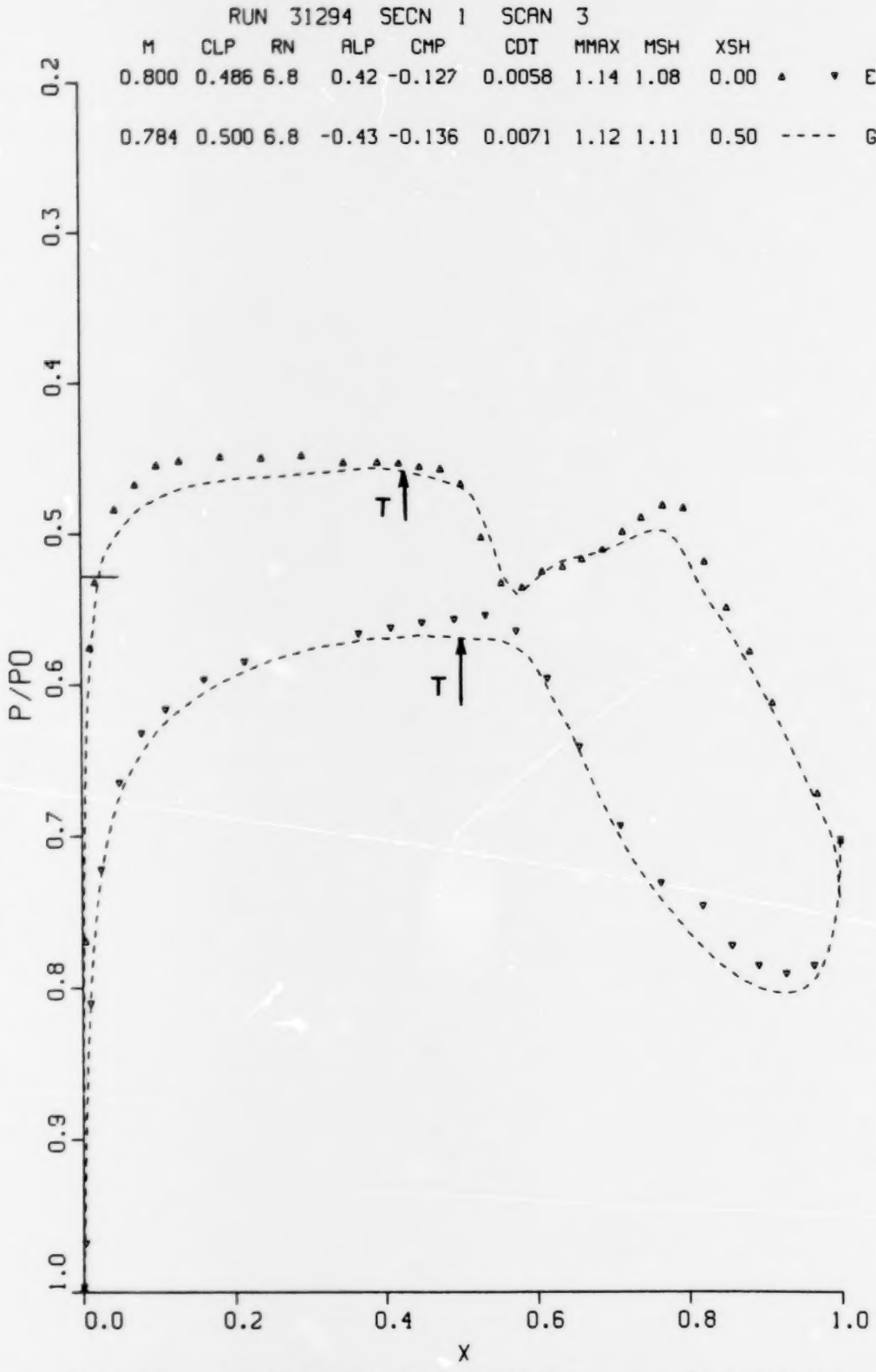


**FIG. 64b: COMPARISON OF GRUMFOIL AND EXPERIMENT, TRANSITION FREE. 10% AIRFOIL. $C_L \approx 0.486$**

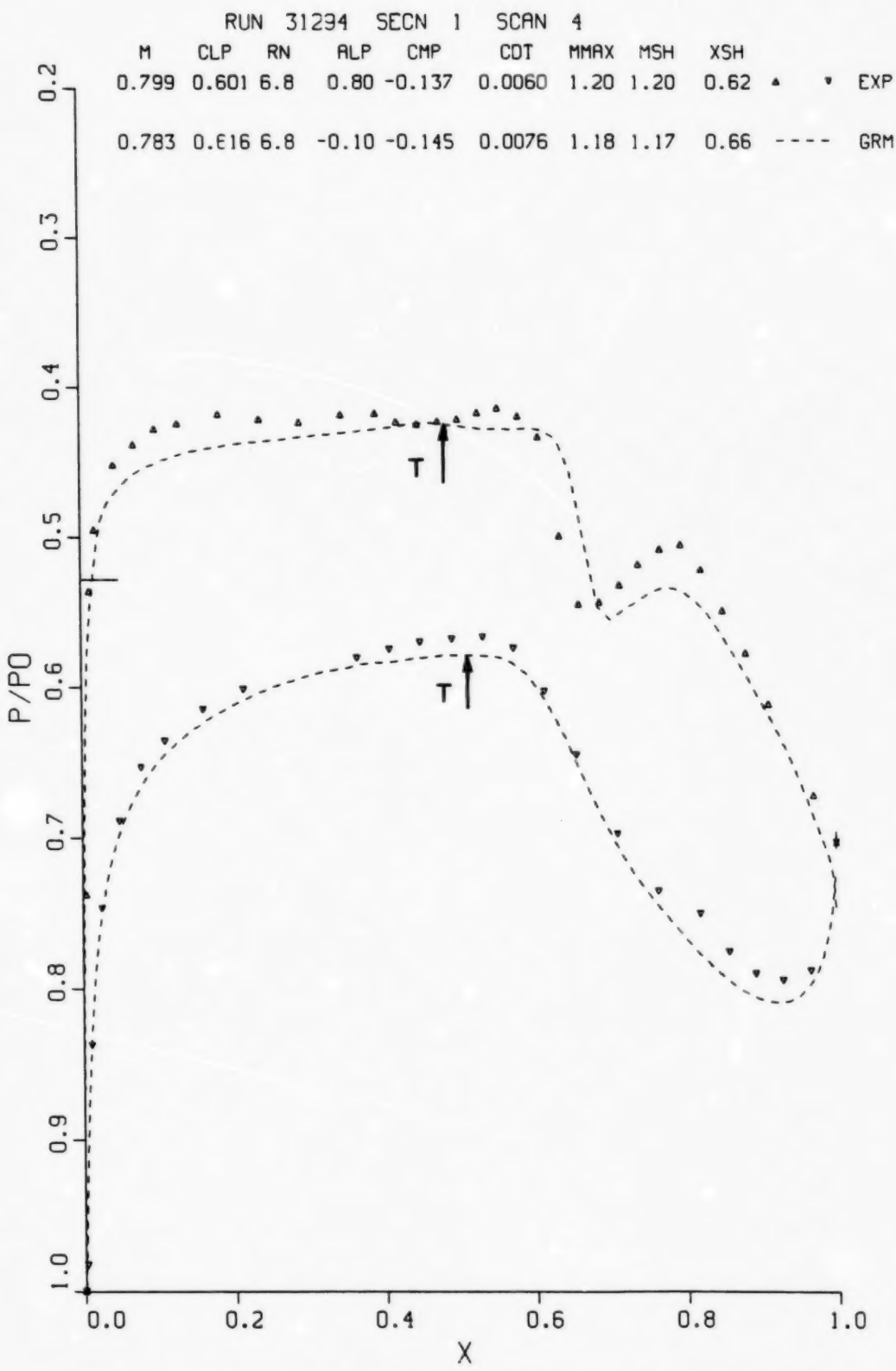


**FIG. 64c: COMPARISON OF GRUMFOIL AND EXPERIMENT, TRANSITION FREE. 10% AIRFOIL. $C_L \sim 0.601$**

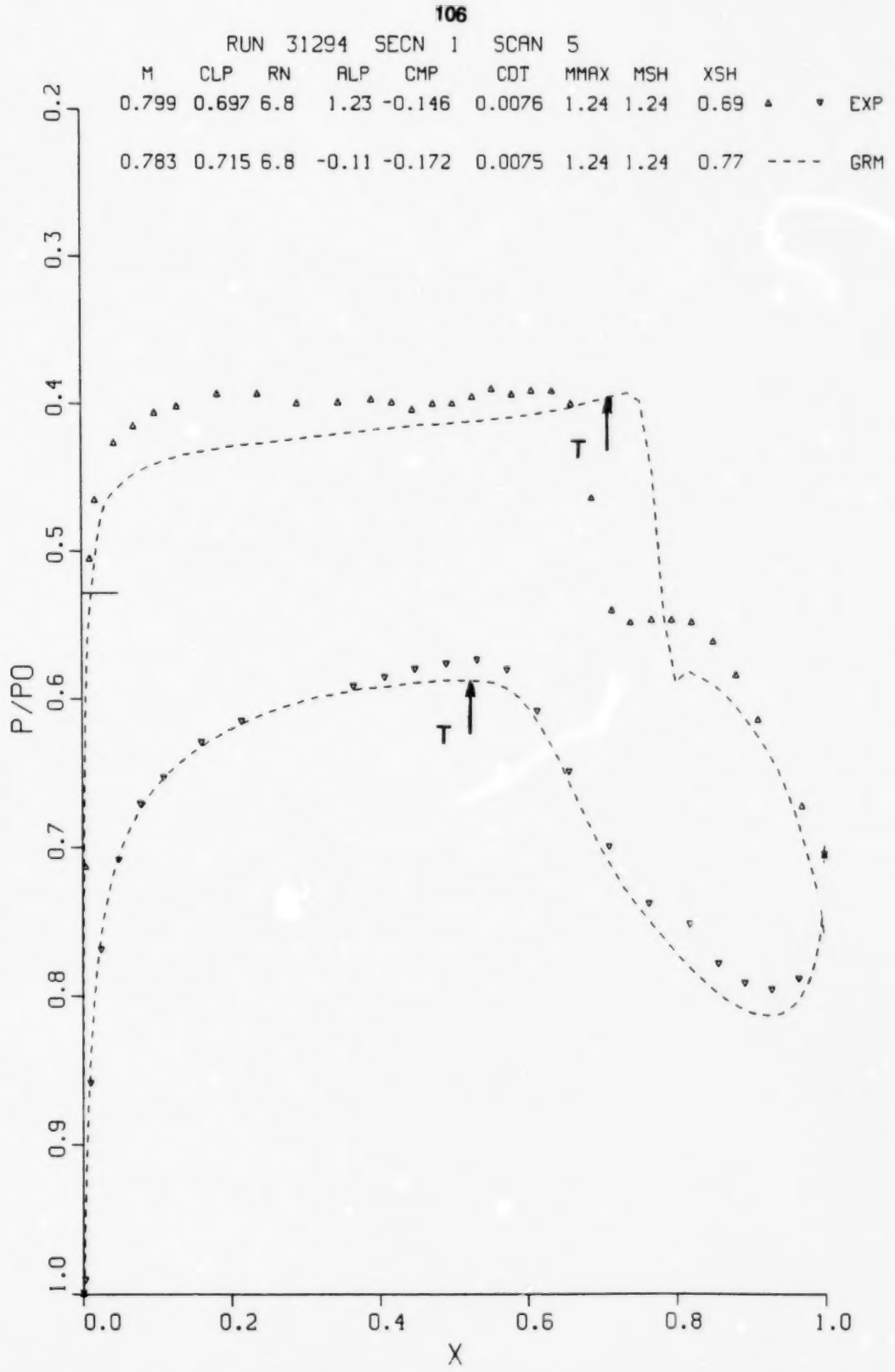


**FIG. 64d: COMPARISON OF GRUMFOIL AND EXPERIMENT, TRTANSITION FREE. 10% AIRFOIL. $C_L \approx 0.697$**

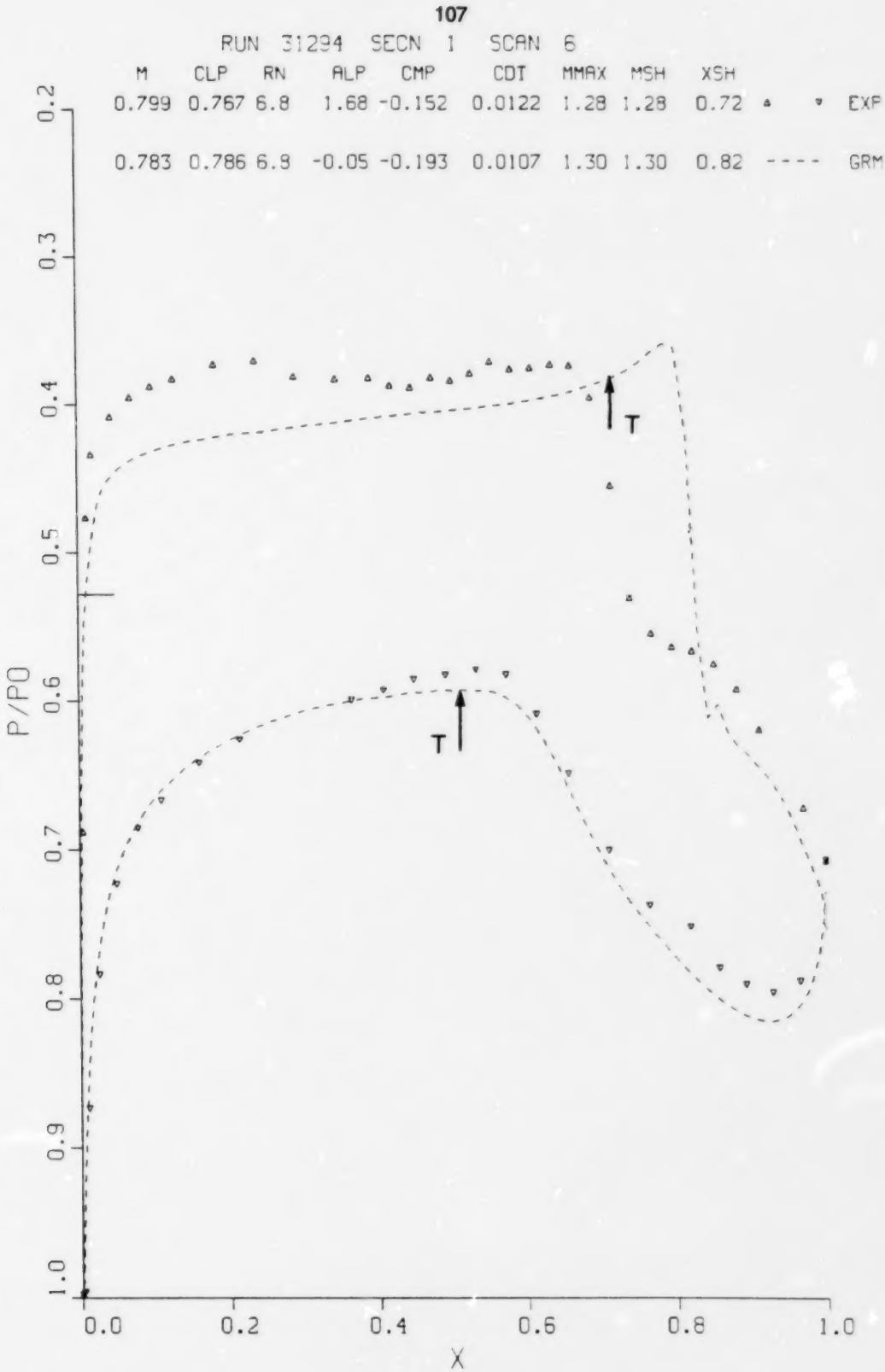


**FIG. 64e: COMPARISON OF GRUMFOIL AND EXPERIMENT, TRANSITION FREE. 10% AIRFOIL. $C_L \approx 0.767$**

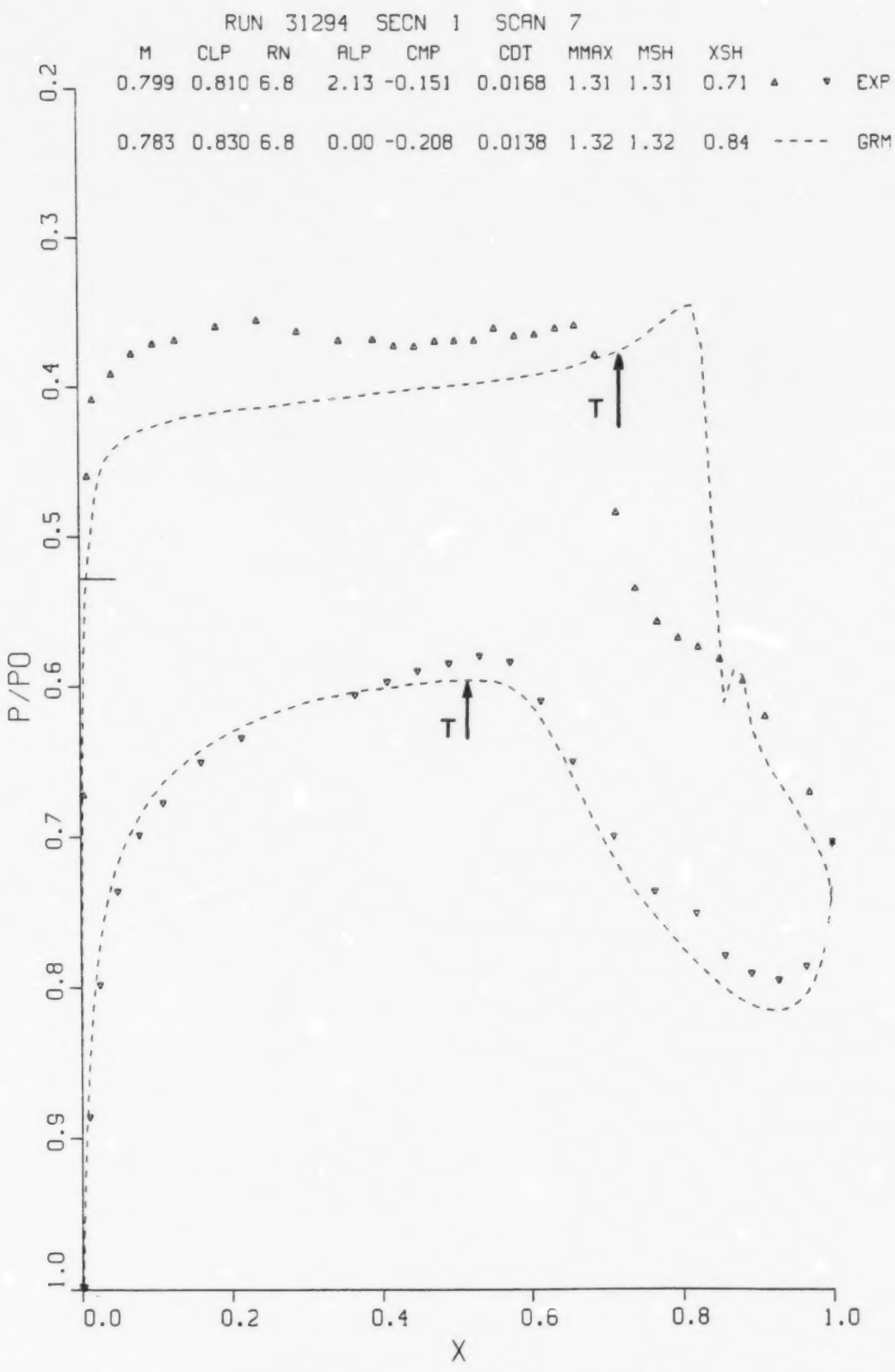


**FIG. 64f: COMPARISON OF GRUMFOIL AND EXPERIMENT, TRANSITION FREE. 10% AIRFOIL. $C_L \approx 0.810$**

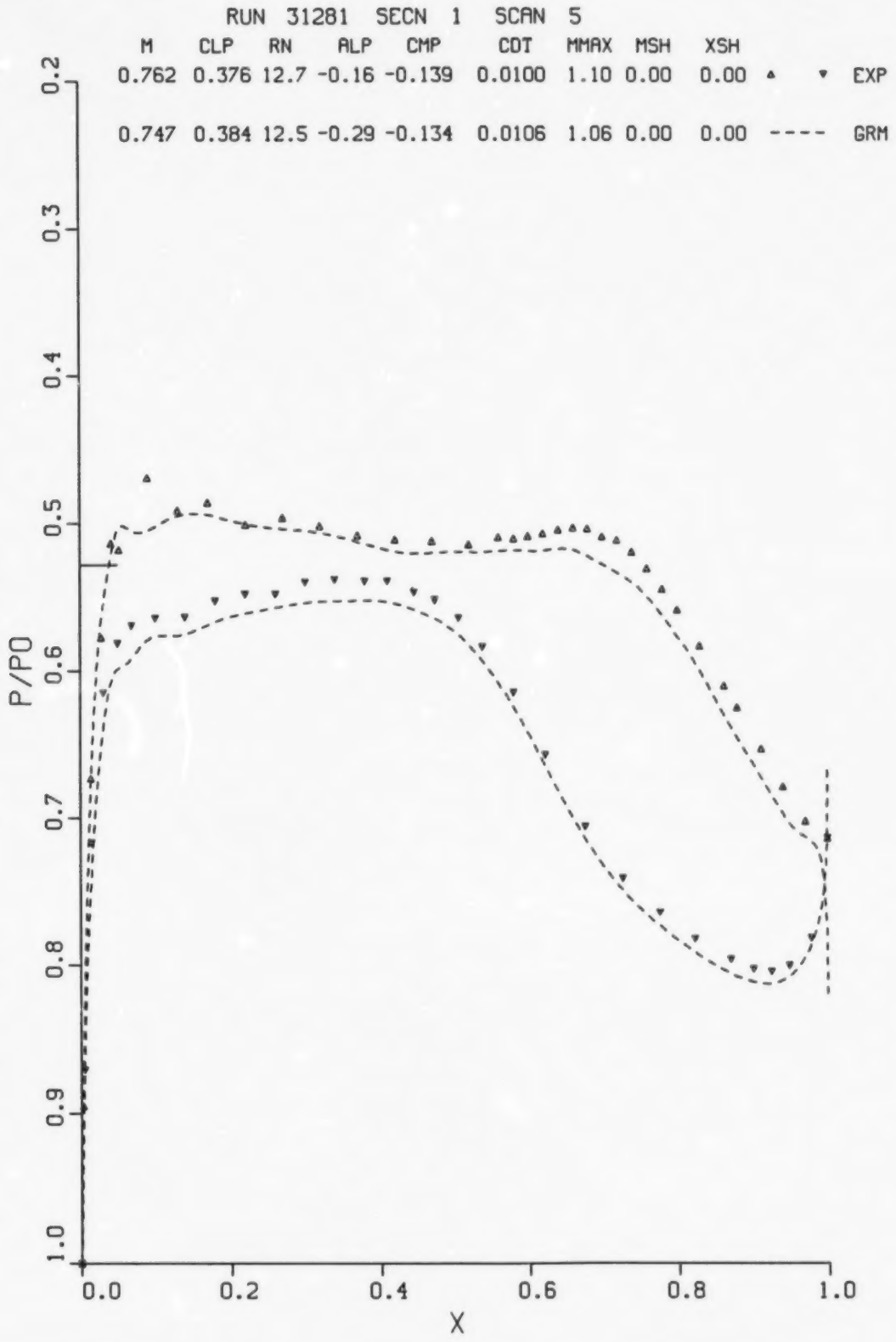


**FIG. 65a: COMPARISON OF GRUMFOIL AND EXPERIMENT, TRANSITION FIXED. 13% AIRFOIL. $C_L \approx 0.376$**

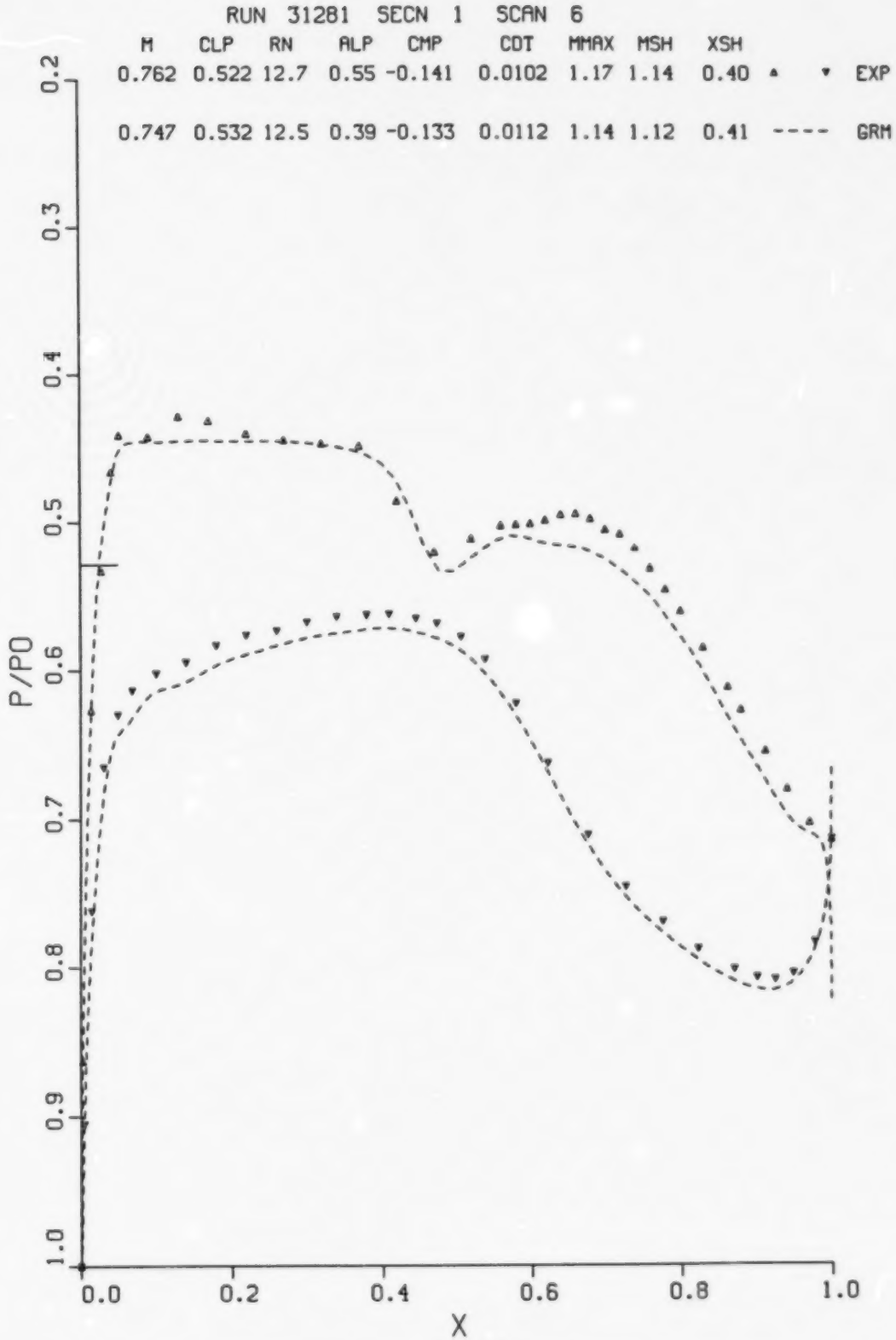


**FIG. 65b: COMPARISON OF GRUMFOIL AND EXPERIMENT, TRANSITION FIXED. 13% AIRFOIL. $C_L \approx 0.522$**

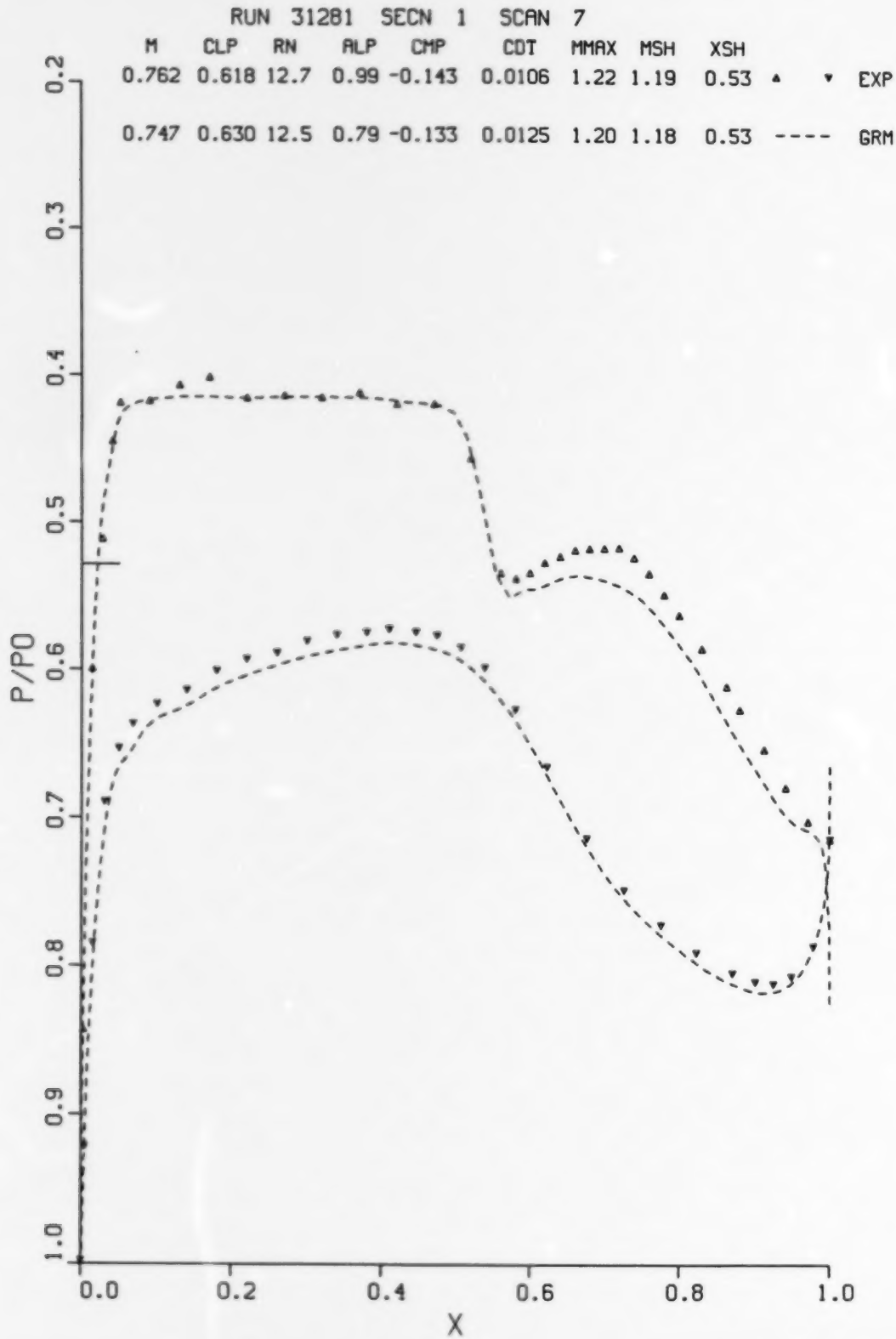


**FIG. 65c: COMPARISON OF GRUMFOIL AND EXPERIMENT, TRANSITION FIXED. 13% AIRFOIL. $C_L \approx 0.618$**

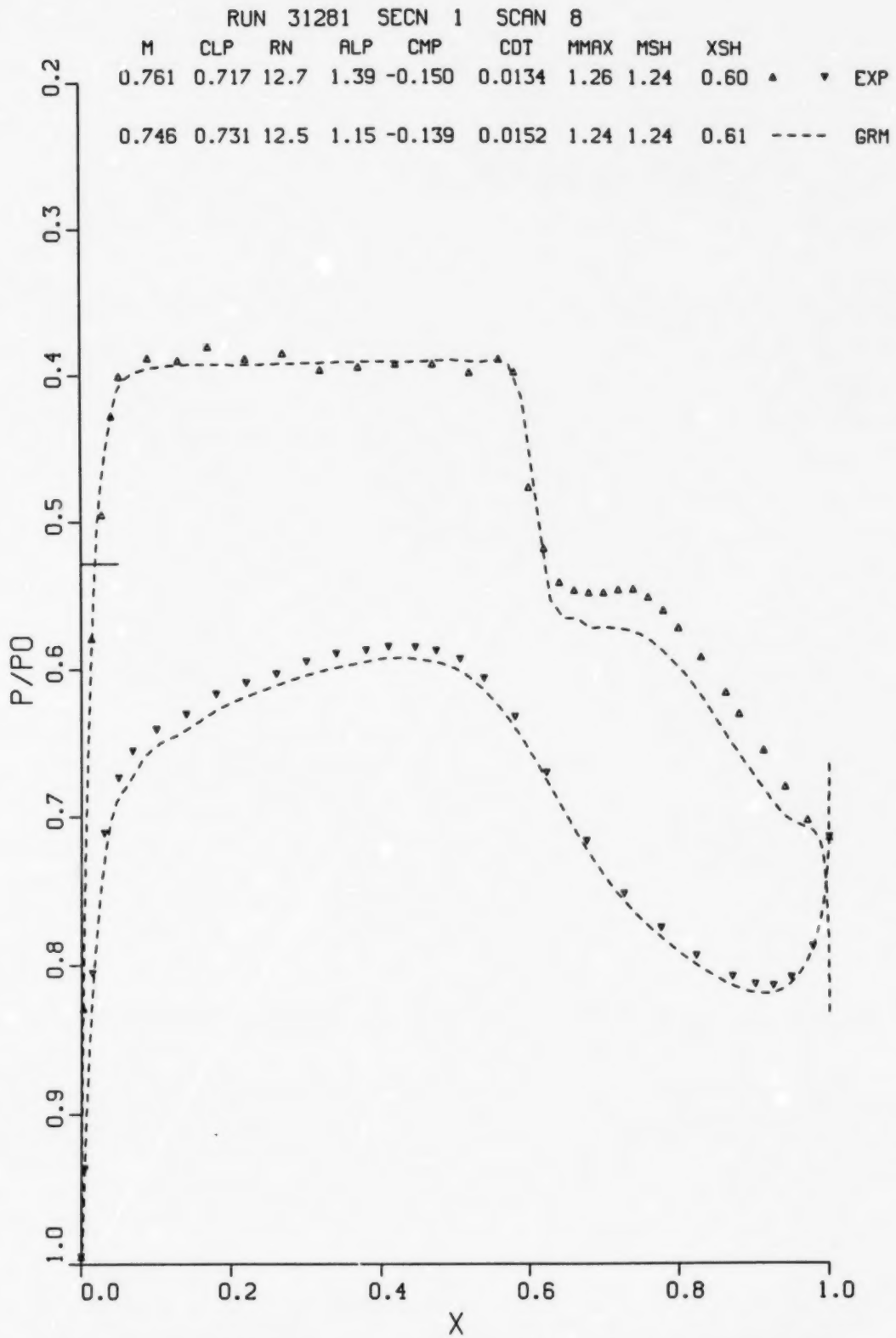


**FIG. 65d: COMPARISON OF GRUMFOIL AND EXPERIMENT, TRANSITION FIXED. 13% AIRFOIL $C_L \approx 0.717$**

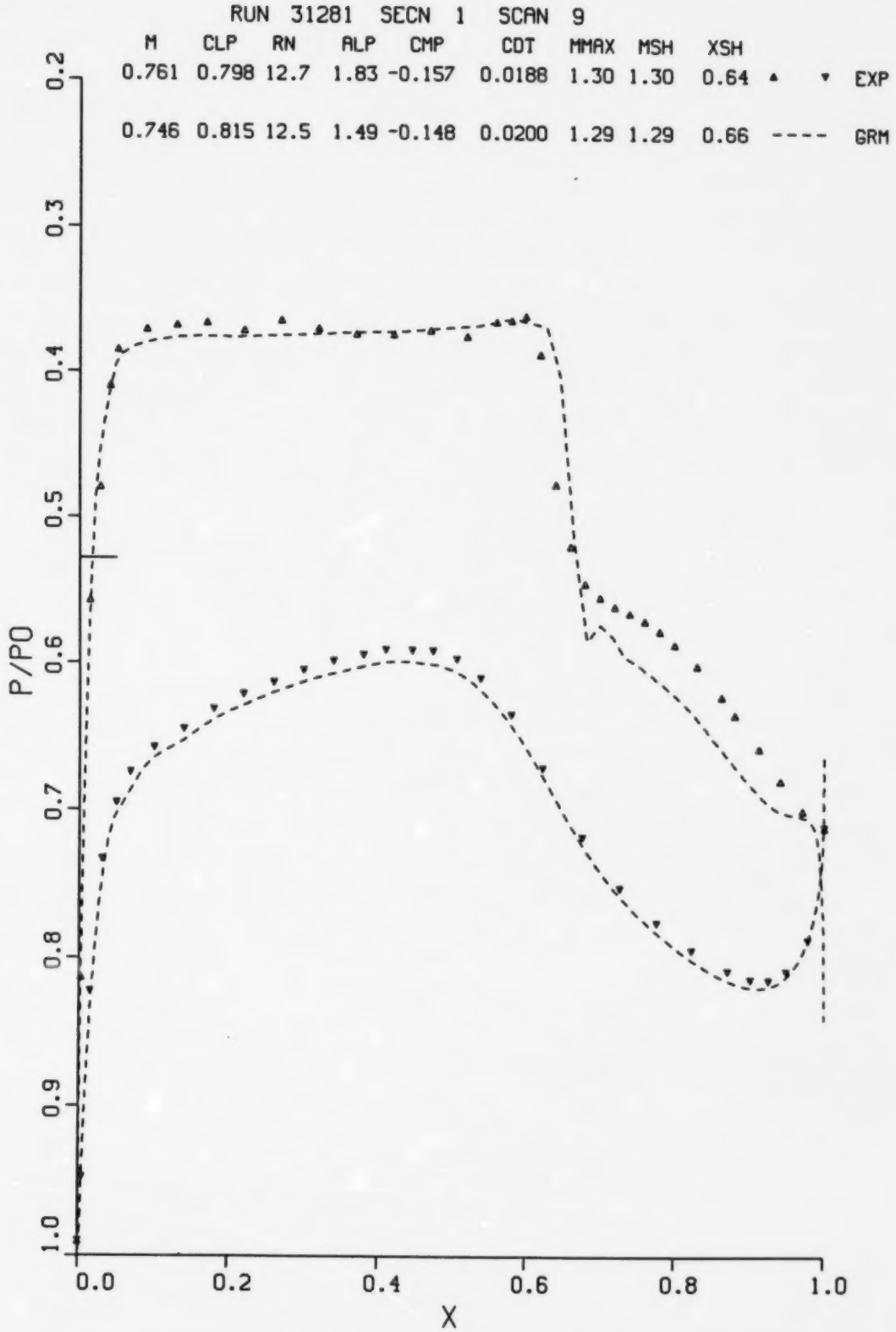


**FIG. 65e: COMPARISON OF GRUMFOIL AND EXPERIMENT, TRANSITION FIXED. 13% AIRFOIL. $C_L$ = 0.798**

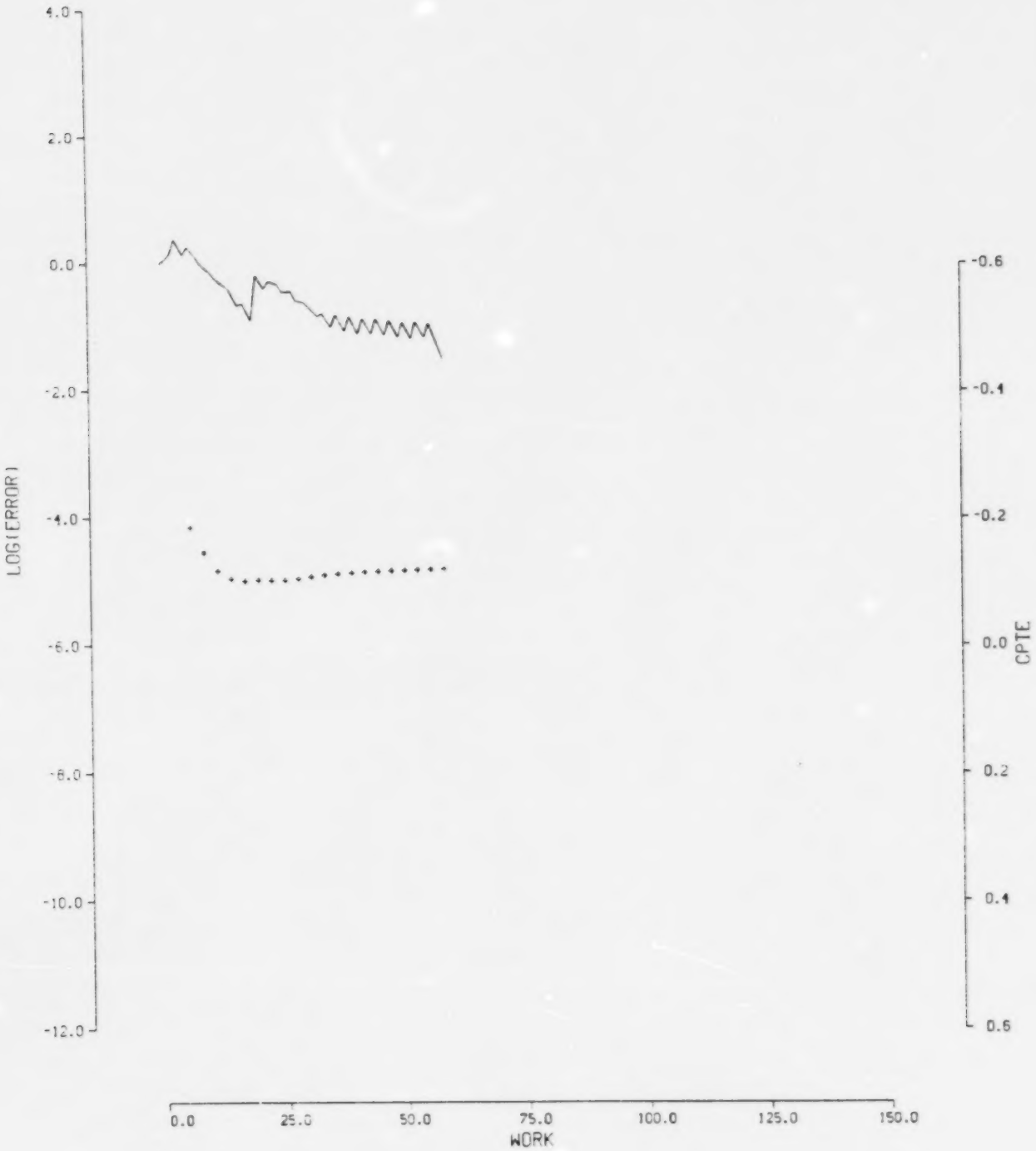


**FIG. 66a: CONVERGENCE OF GRUMFOIL FOR CASE IN FIG. 64c**

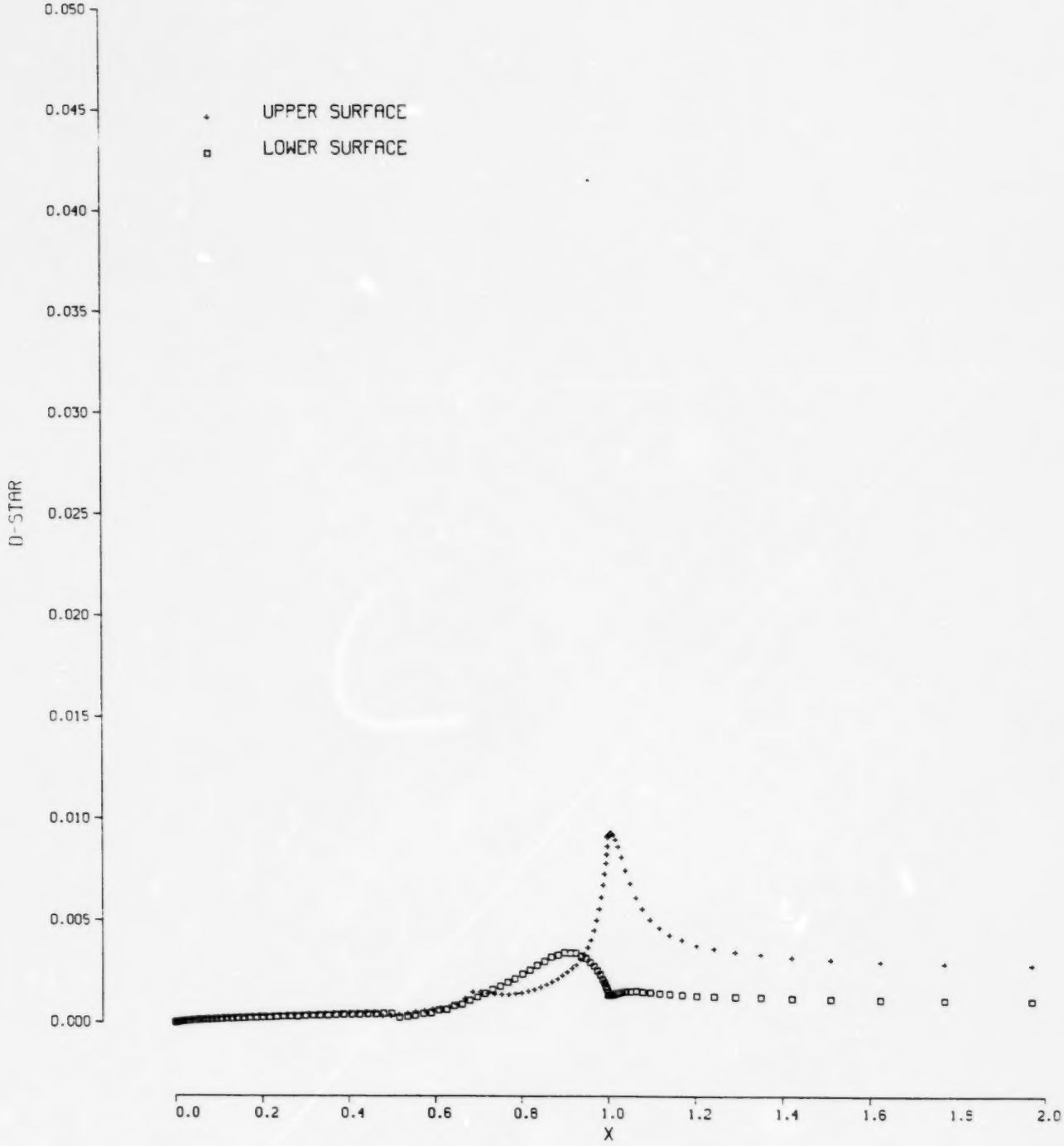


**FIG. 66b: δ* COMPUTED BY GRUMFOIL CODE FOR CASE IN FIG. 64c**

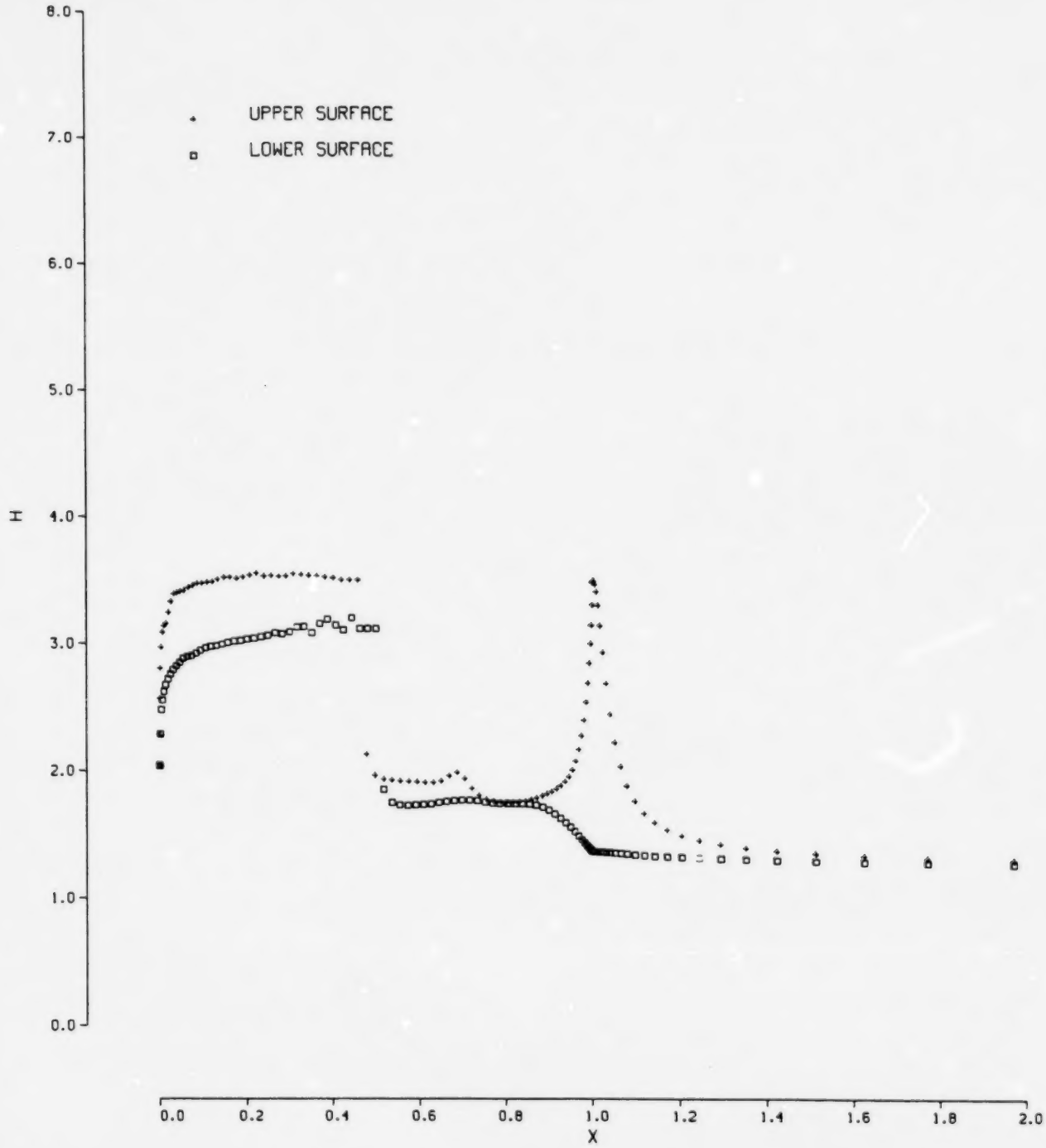


**FIG. 66c: SHAPE FACTOR PREDICTED BY GRUMFOIL FOR CASE IN FIG. 64c**

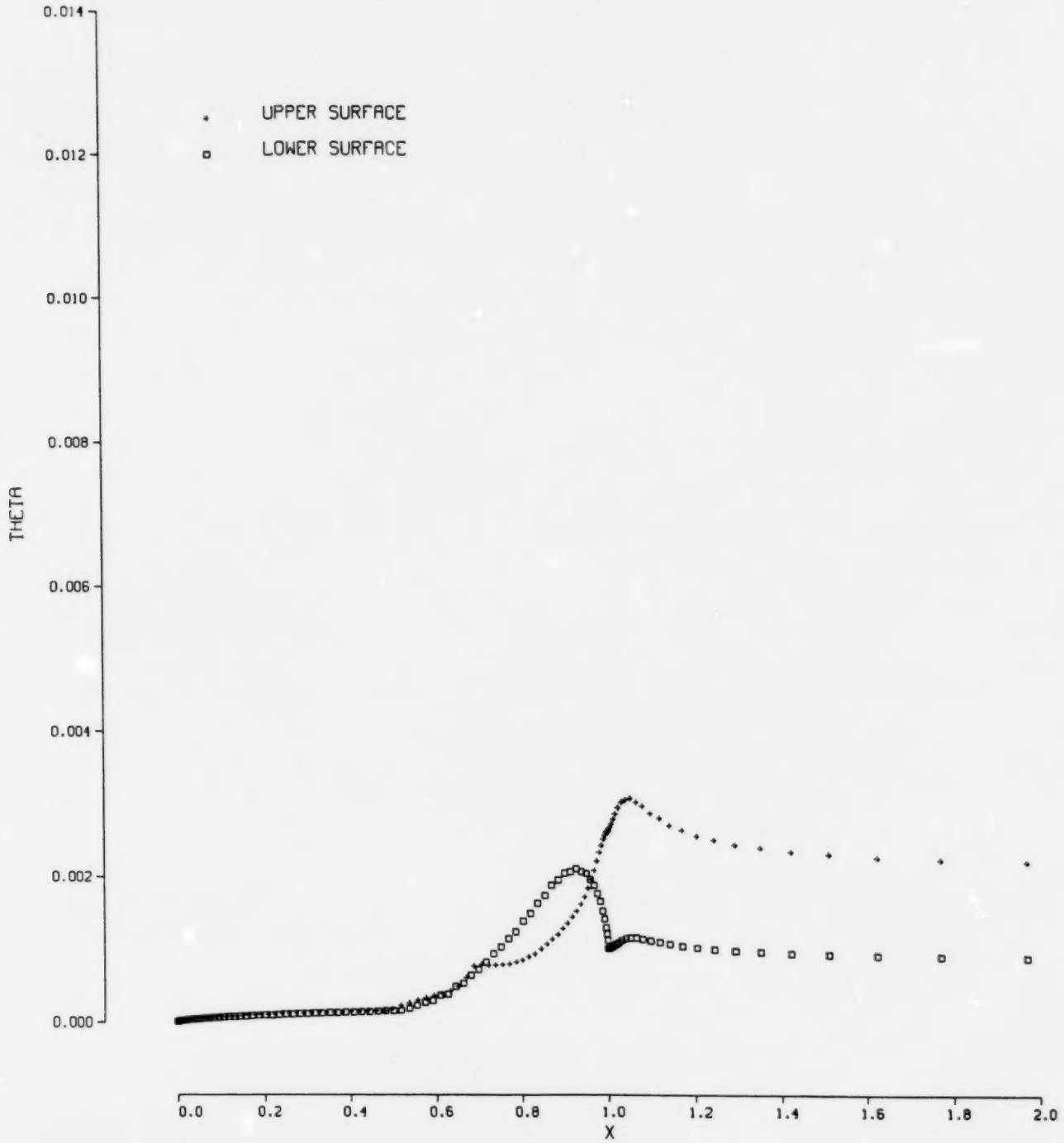


**FIG. 66d: MOMENTUM THICKNESS PREDICTED BY GRUMFOIL FOR CASE IN FIG. 64c**

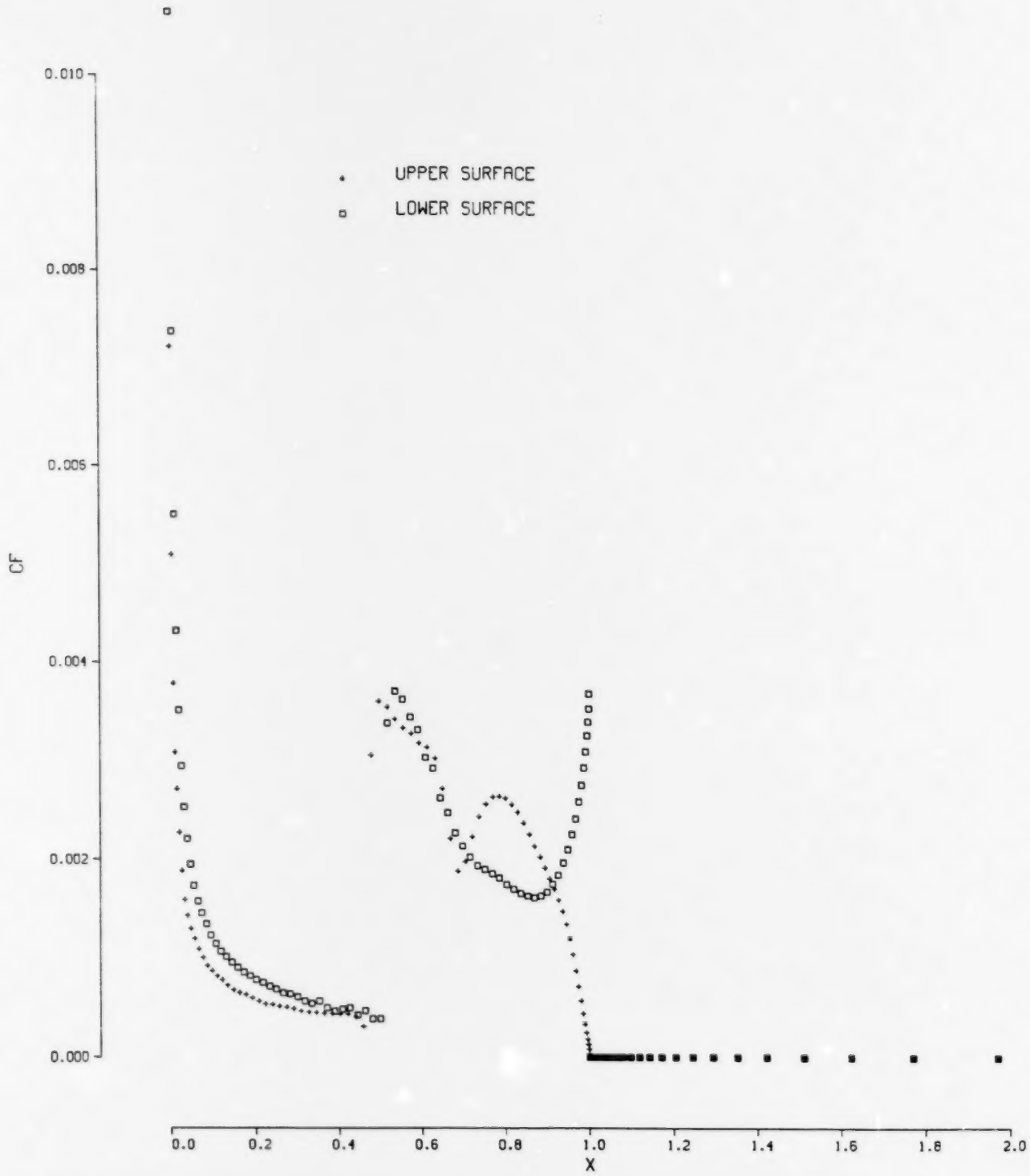


**FIG. 66e: SKIN FRICTION AS PREDICTED BY GRUMFOIL FOR CASE IN FIG. 64c**

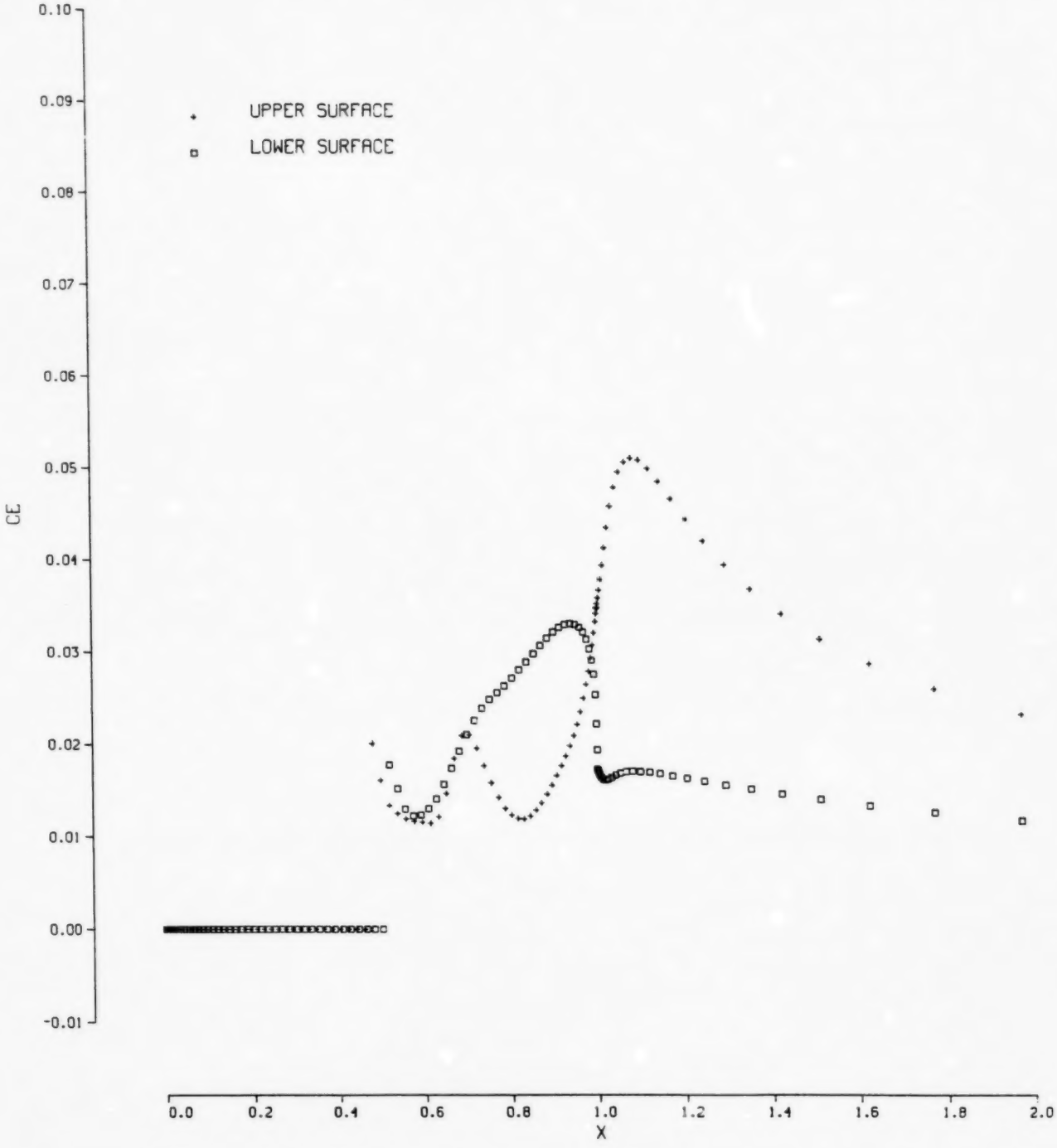


**FIG. 66f: ENTRAINMENT COEFFICIENT PREDICTED BY GRUMFOIL FOR CASE IN FIG. 64c**

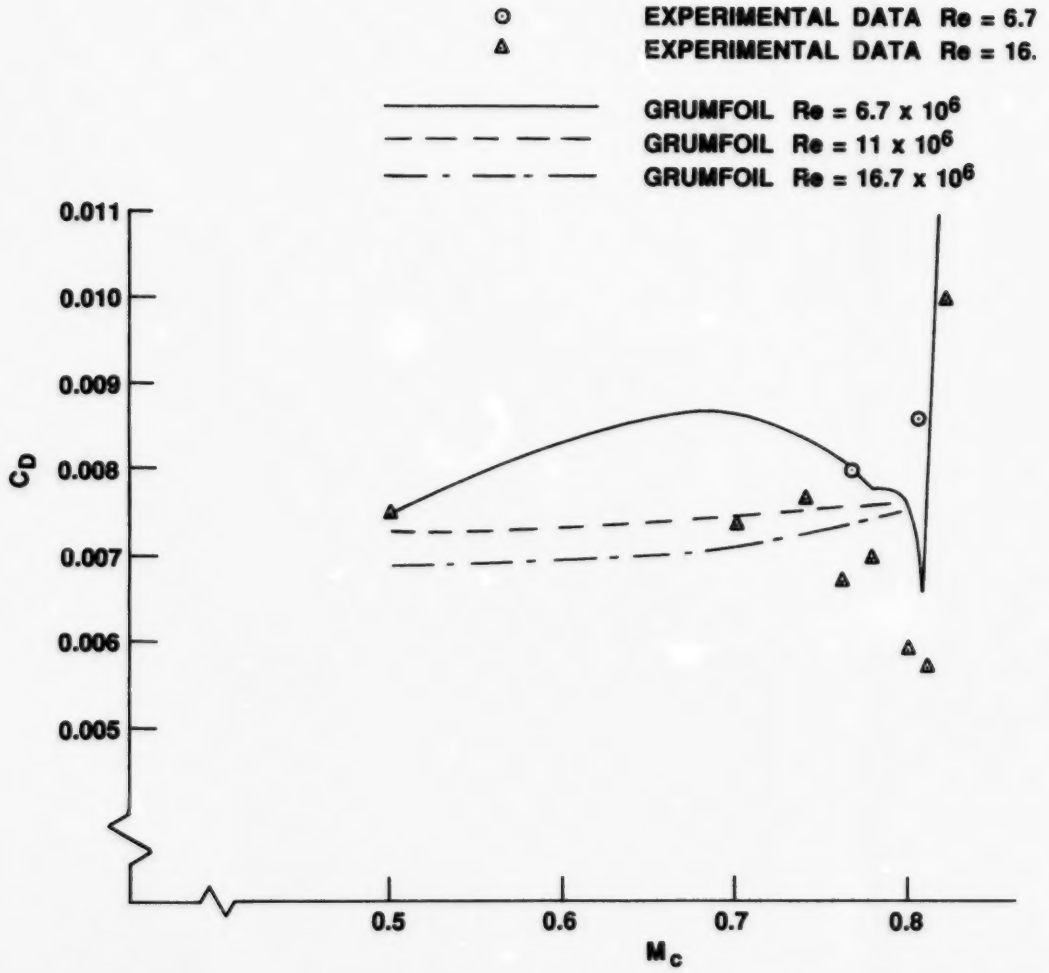


**FIG. 67: A COMPARISON OF EXPERIMENTAL AND GRUMFOIL D VALUES $C_L \approx 0.6$. 10% AIRFOIL**

## REPORT DOCUMENTATION PAGE / PAGE DE DOCUMENTATION DE RAPPORT

| REPORT/RAPPORT | REPORT/RAPPORT |
|---|---|
| NAE-AN-65<br>1a | NRC No. 31608<br>1b |
| REPORT SECURITY CLASSIFICATION<br>CLASSIFICATION DE SÉCURITÉ DE RAPPORT<br>Unclassified<br>2 | DISTRIBUTION (LIMITATIONS)<br>Unlimited<br>3 |

TITLE/SUBTITLE/TITRE/SOUS-TITRE

A Summary of Transonic Natural Laminar Flow Airfoil Development at NAE

4

AUTHOR(S)/AUTEUR(S)

M. Khalid and D.J. Jones

5

SERIES/SÉRIE

Aeronautical Note

6

CORPORATE AUTHOR/PERFORMING AGENCY/AUTEUR D'ENTREPRISE/AGENCE D'EXÉCUTION

National Research Council Canada
National Aeronautical Establishment
High Speed Aerodynamics Laboratory

7

SPONSORING AGENCY/AGENCE DE SUBVENTION

8

| DATE | FILE/DOSSIER | LAB. ORDER<br>COMMANDE DE LAB. | PAGES | FIGS./DIAGRAMMES |
|---|---|---|---|---|
| 05-90<br>9 | 10 | 11 | 134<br>12a | 67<br>12b |

NOTES

13

DESCRIPTORS (KEY WORDS)/MOTS-CLÉS

14
1. Laminar flow airfoils
2. Transonic flow
3. Supercritical airfoils
4. High Reynolds number

SUMMARY/SOMMAIRE

This report contains an analysis of the experimental results obtained from four supercritical natural laminar flow (NLF) airfoils investigated in the NAE High Reynolds Number Test Facility. The airfoils have maximum thickness to chord ratios of 0.10, 0.13, 0.16 and 0.21 and were designed for a lift coefficient of $C_L$ = 0.6. Their design Mach numbers were 0.8, 0.76, 0.72 and 0.68 respectively and the design chord Reynolds number was 12.5 million. It was found that all the airfoils showed the presence of a drag bucket close to design conditions and long lengths (in some cases about 70%) of natural laminar flow at Reynolds number 6.7 million. The minimum drag for the airfoils was found to range from 0.0045 to 0.0051, representing far lower levels than any airfoil dominated by turbulent boundary layer. It is also indicated that with transition fixed at about 10% chord the drag levels were similar to other airfoils with turbulent boundary layers.

15